NASA TECHNICAL NOTE

NASA TN D-6551

PRELIMINARY DETERMINATION OF SPACECRAFT TRAJECTORIES USING ON-BOARD OPTICAL MEASUREMENTS

by John D. McLean

Ames Research Center

Moffett Field, Calif. 94035

NATIONAL AERONAUTICS AND SPACE ADMINISTRATION • WASHINGTON, D. C. • OCTOBER 1971

1. Report No.	2. Government Accession No.	3. Recipient's Catalog No.
NASA TN D-6551		

4. Title and Subtitle

PRELIMINARY DETERMINATION OF SPACECRAFT TRAJECTORIES USING ON-BOARD OPTICAL MEASUREMENTS

5. Report Date: October 1971

6. Performing Organization Code

7. Author(s)

John D. McLean

8. Performing Organization Report No.: A-3522

9. Performing Organization Name and Address

NASA Ames Research Center
Moffett Field, Calif., 94035

10. Work Unit No.: 125-17-10-07

11. Contract or Grant No.

12. Sponsoring Agency Name and Address

National Aeronautics and Space Administration
Washington, D. C., 20546

13. Type of Report and Period Covered: Technical Note

14. Sponsoring Agency Code

15. Supplementary Notes

16. Abstract

This report deals with the problem of determining the trajectory of a spacecraft from on-board optical measurements without a priori information. Only sufficient information to determine the trajectory is used, and it is assumed that this preliminary estimate will be improved later by the use of differential corrections and redundant data.

Five basic types of measurements, representing instruments considered feasible or within the state of the art, are considered. The effects of random and bias type measurement errors and interpolation errors arising from nonsimultaneous measurements are analyzed. Only observations of the central body and two stars are considered.

Within certain limitations all five types of measurements will give satisfactory results. Two important factors discussed in the report are the proper choice of stars and the calibration for eliminating bias errors.

17. Key Words (Suggested by Author(s))	18. Distribution Statement
Navigation On-board Optical simplified Manual Back-up	Unclassified – Unlimited

19. Security Classif. (of this report)	20. Security Classif. (of this page)	21. No. of Pages	22. Price*
Unclassified	Unclassified	90	$3.00

* For sale by the National Technical Information Service, Springfield, Virginia 22151

TABLE OF CONTENTS

NOTATION

$\bar{A}$	vector of gravitational forces
B	angle between planes formed by unit vectors from spacecraft to planet and two stars
b	bias error
D	declination of planet
E	expected value
e	orbital eccentricity
h	orbital angular momentum
$\bar{i},\bar{j},\bar{k}$	unit vectors along Cartesian axis
M	maximum ratio of interpolation error to measurement error
RA	right ascension of planet defined with respect to star-fixed coordinates
$\bar{r}$	range vector from spacecraft to center of planet
r	magnitude of $\bar{r}$
S	half the planet subtense angle
t	time
$\bar{u}$	unit vector along $\bar{r}$
u_1,u_2,u_3	Cartesian components of $\bar{u}$
$\bar{v}$	velocity vector
v	magnitude of $\bar{v}$
$\bar{W}_1,\bar{W}_2$	unit vectors to star number 1 and star number 2
X,Y,Z	Cartesian axis
γ	angle between star and limb of planet
Δt	half the time interval between measurements
δ	small random increment
μ	product of universal gravitational constant and mass of planet

σ standard deviation

ϕ angle between stars

Subscripts

I irradiance

i integer

n normal

r radial

PRELIMINARY DETERMINATION OF SPACECRAFT TRAJECTORIES USING ON-BOARD OPTICAL MEASUREMENTS

John D. McLean

Ames Research Center

SUMMARY

This report deals with the problem of determining the trajectory of a spacecraft from on-board optical measurements without a priori information. Only sufficient information to determine the trajectory is used, and it is assumed that this preliminary estimate will be improved later by the use of differential corrections and redundant data.

Five basic types of measurements, representing instruments considered feasible or within the state of the art, are considered. The effects of random and bias type measurement errors and interpolation errors arising from nonsimultaneous measurements are analyzed. Only observations of the central body and two stars are considered.

Within certain limitations all five measurement types will give satisfactory results. Two important factors are the proper choice of stars and the calibration for eliminating bias errors. The errors for four types of measurements are strongly dependent on the relative location of the projection of the radius vector from the vehicle to the central body onto the plane formed by the unit vectors directed from the central body toward the two stars. The choice of stars is greatly enhanced by allowing measured angles as large as 90°, substantially larger than the present state of the art. Irradiance is a major source of bias error, and every effort should be made to correct for it; even a crude correction would be helpful.

The random position error can be approximated by the radial error from a single subtense angle measurement, and the accuracy of this approximation increases with range from the central body. This approximation can be used to show that within the present state of the art, the maximum distance from the central body at which the measurements considered in the study would be useful is about 200 times its radius. The usefulness of the methods at ranges of less than $\sqrt{2}$ times the radius of the central body, while theoretically possible, is of questionable practicality.

INTRODUCTION

Many navigation schemes require an initial estimate of the trajectory and use very sophisticated data processing techniques. Such systems are subject to partial failures, which, if not discovered immediately, make the information in the on-board computer useless. It is thus essential to have

available a simple back-up navigation scheme that can determine an orbit to a reasonable accuracy with no a priori information.

So far, studies of back-up navigation methods have concentrated on the use of manual computations and on the calculation of perigee altitude (e.g., refs. 1 and 2). A more desirable system, however, would consider all elements of the trajectory. Reference 3 describes such a system, which is designed for near-earth orbits of very small eccentricity. This approach uses manual calculations and a large amount of precomputed graphical data. For more general applications, such as lunar and interplanetary trajectories, greater accuracy, in terms of significant figures, is required, and it appears impractical to obtain this accuracy without the use of redundant data.

The approach used in this study is the same as that used by astronomers in determining the orbit of a newly discovered body. That is, a preliminary estimate of the trajectory is made using only enough data to determine the position and velocity vectors at a given time. The estimate is then improved by the use of redundant data from additional observations. This technique does not require any greater accuracy in measurements but it does require the use of a small automatic computer.

This report is concerned with the first part of the problem, that is, with a preliminary determination of the trajectory, or, in other words, the position and velocity vectors of the spacecraft at some given time. The determination of velocity consists essentially in making two position fixes and then interpolating to find position and velocity at some intermediate time.

Hamer and Mayo (ref. 4) reported on the accuracy of obtaining position fixes using a number of different combinations of simultaneous on-board measurements including radar ranging. This report presents a more detailed error analysis of several possible methods that require fewer measurements and include some practical constraints. This analysis is carried out by the linear perturbation method, which Hamer and Mayo have shown to be valid for fairly large errors in the type of measurements considered.

Only optical observations of two stars and the central attracting body involving measured angles no greater than 90° are considered. Five different types of measurements are investigated. The instruments used are either within the present state of the art or are considered to be potentially feasible. In some cases a complete position fix cannot be made with a single observation, and it is then necessary to refer the data to a common epoch by interpolation. The report considers errors due to interpolation as well as to measurement inaccuracy.

Since the velocity is determined directly from position-fix data, most of the error analysis deals with the accuracy of position fixes, and the errors in determining the corresponding velocities require only a brief treatment. The object of the error analysis is to determine whether the preliminary estimate of the trajectory is accurate enough to allow the use of linear perturbation theory to process subsequent redundant data for improving the estimate.

It is difficult to assign numbers to such an accuracy criterion since the errors in the linear perturbation theory depend upon the time before additional data are acquired and the nature of the trajectory as well as the errors in the preliminary estimate. In most cases, however, the preliminary estimate should be accurate enough if the magnitude of the errors in position and velocity do not exceed 2 or 3 percent of the magnitudes of the total position and velocity, respectively.

DESCRIPTION OF MEASUREMENTS

The measuring instruments for a back-up navigation system should be simple and reliable; therefore, only optical instruments have been considered. In addition, only observations of two stars and the central body were used in order to simplify the measurements and computations. Triangulation of two celestial bodies, which usually gives the range more accurately than the central body subtense angle (ref. 4), was excluded. This was done because of the number of measurements required and the difficulty of interpolation if the necessary angles cannot be measured simultaneously.

The error analysis methods described later in the report are valid for angles as large as 180° between the two stars and between each star and the center of the central body. For the computation of data, however, these angles were restricted to magnitudes of 90° or less, giving 90° total field of view. This restriction is reasonable since it can be shown that if stars are available anywhere within this allowable measurement range, then accuracy will not be improved by increasing this measurement range. Angles up to 90° are included for completeness, even though this limit is beyond the present state of the art. For example, the Apollo and Gemini spacecraft windows restrict the angles measured with the hand-held sextant (ref. 5), to be within a field of view of about 50°. The Apollo space sextant can measure angles up to 57° from the principal axis to give a field of measurement of 114°. Even so, the fact that the measured angles cannot exceed 57° prevents the use of many pairs of stars within the field of view.

Definition of Variables

We wish to determine the position of the spacecraft in a Cartesian coordinate system having the origin at the center of the dominant attracting body. However, for convenience we will translate the origin from the central body to the spacecraft as shown in figure 1. The vector $\bar{r}$ in the figure is the position vector of the planet[1] with respect to the spacecraft and is the negative of the desired position vector.

[1]In the remainder of the report the word "planet" will be used to refer to the central attracting body even though that body might actually be the Sun or Moon.

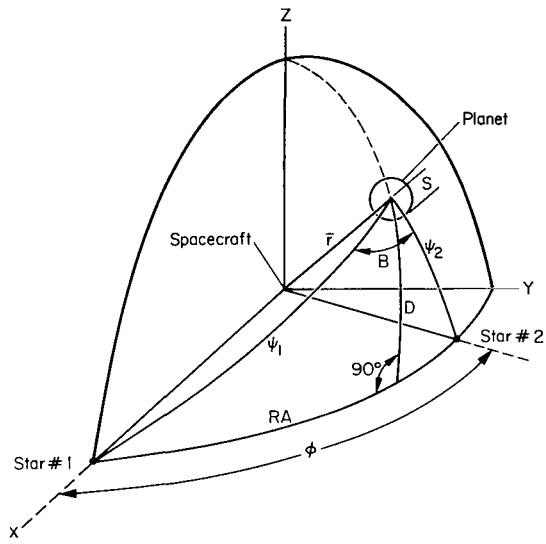

Figure 1.- Geometry for position fix.

For convenience the coordinate system used will be a Cartesian system as follows: The positive X axis lies in the direction of star number 1, while the Y axis is in the plane of the two stars, normal to the X axis and positive when on the same side of the X axis as star number 2. The Z axis completes a right-handed orthogonal system. This report deals only with finding $\bar{r}$ in the coordinate system, but the coordinates can be transformed readily into any inertial system in which the directions of the stars are known.

The angles RA and D in figure 1 are, respectively, the right ascension of the planet measured in the X-Y plane from the X axis and its declination above (or below) the X-Y plane. It is pointed out in reference 4 that another star must be observed to avoid ambiguity. The ambiguity occurs here as an uncertainty in the sign of D, but the observer can determine the proper sign easily from the relative positions of the planet and the two stars. (If one draws an arrow from star 1 to star 2, D is positive when the planet is to the left of the arrow.)

The "star-center" angles ψ_1 and ψ_2 are measured from stars 1 and 2, respectively, to the center of the planet, while S is defined as half the planet subtense angle.

We define the corresponding star-limb angles γ_1 and γ_2, respectively, so that

$$\psi_i = \gamma_i + k_i S \tag{1}$$

where

$$k_i = \pm 1$$

The positive sign is used for γ_i measured to the limb nearest the star and the negative sign for the far limb. The angle between the planes formed by $\bar{r}$ and the lines of sight to the two stars is denoted by B, and ϕ is the angle between the two stars.

If $\bar{u}$ is a unit vector in the direction of $\bar{r}$ then

$$\bar{r} = r\bar{u} = r \begin{pmatrix} u_1 \\ u_2 \\ u_3 \end{pmatrix} \tag{2}$$

and

$$\left.\begin{aligned} u_1 &= \cos RA \cos D \\ u_2 &= \sin RA \cos D \\ u_3 &= \sin D \end{aligned}\right\} \tag{3}$$

while

$$r = R \csc S$$

where R is the radius of the central body. If we normalize by using the planet radius as the unit of length, then $R = 1$ and

$$r = \csc S \tag{4}$$

Measuring Instruments

Three general types of measuring instruments were considered. The first type would measure RA, D, and S or ψ_1, ψ_2, and S simultaneously. The photographic technique investigated by Walsh (ref. 6) could be used for this purpose. Walsh's approach uses a sextant-type measuring instrument with the human eye replaced by photographic film. Sketch (a) illustrates one possible example of such an instrument for two dimensions. The star and central body need only be within a relatively large field of view, and the incremental angle, which must be added to α (the angle between the optical axes), can be measured from the film. The subtense angle and center of the planet can be determined from the film and, therefore, the star-center angle can be measured directly. Walsh's results indicate the photographic method to be potentially feasible, and although he considered no more than two lines of sight, the method could be extended to three. The three-line-of-sight method would allow the simultaneous measurement of S and either ψ_1 and ψ_2 or RA and D, depending on the configuration of the instrument. The latter combination,

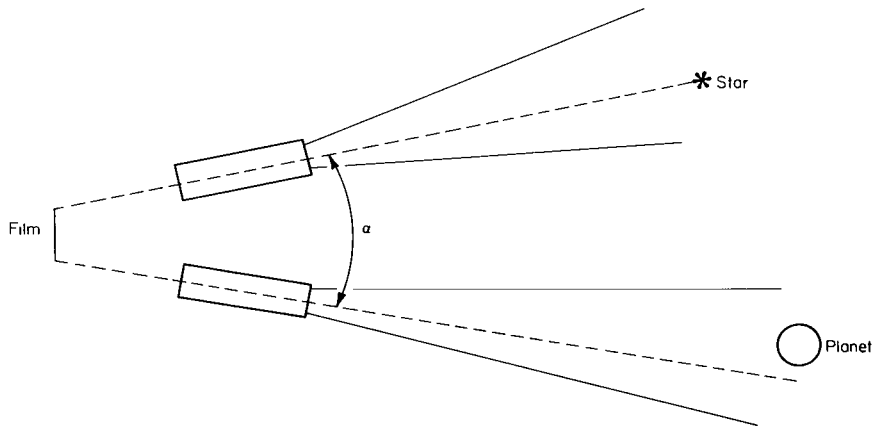

Sketch (a)

which could also be measured by a theodolite mounted on a stable platform, will be used as a standard for comparison in this study.

The second type of instrument considered is capable of measuring two or three angles simultaneously without the use of photography. The trisextant reported on by Novak (ref. 7) is an example of such an instrument. The trisextant has three lines of sight and the principal line of sight has (or could have) a field of view large enough to observe a substantial portion of the planet, while the two secondary lines of sight observe stars. The operator sets the images of the stars tangent to the disk of the planet simultaneously as shown in sketch (b). The readout scales on the instrument provide the angles γ_1, γ_2, and B. The portion of the planet between the two stars must be within the field of view of the principal line of sight, and this requirement restricts the possible location of stars when the spacecraft is near the planet. This restriction may be dealt with in a number of different ways, such as using a larger field of view and less magnification at shorter ranges, and has not been considered in this study. An experimental model of the Martin trisextant has been tested at Ames Research Center and found to be feasible from the operational standpoint. However, this model was not sufficiently accurate for space navigation, and the ultimate accuracy obtainable with such an instrument is unknown.

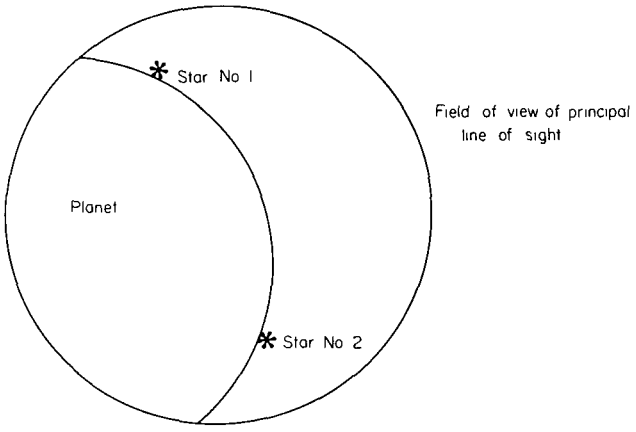

Sketch (b)

The third instrument considered, which measures only a single angle at a time, is typified by the hand-held sextant described in reference 5. Data obtained from the instrument in ground tests and space flight (refs. 5 and 8) were found to have random errors of less than 10 arc seconds standard deviation. Bias errors ranged in magnitude from 0 to 28.7 arc seconds, depending on the measurement conditions. Further studies may lead to the reduction or calibration of part of the bias errors.

In tests of instruments such as the hand-held sextant it has been found difficult to estimate the planet center accurately, especially when the full disk is not visible. Therefore star-center measurements are considered only when photography is used.

Types of Measurements

In order to determine the position vector, at least three of the angles defined must be known at a given time. The consideration of different practical combinations led to the following five types of measurements.

Type 1- Simultaneous measurement of the right ascension, RA, declination, D, and subtense angle, 2S, by means of photography (or an inertially stabilized theodolite). As will be seen in the section on Error Analysis Methods, this is the only one of the five types of measurements for which the error equations do not contain singularities. Therefore type 1 measurements have been used as a standard of comparison for the other types.

Type 2- Simultaneous measurement of γ_1, γ_2, and 2s. This measurement would require photography, but it could be approximated by using the trisextant to measure 2S, then γ_1 and γ_2 simultaneously, followed by another measurement of 2S. Linear interpolation, discussed later in the report, would be used to refer S to the same epoch as γ_1 and γ_2. This approximation is not analyzed.

Type 3- Simultaneous measurements of γ_1, γ_2, and angle B, between the planes of the two star-limb angles. This single measurement with the trisextant would allow a complete position fix.

Type 4- Simultaneous measurement of one star-limb angle and the subtense angle followed by simultaneous measurement of the other star-limb angle and the subtense angle at a later time. Interpolation is used to refer these two sets of measurements to a common epoch. This is another possible application of the trisextant, or it could be done with the two-lines-of-sight photographic sextant described by Walsh.

Type 5- Measurements of the two star-limb angles and the subtense angle, one at a time in a suitable sequence, followed by interpolation to refer the measurements to a common epoch. These measurements, which could be performed with the hand-held space sextant described in reference 5, constitute the only one of the five types that is truly within the present state of the art.

DETERMINATION OF POSITION AND VELOCITY

This section of the report presents the equations used for determining position and velocity from the measured angles. The angles RA and D are measured directly only in type 1 measurements, and for the other types the u_i in equation (3) must be expressed in terms of the angles (γ_1, γ_2, S or B) actually measured. However, it is more convenient to combine the γ_i with S using equation (1) in order to get the star-center angles ψ_i. The resulting equations for the u_i and the equations for determining S from type 3 measurements are derived in appendix A. Types 4 and 5 also require interpolation formulas for determining position and these are derived in appendix B along with those used for determining velocity.

The position-fix equations for all types of measurements are summarized in the following paragraphs after which the computation of velocity is discussed.

Position Fix Equations

Type 1 measurements- In this case equation (3) can be used for $\bar{u}$ while r is given by equation (4).

Type 2 measurements- Again, r is given by equation (4), but $\bar{u}$ is given by equation (A8) as

$$\bar{u} = \begin{bmatrix} \cos \psi_1 \\ \dfrac{\cos \psi_2 - \cos \psi_1 \cos \phi}{\sin \phi} \\ \pm \sqrt{1 - u_1^2 - u_2^2} \end{bmatrix} \tag{5}$$

The third component is equal to sin D and the sign is chosen by the method described earlier.

Type 3 measurements- For these observations S is computed in terms of γ_1, γ_2, and B using the following equation from appendix A:

$$\cos(2S + k_1\gamma_1 + k_2\gamma_2) = \frac{2 \cos \phi - \cos(k_1\gamma_1 - k_2\gamma_2)(1 + k_1k_2 \cos B)}{1 - k_1k_2 \cos B} \tag{6}$$

where k_1 and k_2 are defined by equation (1). Once S is known, ψ_1 and ψ_2 can be found using equation (1), and $\bar{u}$ is determined by equation (5). Equation (A15) is an alternate equation for $\bar{u}$

$$\bar{u} = \begin{bmatrix} \cos \psi_1 \\ \dfrac{\cos \psi_2 - \cos \psi_1 \cos \phi}{\sin \phi} \\ \dfrac{\pm \sin \psi_1 \sin \psi_2 \sin B}{\sin \phi} \end{bmatrix}$$

Type 4 measurements- This is the first case in which it is necessary to use interpolation. Measurements of one star-limb angle and the subtense angle at each of the times are indicated in table 1.

TABLE 1.- REGULAR SCHEDULE FOR TYPE 4 MEASUREMENTS

Time	t_1	t_2	t_3
Angles measured	γ_1 and S	γ_2 and S	γ_1 and S

Equation (4) can be used to compute r at each time in the table while equation (1) gives ψ_1 at t_1 and t_3 and ψ_2 at t_2.

Next Gibb's method (ref. 9) is used for interpolation to find $\psi_1(t_2)$. The interpolation formula, derived in appendix B, is equivalent to third order in time. For convenience t_2 is assumed to be zero, in which case

$$\bar{r}(t_2) = \frac{1}{t_3 - t_1}\left[t_3\bar{r}(t_1) - t_1\bar{r}(t_3) - \frac{\bar{A}(t_1)}{6}t_1t_3(t_1 - 2t_3)\right.$$

$$\left. - \frac{\bar{A}(t_3)}{6}t_1t_3(2t_1 - t_3)\right] \tag{7}$$

where $\bar{A}(t)$ is the gravitational force acting on the spacecraft at time t.

At times t_1 and t_3, r and ψ_1 have been determined so that if $\bar{w}_1$ is the unit vector in the direction of star number 1 it is possible to compute

$$\bar{r}(t_i) \cdot \bar{w}_1 = r(t_i)\cos\psi_1(t_i)$$

Thus equation (7) can be used to find $\cos\psi_1(t_2)$ by taking the dot product of both sides with $\bar{w}_1$ if a conic trajectory is assumed. In this case

$$\bar{A}(t) = -\frac{\mu\bar{r}(t)}{r^3(t)}$$

and, using equation (7),

$$\bar{A}(t) \cdot \bar{w}_1 = -\frac{\mu}{r^2(t)}\cos\psi_1(t)$$

This approximation is necessary since all three components of $\bar{r}(t)$ would be needed to compute $\bar{A}(t) \cdot \bar{w}_1$ for the n-body case. The resulting expression for $\cos\psi_1(t_2)$ is

$$\cos\psi_1(t_2) = \frac{1}{t_3 - t_1}\left\{\frac{r(t_1)}{r(t_2)}\left[t_3 - \frac{\mu t_1t_3(t_1 - 2t_3)}{6r^3(t_1)}\right]\cos\psi_1(t_1)\right.$$

$$\left. - \frac{r(t_3)}{r(t_2)}\left[t_1 - \frac{\mu t_1t_3(t_3 - 2t_1)}{6r^3(t_3)}\right]\cos\psi_1(t_3)\right\} \tag{8}$$

Since $\cos\psi_2(t_2)$ and $r(t_2)$ can be computed directly from measurements at t_2, enough information is available to compute $r(t_2)$ using equations (2), (4), and (5).

Type 5 measurements- In this case it is possible to measure only one angle at a time, and it is necessary to depend partly on linear interpolation. Either the range, r, or one or both of the star-limb angles may be interpolated, but it will be shown later that linear interpolation is somewhat more accurate for r than for γ. Therefore, from the standpoint of interpolation accuracy, the schedule in table 2 was considered best.

TABLE 2.- REGULAR SCHEDULE FOR TYPE 5 MEASUREMENTS

Time	t_1	t_2	t_3	t_4	t_5	t_6	t_7
Angle measured	S	γ_1	S	γ_2	S	γ_1	S

Linear interpolation gives the range at t_2, t_4, and t_6 as

$$r(t_i) = \frac{(t_{i+1} - t_i)r(t_{i-1}) + (t_i - t_{i-1})r(t_{i+1})}{(t_{i+1}) - (t_{i-1})} \tag{9}$$

Once $r(t_2)$, $r(t_4)$, and $r(t_6)$ are known, equation (8), with the proper substitutions for the t_i, can be used to compute $\cos \psi_1(t_4)$. Then $\cos \psi_2(t_4)$ is determined from a direct measurement, and equations (2), (4), and (5) give $\bar{r}(t_4)$.

The procedure just outlined uses linear interpolation to determine r at times t_2, t_4, and t_6, after which Gibb's method is used for interpolation to determine $\cos \psi_1(t_4)$. Two alternate schedules which use only linear interpolation are shown in table 3. The same time indices are used for comparison with table 2. For case 1 equation (9) is used to compute $r(t_4)$; $\gamma(t)$ is substituted for $r(t)$ in equation (9) to obtain $\gamma_1(t_4)$ which can be used with $r(t_4)$ and $\gamma_2(t_4)$ in equation (1) to give $\psi_1(t_4)$ and $\psi_2(t_4)$. For case 2 equation (9) is used to compute $\gamma_1(t_4)$ and $\gamma_2(t_4)$, and $S(t_4)$ is known from direct measurement. Each of these alternate schedules uses equation (9) twice, whereas the regular type 5 schedule uses equation (9) three times and equation (8) (from Gibb's method) once. Therefore, the alternate schedules require less computation but have larger interpolation errors; this is because $(t_6 - t_2)$ is larger than the time intervals used for linear interpolation in the regular schedule, and Gibb's method is more accurate than linear interpolation.

TABLE 3.- ALTERNATE SCHEDULES FOR TYPE 5 USING ONLY LINEAR INTERPOLATION

Time	t_1	t_2	t_3	t_4	t_5	t_6	t_7
Angle measured, case 1	-	S	γ_1	γ_2	γ_1	S	-
Angle measured, case 2	-	γ_1	γ_2	S	γ_2	γ_1	-

Computation of Velocity

It is a well-known principle of celestial mechanics that if the position vector on an orbit is known at two different times, the velocities can be calculated. In the two-body case this determination of velocity is known as Lambert's problem, and a number of methods of solution are in the literature. However, these computational procedures are valid for large time intervals and are fairly complex. For shorter time intervals Gibb's method (appendix B) will provide a reasonably accurate solution with much less computation and allow the inclusion of perturbing gravitational forces.

Two separate sets of measurements of any of the five types already discussed will provide two independent position fixes. With types 4 and 5 it is also possible to obtain two position fixes by extending a single measurement schedule to include one additional measurement each of a star-limb angle and the subtense angle. The use of the two independent position fixes and the extended schedules is discussed in the following paragraphs.

Two independent position fixes- If $\bar{r}(t_1)$ and $\bar{r}(t_3)$ have been determined by two sets of any of the five measurement types, then the velocity $\bar{v}(t_2)$ at some intermediate time t_2 can be computed by Gibb's method. It is shown in appendix B that if it is assumed that $t_2 = 0$, then

$$\bar{v}(t_2) = \frac{1}{t_3 - t_1}\left[\bar{r}(t_3) - \bar{r}(t_1) - \frac{\bar{A}(t_1)}{6}(2t_3^2 + 2t_1t_3 - t_1^2) - \frac{\bar{A}(t_3)}{6}(t_3^2 - 2t_1t_3 - 2t_1^2)\right] \tag{10}$$

while $\bar{r}(t_2)$ is given by equation (7). These formulas can also be used if the epoch t_2 is chosen to coincide with the beginning or end of the interpolation interval by letting $t_2 = t_1 = 0$ or $t_2 = t_3 = 0$. If, for example, the second choice is used equation (7) reduces to

$$\bar{r}(t_2) = \bar{r}(t_3)$$

and equation (10) becomes

$$\bar{v}(t_2) = \frac{\bar{r}(t_1) - \bar{r}(t_3)}{t_1} + \frac{t_1}{6}[\bar{A}(t_1) + 2\bar{A}(t_3)] \tag{11}$$

The choice of epoch requires less computation but is less accurate, as will be shown in the section on Error Analysis Methods.

Extended schedules- The schedules of types 4 and 5 can be extended to provide enough information for computing both $\bar{r}$ and $\bar{v}$ from a single set of measurements. The measurement schedules and the necessary computations for type 4 are shown in table 4.

TABLE 4.- EXTENDED SCHEDULE FOR TYPE 4 MEASUREMENTS

Time	t_1	t_2	t_3	t_4	t_5
Angles measured	γ_1 and S	γ_2 and S		γ_1 and S	γ_2 and S
Computed from measurements	$r(t_1)$, $\psi_1(t_1)$	$r(t_2)$, $\psi_2(t_2)$		$r(t_4)$, $\psi_1(t_4)$	$r(t_5)$, $\psi_2(t_5)$
From interpolation (eq. (8))		$\cos\ \psi_1(t_2)$		$\cos\ \psi_2(t_4)$	
Computed from measured and interpolated quantities		$\bar{r}(t_2)$		$\bar{r}(t_4)$	
From interpolation (eqs. (7) and (10))			$\bar{r}(t_3), \bar{v}(t_3)$		

Note that this is essentially the same procedure as is used for two separate position fixes, the difference being that the extended schedule uses some of the measured angles twice. Reusing the data makes no difference in the position fix computations, but, as will be seen in the next section of the report, it does affect the error analysis.

The extended schedule and associated computations for type 5 measurements are shown in table 5. In this case only 9 measurements are required compared

TABLE 5.- EXTENDED SCHEDULES FOR TYPE 5 MEASUREMENTS

Time	t_1	t_2	t_3	t_4	t_5	t_6	t_7	t_8	t_9
Angle measured	$S(t_1)$	$\gamma_1(t_2)$	$S(t_3)$	$\gamma_2(t_4)$	$S(t_5)$	$\gamma_1(t_6)$	$S(t_7)$	$\gamma_2(t_8)$	$S(t_9)$
Computed from measured angle	$r(t_1)$		$r(t_3)$		$r(t_5)$		$r(t_7)$		$r(t_9)$
From linear interpolation (eq. (9))		$r(t_2)$		$r(t_4)$		$r(t_6)$		$r(t_8)$	
From measured and interpolated quantities		$\psi_1(t_2)$		$\psi_2(t_4)$		$\psi_1(t_6)$		$\psi_2(t_8)$	
From interpolation (eq. (8))				$\psi_1(t_4)$		$\psi_2(t_6)$			
From measured and interpolated quantities				$\bar{r}(t_4)$		$\bar{r}(t_6)$			
From interpolation (eqs. (7) and (10))					$\bar{r}(t_5)$ $\bar{v}(t_5)$				

to the 14 needed for two independent position fixes, but the amount of computation is the same. As in the type 4 measurements the error analysis is substantially different from that for the regular schedule.

This approach of making only one set of observations to determine both position and velocity is discussed further in the section on error analysis and in appendix C. However, as will be shown later, the procedure appears to have limited practical value because of accuracy limitations.

ERROR ANALYSIS METHODS

The previous section presented equations for finding the position and velocity vectors from appropriate sets of measured angles. This section deals with the equations used to evaluate the errors produced in the computed position and velocity by measurement errors and by the use of linear interpolation. The errors in position due to measurement errors are discussed first and then those in velocity. These errors are evaluated to a first-order approximation by differentiating the position fix equations from the previous section with respect to the measured angles. The errors due to the use of linear interpolation are then dealt with briefly. The equations used for evaluating the measurement errors are derived in appendix C and those for the interpolation errors in appendix D.

The measurement error in each angle is assumed to consist of a bias and a random component. It is assumed that the random component is gaussian with zero mean and independent of the random components of errors in the other measured angles, but errors in γ_1 and γ_2 have the same standard deviations. The resulting errors in position and velocity are evaluated on the basis of the standard deviations of their components. The bias errors are discussed in detail in the following paragraphs.

Data presented in reference 5 indicate that even after careful calibration there may be fairly large mean errors in a series of measurements taken over a short period of time. It is customary to treat such unknown biases as random variables in order to determine the rms error for the ensemble of measurements using different instruments and operators at different times. In this study, however, it was desired to assess the relative importance of the bias errors in a given practical case where one instrument is used by the same operator over a short period of time. Therefore the bias in each measured angle is assumed to be a constant, and the resulting errors in position are determined directly.

The biases are separated into two parts, one part due to irradiance or other uncertainty in planet diameter and the other part due to instrument inaccuracy, including operator error. This separation is made because it is pointed out in reference 5 that irradiance is a major source of bias error which can be corrected for only approximately at the present time.[2] It can be

[2]Another important source of bias error is the window-induced error mentioned in reference 5. This error can be corrected for by the method described in reference 10 and will not be considered here.

seen from sketch (c) (taken from ref. 5) that when γ is measured to the near limb, it is reduced by the irradiance bias b_I. On the other hand, if γ is measured to the far limb, it is increased by b_I.

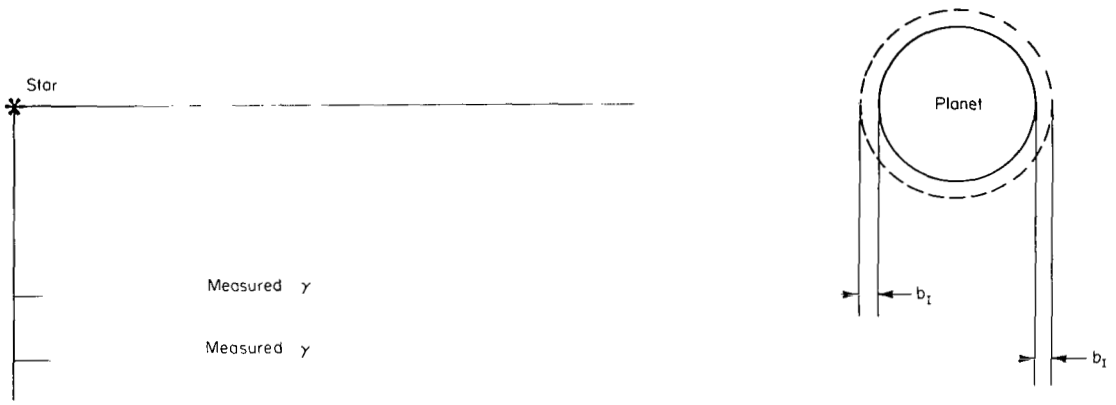

Sketch (c)

Data presented in references 5 and 7 indicate that a zero calibration error may account for a fairly large part of the instrument bias. This calibration error, which would be a constant for a given instrument line of sight, will be discussed with the error equations. For numerical evaluation of the effects of the bias errors, to be discussed in the section on results, the signs of the individual instrument biases were chosen to give the largest possible error.

The treatment of these bias errors is pessimistic, and quite simplified, but it does show how such biases affect the accuracy of the trajectory determination and indicate the need for better calibration.

The equations used for evaluating the position errors produced by measurement errors are presented next.

Measurement Errors in Position

The measurement errors are evaulated to a first-order approximation by differentiating the position fix equations with respect to the measured angles. The differentials of the angles are replaced with the various error components described earlier as follows:

$$\left.\begin{aligned} dRA &= \delta_{RA} + b_{RA} \\ dB &= \delta_B + b_B \\ dS &= \delta_S + b_S + b_I \\ d\gamma_1 &= \delta_1 + b_1 - k_1 b_I \\ d\gamma_2 &= \delta_2 + b_2 - k_2 b_I \end{aligned}\right\} \qquad (12)$$

The k_i are defined by equation (1) while δ and b subscripted by the measured angle are the random errors and instrument bias in that angle. The irradiance bias is denoted by b_I.

If the spacecraft-planet vector $\bar{r}$ given by equation (2) is differentiated, then

$$d\bar{r} = dr \begin{pmatrix} u_1 \\ u_2 \\ u_3 \end{pmatrix} + r \begin{pmatrix} du_1 \\ du_2 \\ du_3 \end{pmatrix}$$

Since $\bar{u}$ and $d\bar{u}$ are orthogonal $d\bar{r}$ can be separated into two components, dr along $\bar{r}$ and $r\, d\bar{u}$ normal to it. The magnitude of $r\, d\bar{u}$ can be written

$$r|d\bar{u}| = r\sqrt{du_1^2 + du_2^2 + du_3^2} \tag{13}$$

The position errors due to measurement biases are found by setting the random errors in equations (12) equal to zero. The radial bias error b_r is obtained by substituting the resulting differentials into the appropriate expression for dr while the normal bias error b_n is obtained from equation (13).

The random errors are evaluated on the basis of the standard deviations of the components of $d\bar{r}$. These standard deviations, denoted σ_r for the radial component and σ_n for the normal component, are given by

$$\left.\begin{aligned} \sigma_r &= \sqrt{E(dr^2) - br^2} \\ \sigma_n &= \sqrt{r^2 E(du_1^2 + du_2^2 + du_3^2) - b_n^2} \end{aligned}\right\} \tag{14}$$

Equations (13) and (14) show that

$$E|d\bar{r}| = \sqrt{(\sigma_r^2 + \sigma_n^2) + (b_r^2 + b_n^2)}$$

and the magnitude of $d\bar{r}$, which is the vector error in $\bar{r}$, is the same as that of a variable having a constant bias of magnitude $\sqrt{b_r^2 + b_n^2}$ and a random component with standard deviation $\sqrt{\sigma_r^2 + \sigma_n^2}$. The following paragraphs give the equations, derived in appendix C, for b_r, b_n, σ_r, and σ_n for the different types of measurements. The standard deviation of each of the random errors $\delta_{(.)}$ in equations (12) is denoted by $\sigma_{(.)}$ where the subscripts are the same except that it is assumed that $\sigma_1 = \sigma_2 = \sigma_\gamma$.

Type 1 measurements- The biases are

$$\left.\begin{aligned} b_r &= -(b_I + b_S) r\sqrt{r^2 - 1} \\ b_n &= r\sqrt{b_D^2 + b_{RA}^2 \cos^2 D} \end{aligned}\right\} \tag{15}$$

and

$$\left.\begin{aligned} \sigma_r &= \sigma_S r\sqrt{r^2 - 1} \\ \sigma_n &= r\sqrt{\sigma_D^2 + \sigma_{RA}^2 \cos^2 D} \end{aligned}\right\} \tag{16}$$

Type 2 measurements- The bias errors are

$$\left.\begin{aligned} b_r &= -(b_I + b_S) r\sqrt{r^2 - 1} \\ b_n &= \frac{r}{\sin B}\left[(b_1 + k_1 b_S)^2 + (b_2 + k_2 b_S)^2 - 2(b_1 + k_1 b_S)(b_2 + k_2 b_S)\cos B\right]^{1/2} \end{aligned}\right\} \tag{17}$$

It was stated earlier that the signs of the biases were chosen to give the largest possible error; therefore if it is also assumed that $|b_1| = |b_2| = |b_S| = b$, then

$$\left.\begin{aligned} |b_r| &\leq (b_I + b) r\sqrt{r^2 - 1} \\ |b_n| &\leq \frac{rb}{\sin B}\sqrt{8(1 + |\cos B|)} \end{aligned}\right\} \tag{18}$$

The standard deviations of the random errors are given by

$$\left.\begin{aligned} \sigma_r &= \sigma_S r\sqrt{r^2 - 1} \\ \sigma_n &= \frac{r}{\sin B}\sqrt{2\sigma_\gamma^2 + 2\sigma_S^2(1 + k_1 k_2 \cos B)} \end{aligned}\right\} \tag{19}$$

For this type of measurement there are singularities in both b_n and σ_n when $B = 0$ or $180°$. Thus, poor accuracy would be expected near these values of B.

Type 3 measurements- In this case the errors are the result of errors in γ_1, γ_2, and B, and

$$b_r = \frac{r\sqrt{r^2 - 1}}{2} [k_1 b_1 (1 + \rho_1) + k_2 b_2 (1 - \rho_1) + 2b_B \rho_2 - 2b_I]$$

$$b_n = \frac{r}{\sin B} \left\{ \frac{(k_1 b_1 - k_2 b_2)^2}{2} [(1 + \rho_1^2) + k_1 k_2 (1 - \rho_1^2) \cos B] \right.$$

$$\left. + 2b_B (k_1 b_1 - k_2 b_2) \rho_1 \rho_2 (1 - k_1 k_2 \cos B) + 2b_B^2 \rho_2^2 (1 - k_1 k_2 \cos B) \right\}^{1/2}$$

If $|b_1| = |b_2| = b$ and the signs of the biases are chosen to give the largest possible error, then

$$\left.
\begin{aligned}
|b_r| &\leq r\sqrt{r^2 - 1} \, [b_I + b(1 + |\rho_1|) + |b_B \rho_2|] \\
|b_n| &\leq \frac{r}{\sin B} \{ b^2 [(1 + \rho_1^2) + k_1 k_2 (1 - \rho_1^2) \cos B] \\
&\quad + 4b |b_B| \, |\rho_1 \rho_2 (1 - k_1 k_2 \cos B)| + 2b_B^2 \rho_2^2 (1 - k_1 k_2 \cos B) \}^{1/2}
\end{aligned}
\right\} \quad (20)$$

The standard deviations of the random errors are

$$\left.
\begin{aligned}
\sigma_r &= r\sqrt{r^2 - 1} \sqrt{\frac{\sigma_\gamma^2}{2} (1 + \rho_1^2) + \sigma_B^2 \rho_2^2} \\
\sigma_n &= \frac{r}{\sin B} \{ \sigma_\gamma^2 [(1 + \rho_1^2) + k_1 k_2 (1 - \rho_1^2) \cos B] + 2\sigma_B^2 \rho_2^2 (1 - k_1 k_2 \cos B) \}^{1/2}
\end{aligned}
\right\} \quad (21)$$

In equations (20) and (21) ρ_1 and ρ_2 are defined by

$$\rho_1 = \frac{\sin(k_1 \psi_1 - k_2 \psi_2)(1 + k_1 k_2 \cos B)}{\sin(k_1 \psi_1 + k_2 \psi_2)(1 - k_1 k_2 \cos B)}$$

and

$$\rho_2 = \frac{\sin \psi_1 \sin \psi_2 \sin B}{\sin(k_1 \psi_1 + k_2 \psi_2)(1 - k_1 k_2 \cos B)}$$

If $k_1 = k_2$, it can be shown that

$$\frac{1 + \rho_1^2 + k_1 k_2 (1 - \rho_1^2) \cos B}{\sin^2 B} = \frac{1}{1 - \cos B} + \frac{\sin^2(\psi_1 - \psi_2)}{\sin^2(\psi_1 + \psi_2)} \cdot \frac{1}{(1 - \cos B)^2}$$

and

$$\frac{\rho_2^2(1 - k_1k_2 \cos B)}{\sin^2 B} = \frac{\sin^2 \psi_1 \sin^2 \psi_2}{\sin^2(\psi_1 + \psi_2)(1 - \cos B)}$$

In that case σ_n for type 3 has singularities for $B = 0$ and $\psi_1 + \psi_2 = 180°$, but none for $B = 180°$. Similarly, if $k_1 = -k_2$ there are singularities for $B = 180°$ and $\psi_1 = \psi_2$ but none for $B = 0$.

Type 4 measurements- The equations for b_r and b_n for type 4 are identical with those for type 2 and are given by equations (18). Also, since r is determined from a single measurement, σ_r is the same as for type 2, and

$$\left.\begin{aligned} \sigma_r &= \sigma_s r\sqrt{r^2 - 1} \\ \sigma_n &= \frac{r}{\sin B}\left\{\frac{3}{2}\sigma_\gamma^2 + \frac{\sigma_s^2}{2}\left[3(r^2 - 1)\operatorname{ctn}^2 \psi_1 + 2\sqrt{r^2 - 1}\operatorname{ctn} \psi_1 (2k_2 \cos B_1 + k_1)\right]\right\}^{1/2} \end{aligned}\right\} \tag{22}$$

The equation for σ_n was derived under the assumption that ψ_1 is the angle interpolated. If ψ_2 is interpolated instead, it replaces ψ_1 in the equation and k_1 and k_2 are interchanged.

In addition to the singularities for $B = 0$ or $180°$ noted for type 2, Gibb's method produces a singularity when the interpolated angle ψ_1 or ψ_2 is zero. This singularity is in the measurement error and should not be confused with the interpolation errors discussed later in the report.

Type 5 measurements- The bias errors for this type of measurement are also given by equations (17), but is was pointed out earlier that a large part of the bias errors appear to be due to zero calibration errors. If the biases in γ and S are attributed entirely to this source, then equations (17) for type 2 biases remain the same. However, since all angles for type 5 are measured with the same instrument $b_1 = b_2 = b_S = b$ and

$$\left.\begin{aligned} |b_r| &\leq (b_I + b)r\sqrt{r^2 - 1} \\ |b_n| &\leq \frac{rb}{\sin B}\left[4 + 2k_1 + 2k_2 - 2(1 + k_1 + k_2 + k_1k_2)\cos B\right]^{1/2} \end{aligned}\right\} \tag{23}$$

These equations were used for type 5 in order to assess the effects of the zero calibration errors. Note that if $k_1 = k_2 = 1$, there is no singularity for $B = 0$, and if $k_1 = k_2 = -1$, then $b_n = 0$.

The standard deviations of the random errors are

$$\left.\begin{aligned}
\sigma_r &= \sigma_s r \sqrt{\frac{r^2 - 1}{2}} \\
\sigma_n &= \frac{r}{\sin B}\left\{3\frac{\sigma_\gamma^2}{2} + \frac{\sigma_s^2}{4}\left[(r^2 - 1)\operatorname{ctn}^2 \psi_1\right.\right. \\
&\qquad \left.\left. +2k_2(\sqrt{r^2 - 1}\ \operatorname{ctn} \psi_1 + k_1)\cos B + 3\right]\right\}^{1/2}
\end{aligned}\right\} \qquad (24)$$

Type 5 has singularities at the same points as type 4, that is, at $B = 0$, $B = 180°$, and $\psi_1 = 0$. Since types 4 and 5 both have terms containing $\operatorname{ctn} \psi_i$ where ψ_i is the angle interpolated, it will be assumed that interpolation will always be carried out with the larger of the two angles.

Note, also, that σ_r for type 5 is reduced by $\sqrt{2}$ compared to that for types 2 and 4 because two measurements of S are used in determining the range.

The two alternate schedules for type 5 (discussed in the section on position fix equations) which use only linear interpolation have nearly the same position errors due to measurement inaccuracies as type 2. These schedules can be evaluated on the basis of data from type 2.

Extended schedules- It was pointed out in the section on the computation of velocity that the velocity could be determined by adding one measurement time to the type 4 schedule or two to the type 5 schedule. The resulting bias errors are unchanged, but the standard deviations of the position errors become, for type 4,

$$\left.\begin{aligned}
\sigma_r &= \sigma_s r \sqrt{\frac{r^2 - 1}{2}} \\
\sigma_n &= \frac{r}{2 \sin B}\left\{5\sigma_\gamma^2 + \frac{\sigma_s^2}{2}\left[(r^2 - 1)(3 \operatorname{ctn}^2 \psi_1 + 3 \operatorname{ctn}^2 \psi_2\right.\right. \\
&\qquad +4 \operatorname{ctn} \psi_1 \operatorname{ctn} \psi_2 \cos B) + \sqrt{r^2 - 1}\ (4k_1 + 6k_2 \cos B)\operatorname{ctn} \psi_1 \\
&\qquad \left.\left. + \sqrt{r^2 - 1}\ (4k_2 + 6k_1 \cos B)\operatorname{ctn} \psi_2 + 10\right]\right\}^{1/2}
\end{aligned}\right\} \qquad (25)$$

and for type 5

$$\sigma_r = \sigma_s r \sqrt{\frac{3(r^2 - 1)}{8}}$$

$$\sigma_n = \frac{r}{2 \sin B} \left\{ 5\sigma_\gamma^2 + \frac{\sigma_s^2}{8} \left[(r^2 - 1)(2 \operatorname{ctn}^2 \psi_1 + 2 \operatorname{ctn}^2 \psi_2 \right.\right. \tag{26}$$

$$\left. + \cos \psi_1 \operatorname{ctn} \psi_2 \cos B \right] + 5\sqrt{r^2 - 1}\,(k_1 \operatorname{ctn} \psi_2 + k_2 \operatorname{ctn} \psi_1) \cos B$$

$$\left. - 15 k_1 k_2 \cos B + 20 \right\}^{1/2}$$

Note that for both measurement types, σ_r is reduced because more measurements of S are used in determining r. On the other hand, singularities are present for both $\psi_1 = 0$ and $\psi_2 = 0$.

Velocity Errors

It is shown in appendix C that, for most conditions, the third-order terms in equation (10) may be neglected in computing the measurement errors in $\bar{v}(t_2)$. That is, we can assume

$$d\bar{v}(t_2) = \frac{d\bar{r}(t_3) - d\bar{r}(t_1)}{t_3 - t_1} \tag{27}$$

Since the biases are considered to be constant over the observation period, the portions of $d\bar{r}(t_1)$ and $d\bar{r}(t_3)$ due to bias errors are equal. Therefore, to a first approximation $d\bar{v}(t_2)$ is due only to random errors, and the standard deviation, σ_v of $|d\bar{v}(t_2)|$ is

$$\sigma_v = \frac{\sqrt{2(\sigma_r^2 + \sigma_n^2)}}{t_3 - t_1} = \frac{\sqrt{\sigma_r^2 + \sigma_n^2}}{\sqrt{2}\,\Delta t} \tag{28}$$

Thus, to a first approximation the standard deviation of random error in the velocity is inversely proportional to the time between the two position fixes. The standard deviation of error in $\bar{r}(t_2)$ (see appendix C) is

$$\sigma_p(t_2) = \frac{\sqrt{(\sigma_r^2 + \sigma_n^2)(t_1^2 + t_3^2)}}{t_3 - t_1} \tag{29}$$

This error is minimized if $-t_1 = t_3 = \Delta t$, in which case

$$\sigma_p(t_2) = \sqrt{\frac{\sigma_r^2 + \sigma_n^2}{2}}$$

and

$$\sigma_v(t_2) = \frac{\sigma_p(t_2)}{\Delta t} \tag{30}$$

If Gibb's method is used to obtain $\bar{v}(t_3)$ instead of $\bar{v}(t_2)$, then $\bar{r}(t_3)$ is assumed to be the correct position, and σ_p increases to $\sqrt{\sigma_r^2 + \sigma_n^2}$ since the information obtained at t_1 is not used. However, σ_v is the same as when $\bar{v}$ is computed at t_2. Equation (30) is roughly the same (usually within a factor of two) for the extended schedule versions of types 4 and 5.

Linear Interpolation Errors

It was pointed out in the description of type 4 and type 5 measurements that it is necessary to use some linear interpolation with type 5. If one component of position (in other words r and either ψ_1 or ψ_2) is known at two times a more accurate interpolation, such as Gibb's method, may be used. Since linear interpolation is simpler than Gibb's method, and in some cases is necessary, we would like to know when the resulting errors are small enough compared to the measurement errors to be acceptable.[3]

The bias and random errors are a function only of the geometry, but errors due to linear interpolation of r or γ depend on the orbit as well. For this reason only upper bounds of these errors were considered. The interpolation error for r was evaluated by taking the maximum magnitude of the second-order term in a Taylor series expansion of r. This error increases as r decreases, and the minimum value r_{min} of r was found for which the interpolation error is less than some fraction, M, of $\sigma_s r\sqrt{r^2 - 1}$ (i.e., of σ_r for type 4). In order to ensure that the second-order term is a valid measure of the interpolation error, an expression was also found for the minimum value of r such that the third-order term is negligible compared to the second-order term.

A conceptually similar, but less direct, approach was used for the errors due to linear interpolation of γ. The minimum value of r was found for which the interpolation error is less than M times $\sqrt{\sigma_r^2 + \sigma_n^2}$ for type 5. The error due to interpolation of γ is in the normal direction, but the radial component is often the dominant part of the measurement error and therefore should be included in determining the relative importance of the interpolation error. The value of r_{min} in this case is a function of B as well as r.

The values of r_{min} for which the interpolation error is less than M times the appropriate standard deviation are presented in the section on results. Appendix D contains the derivations of the equations used and the

[3]There is also an interpolation error due to the use of Gibb's method which is much smaller than that due to linear interpolation. This error, which cannot be analyzed by linear perturbation methods is discussed briefly in the section on results.

values of r_{min} for neglecting the various higher order terms. The latter results indicate that in most practical cases the second-order terms are a valid measure of the interpolation error.

RESULTS AND DISCUSSION

The standard deviation of position error, $\sqrt{\sigma_r^2 + \sigma_n^2}$, and the total bias error, $\sqrt{b_r^2 + b_n^2}$ were computed for all five types of measurements with various values of RA, D, and ϕ at several different ranges from the planet. At each value of r sufficient cases were computed to cover the range of angles considered ($-90° \leq RA \leq 90°$, $0 \leq D \leq 90°$ and $0 \leq \phi \leq 90°$).

It was found that, except for type 1, the errors depend strongly on the location of the projection of $\bar{r}$ onto the X-Y plane relative to the unit vectors to the two stars. Three different star-planet configurations, two of them extreme possibilities for location of the projection and the third an intermediate value, are illustrated in figure 2. In the first configuration

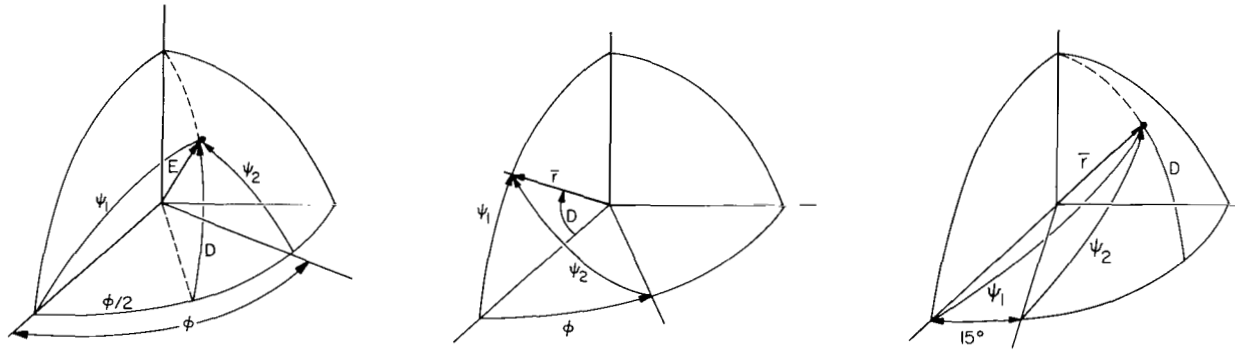

(a) First configuration, $A = \phi/2$. (b) Second configuration, $A = 0$. (c) Third configuration, $A > \phi$.

Figure 2.- Star-planet configurations.

(fig. 2(a)) the projection of $\bar{r}$ on the X-Y plane lies midway between the two stars. In figure 2(b) the projection of $\bar{r}$ is in the direction of one of the stars. In this case, star number 1 and RA = 0, but it could be in the direction star number 2 instead. In figure 2(c) the projection of $\bar{r}$ lies well outside the smaller angle between the two stars.

The values of $\sqrt{\sigma_r^2 + \sigma_n^2}$ and $\sqrt{b_r^2 + b_n^2}$ obtained for these three geometric configurations are discussed separately in the next two sections after which the errors caused by linear interpolation are compared with those due to measurement errors.

Random Errors

The standard deviations for the random position errors were computed assuming the same standard deviations of error in each angle measured, that is,

$\sigma_{RA} = \sigma_D = \sigma_\gamma = \sigma_S = \sigma_B = \sigma$, except for a special set of data for type 3 measurements. Tests made on the trisextant at Ames Research Center indicated that it may not be possible to measure B as accurately as the other angles. Therefore, an additional set of data was obtained for type 3 measurements with $\sigma_B = 10\sigma$.

The value of $\sqrt{\sigma_r^2 + \sigma_n^2}$ for type 1 measurements is presented in figure 3. The standard deviation in units of (planet radii)/(arc sec) is plotted as a function of the declination D for four ranges. The corresponding values of σ_r (dashed lines) are also presented. Note that as r increases the importance of σ_r in the total standard deviation becomes greater, and for $r \geqslant \sqrt{10}$ it accounts for nearly all of $\sqrt{\sigma_r^2 + \sigma_n^2}$. Since σ_r is independent of D, there is negligible variation of the total standard deviation with D at the larger ranges. It can be seen from equations (16) that these results are to be expected and that for large values of r the type 1 error may be regarded as consisting only of the radial component.

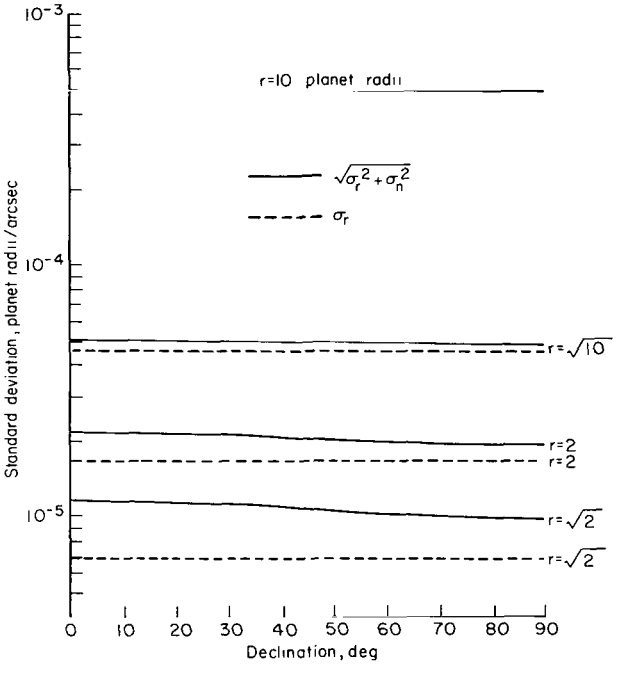

Figure 3.- Standard deviations of random error for type 1 measurements.

The errors from measurements of type 2, 3, 4, or 5 are functions not only of the range but also of the relative location of the stars and planet and whether the star-limb angles are measured to the limb near the star or the far limb. The ratios of the standard deviations for these types of measurements to those for type 1 were computed in order to facilitate comparison between the various methods. The effects of the relative locations of stars and planet were evaluated by using the three different configurations (fig. 2) discussed earlier. Two different values of r, $\sqrt{10}$, and 10, were found to be sufficient to show the effect of changing range. The results of measuring γ_1

and γ_2 to the near and far limbs were accounted for by computing the 22 cases described in table 6.

TABLE 6.- CASES FOR WHICH ERROR RATIOS WERE COMPUTED

Case	Measurement type	Description
2a	2	γ_1 and γ_2 to same limb
2b		γ_1 and γ_2 to opposite limbs
3a	3	γ_1 and γ_2 to same limb, $\sigma_B = 0$
3b		γ_1 and γ_2 to same limb, $\sigma_B = 10\ \sigma$
3c		γ_1 and γ_2 to opposite limbs, $\sigma_B = \sigma$
3d		γ_1 and γ_2 to opposite limbs, $\sigma_B = 10\ \sigma$
4a	4	γ_1 and γ_2 to near limb
4b		γ_1 and γ_2 to far limb
4c		γ_1 to near limb, γ_2 to far limb
4d		γ_1 to far limb, γ_2 to near limb
4e-4h	4	Same as 4a-4d with extended schedule
5a-5h	5	Same as 4a-4h

The resulting ratios of $\sqrt{\sigma_r^2 + \sigma_n^2}$ for types 2, 3, 4, and 5 to those for type 1 were computed for each of the geometric configurations and each of the two values of r. These results are presented graphically in figures 4 through 12. The curves for type 2 are presented with each of the other types separately for ease of comparison. Only the maximum and minimum values from cases 4(a) through (d) are shown and are labeled as type 4, while the maximum and minimum values for the extended schedule are labeled 4X. An equivalent set of data is presented for type 5 measurements, and the curves are labeled 5 and 5X.

The data for the configuration with $RA = \phi/2$ (fig. 2(a)) are presented in figures 4, 5, and 6. Three values of ϕ are used with $r = \sqrt{10}$, and one is also used with $r = 10$ (figs. 4(c), 5(c), and 6(c)) in order to show the effects of range.

Figure 4 shows the ratio for types 2 and 3. For this configuration $B = 180°$ when $D = 0$ and decreases as D increases so that $\sqrt{\sigma_r^2 + \sigma_n^2}$ for type 2 is infinite when $D = 0$, reaches a minimum at the value of D for which $B = 90°$ and then increases again. This effect is most noticeable for the smallest value of ϕ since the minimum value of B increases with ϕ. On the other hand, the curves for types 3a and 3b are at a minimum for $D = 0$ and increase rapidly for larger values of D. When $RA = \phi/2$, we can see that $\psi_1 = \psi_2$, causing (as was pointed out in the section on Error Analysis Methods) the errors for types 3c and 3d to be infinite, and those curves have been omitted. For $\phi = 30°$ and $D \geqslant 5°$, type 2 errors are less than twice those for type 1, and the ratio is smaller for larger values of ϕ. Also, comparison of figures 4(b) and 4(c) shows that as r increases, the ratios for both types decrease and the spread between the curves of the same type becomes smaller. From the equations for the standard deviations we would expect the

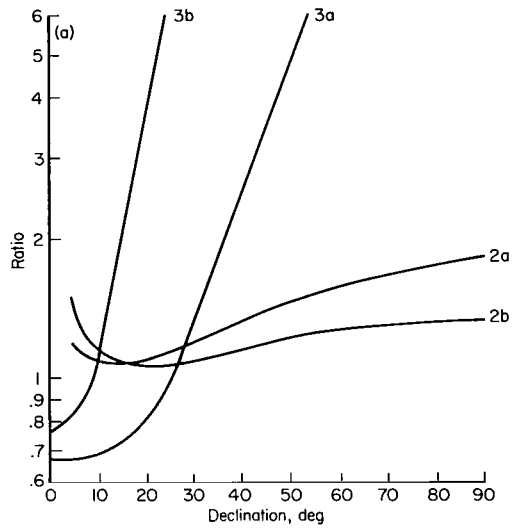

(a) $\phi = 30°$, RA = 15°, $r = \sqrt{10}$

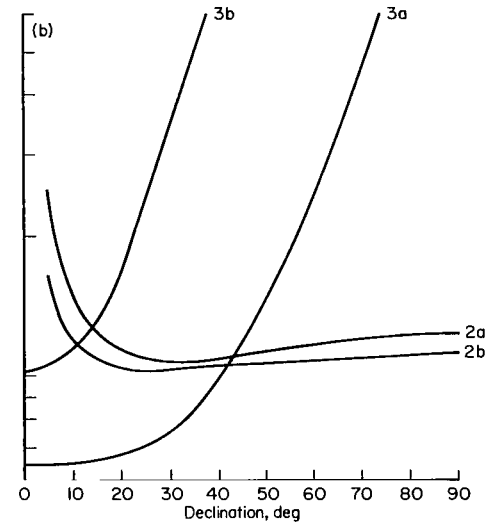

(b) $\phi = 60°$, RA = 30°, $r = \sqrt{10}$

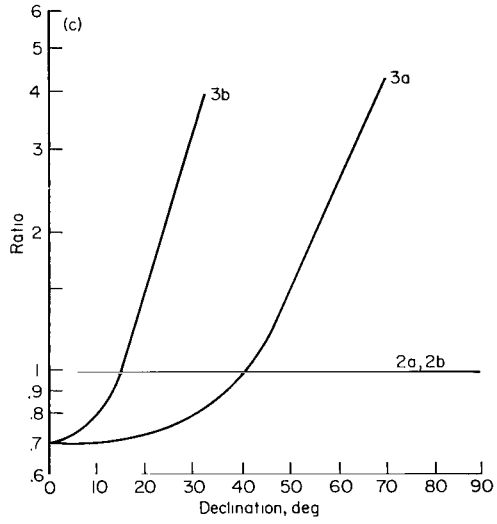

(c) $\phi = 60°$, RA = 30°, r = 10

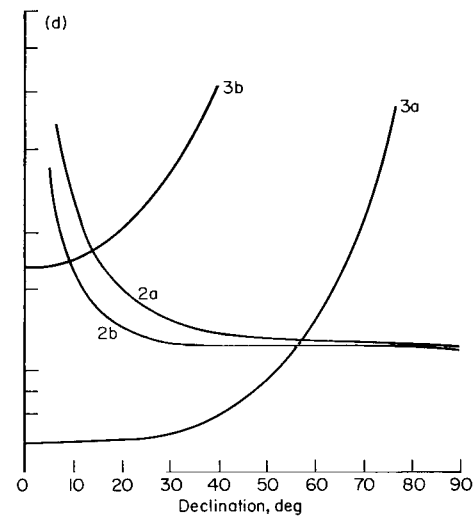

(d) $\phi = 90°$, RA = 45°, $r = \sqrt{10}$

Figure 4.- Ratio of $\sqrt{\sigma_r^2 + \sigma_n^2}$ for types 2 and 3 with RA = $\phi/2$ to $\sqrt{\sigma_r^2 + \sigma_n^2}$ for type 1.

sensitivity to changes in r to be greater for small values of r. Therefore, for $\phi \geq 30°$, $r \geq \sqrt{10}$ and any given value of D. One or both of these measurement types (type 2 and type 3) will provide a standard deviation less than twice that for type 1.

The ratio for type 4 (fig. 5) follows the same trends for changes in r or ϕ as the corresponding data for type 2. However, type 4 is generally poorer than type 2, particularly for small values of D. The use of the extended schedule improves the results somewhat and produces lower ratios (to type 1 values) than type 2 for the larger values of D. This improvement is due mainly to the increase in the number of measurements used.

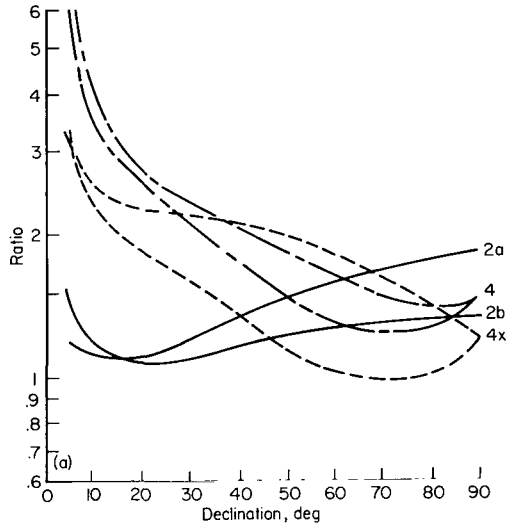

(a) $\phi = 30°$, RA = 15°, r = $\sqrt{10}$

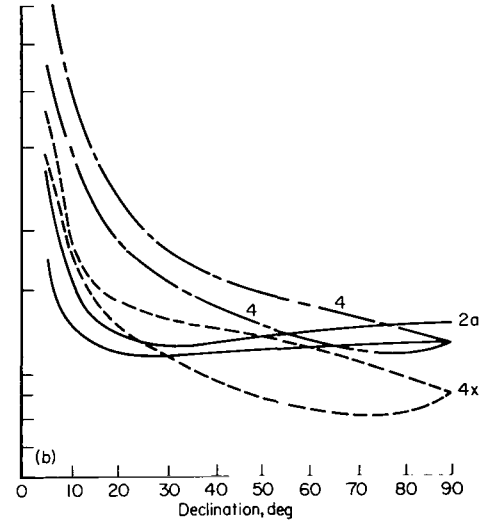

(b) $\phi = 60°$, RA = 30°, r = $\sqrt{10}$

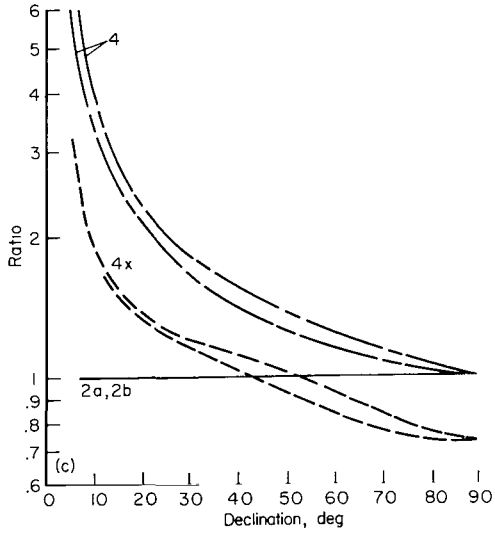

(c) $\phi = 60°$, RA = 30°, r = 10

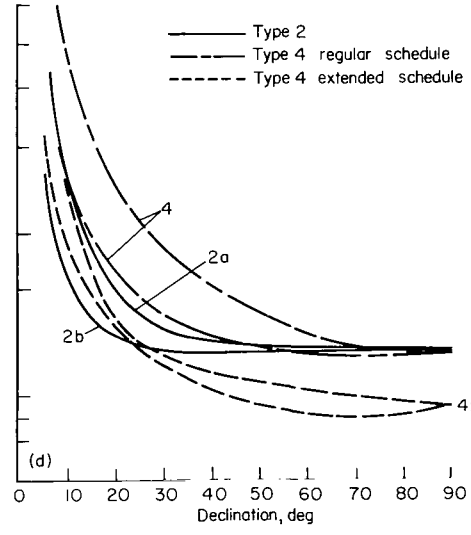

(d) $\phi = 90°$, RA = 45°, r = $\sqrt{10}$

Figure 5.- Ratio of $\sqrt{\sigma_r^2 + \sigma_n^2}$ for type 2 and type 4 with RA = $\phi/2$ to $\sqrt{\sigma_r^2 + \sigma_n^2}$ for type 1.

The results for type 5 are given in figure 6, and the trends with changes in r and ϕ are the same as those for types 2 and 4. Type 5 has substantially smaller errors than type 4 and less spread between maximum and minimum. The singularities at D = 0 have a greater effect on type 5 than on type 2, but for D > 25° the type 5 errors are smaller than those for type 2. This improvement in performance is probably due to the increased number of observations for type 5, and for the same reason the use of the extended schedule provides a small improvement over the regular schedule for type 5.

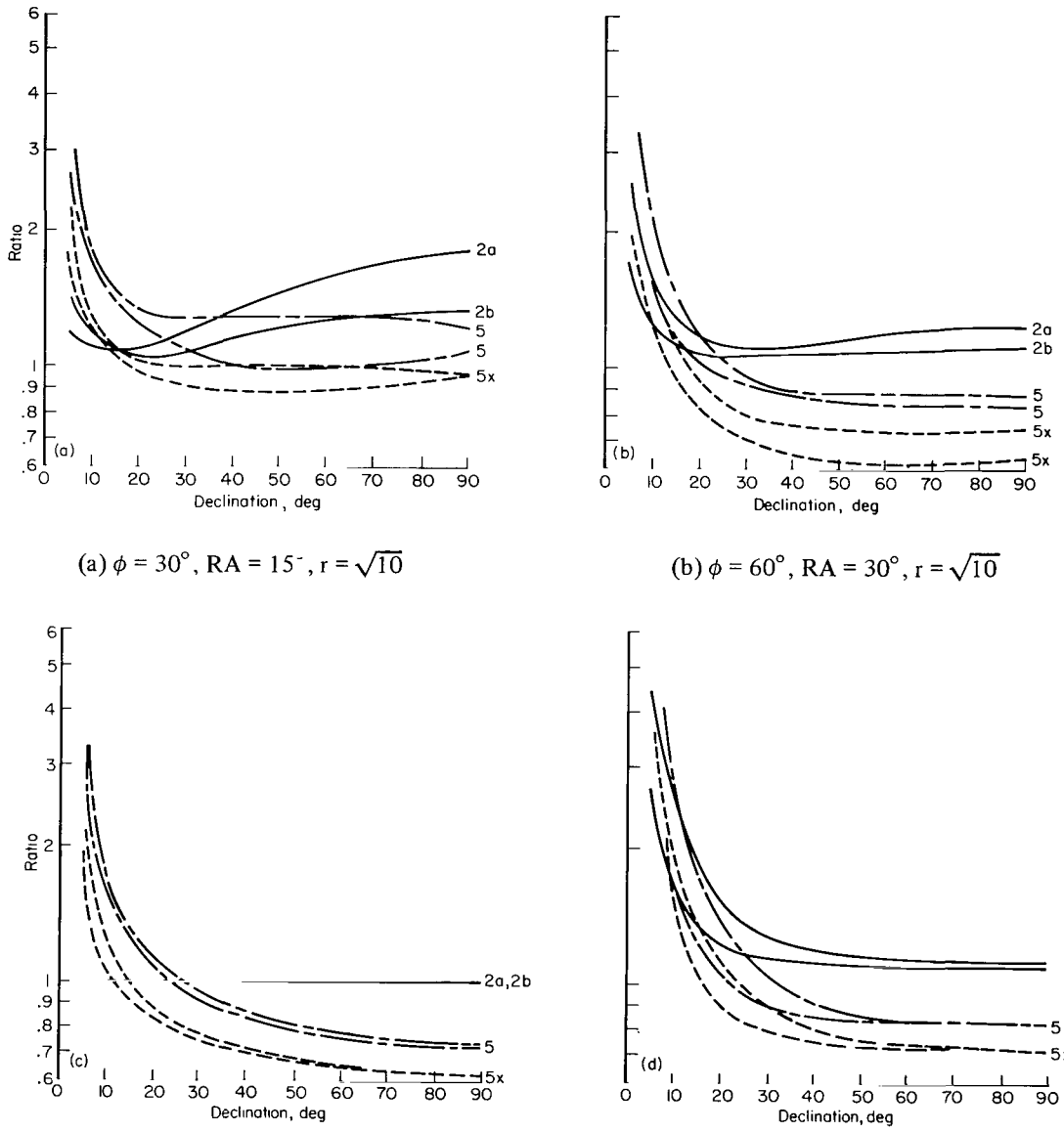

(a) $\phi = 30°$, RA = 15°, $r = \sqrt{10}$

(b) $\phi = 60°$, RA = 30°, $r = \sqrt{10}$

(c) $\phi = 60°$, RA = 30°, r = 10

(d) $\phi = 90°$, RA = 45°, $r = \sqrt{10}$

Figure 6.- Ratio of $\sqrt{\sigma_r^2 + \sigma_n^2}$ for type 2 and type 5 with RA = $\phi/2$ to $\sqrt{\sigma_r^2 + \sigma_n^2}$ for type 1.

The corresponding data for the configuration (fig. 2(b)) where the projection of $\bar{r}$ on the X-Y plane is alined with one of the stars are presented in figures 7, 8, and 9. The errors for this configuration show the same trends with r and ϕ as shown in figures 4, 5, and 6; namely as r or ϕ increases, the ratios of the standard deviations to those for type 1 become smaller, and the spread between the maximum and minimum curves is reduced. The effect on types 2 and 3 of changing the geometric configuration can be seen by comparing figure 4(a) with figure 7(b) and figure 4(b) with figure 7(d). These pairs of figures have the same values of ϕ and r and the curves for type 2 are nearly same except for small values of D. The type 2

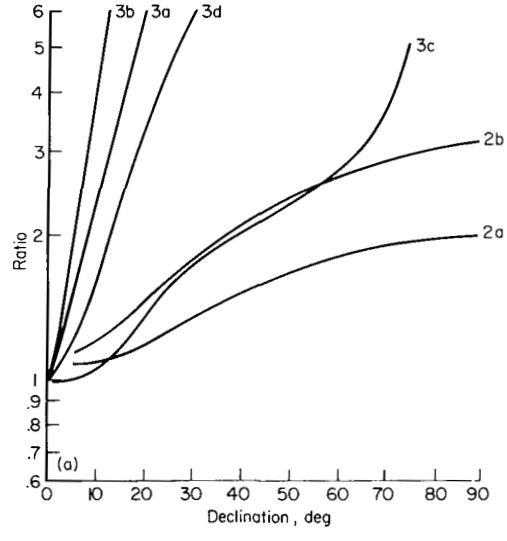

(a) $\phi = 15°$, RA = 0, r = $\sqrt{10}$

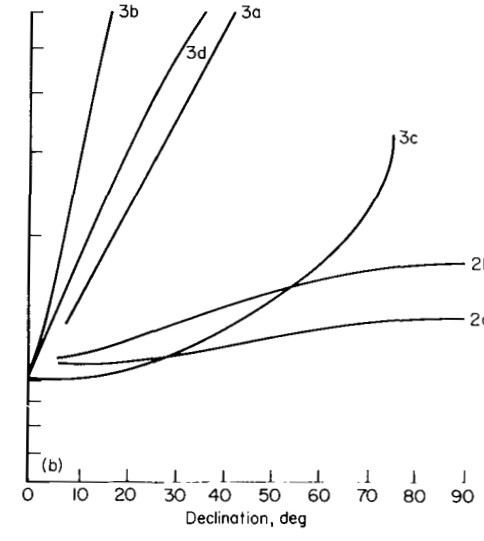

(b) $\phi = 30°$, RA = 0, r = $\sqrt{10}$

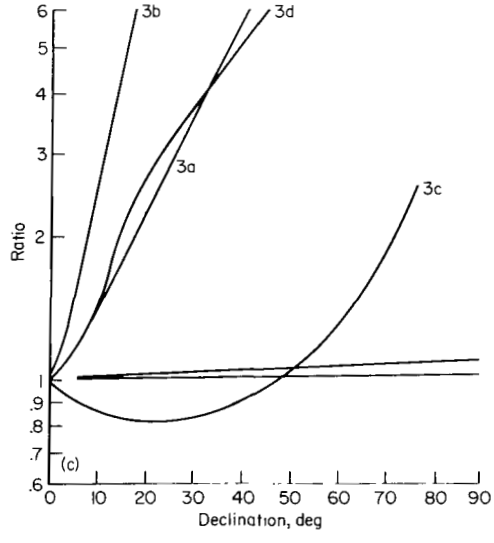

(c) $\phi = 30°$, RA = 0, r = 10

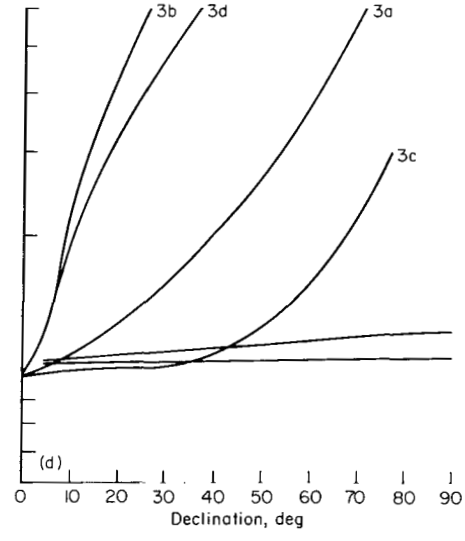

(d) $\phi = 60°$, RA = 0, r = $\sqrt{10}$

Figure 7.- Ratio of $\sqrt{\sigma_r^2 + \sigma_n^2}$ for type 2 and type 3 with RA = 0 to $\sqrt{\sigma_r^2 + \sigma_n^2}$ for type 1.

errors for RA = $\phi/2$ increase quite rapidly for $D < 20°$ while there is little noticeable increase for RA = 0. On the other hand, the errors for type 3 are much larger for RA = 0 than for RA = $\phi/2$, but the combination[4] of types 2 and 3 will still provide a standard deviation less than twice that of type 1 for all values of D if $\phi \geq 30°$ and $r \geq \sqrt{10}$.

When the regular schedule is used, the errors for type 4, shown in figure 8, are not affected as strongly by the singularities near D = 0 as

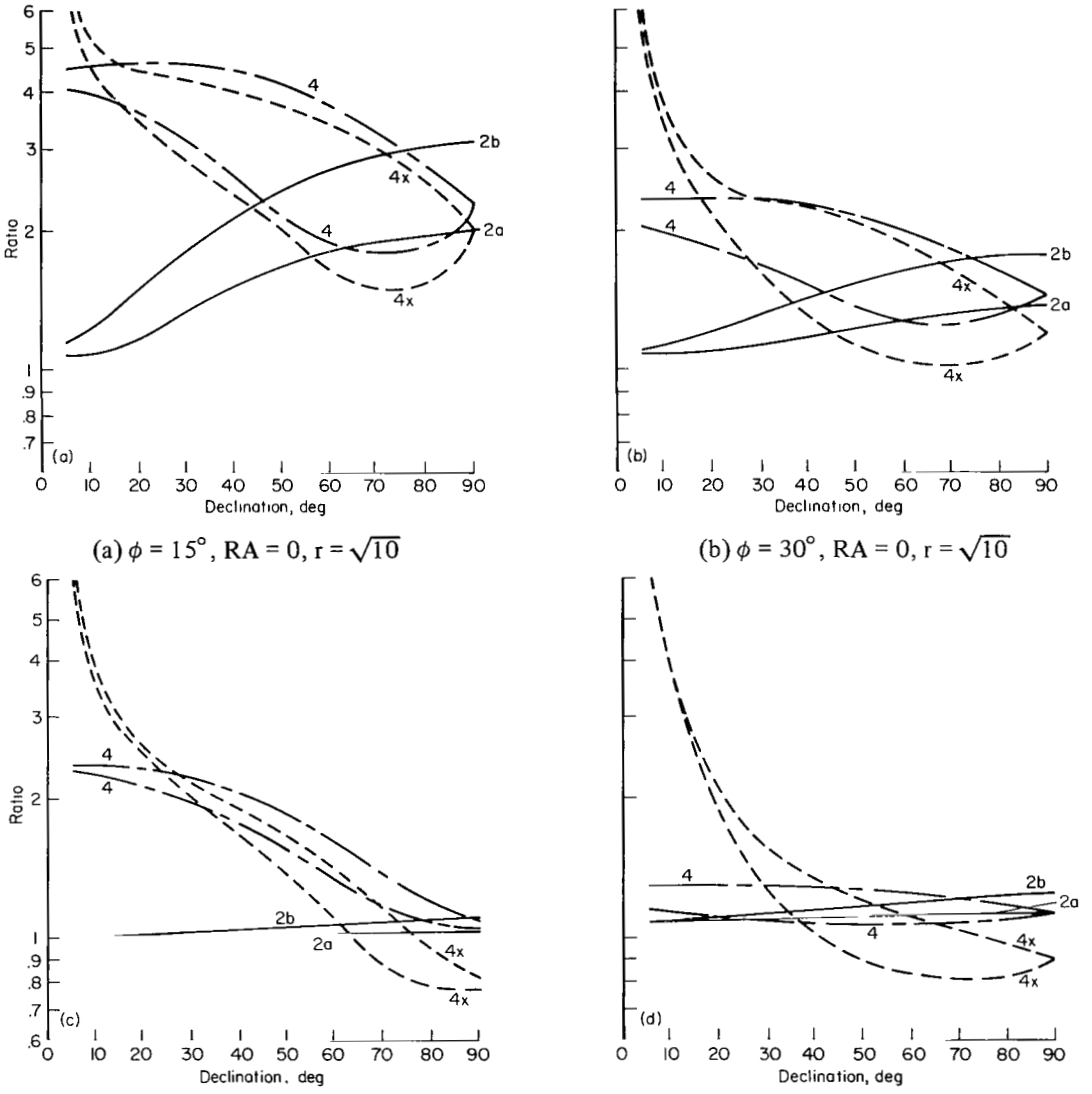

(a) $\phi = 15°$, RA = 0, $r = \sqrt{10}$

(b) $\phi = 30°$, RA = 0, $r = \sqrt{10}$

(c) $\phi = 30°$, RA = 0, r = 10

(d) $\phi = 60°$, RA = 0, $r = \sqrt{10}$

Figure 8.- Ratio of $\sqrt{\sigma_r^2 + \sigma_n^2}$ for type 2 and type 4 with RA = 0 to $\sqrt{\sigma_r^2 + \sigma_n^2}$ for type 1.

[4]Note that if RA is exactly zero then $\lim_{D \to 0} B = 90°$, and σ_r for type 2 (eq. (19)) is bounded. However, for RA slightly different from zero, σ_r will approach infinity and it would be necessary to use type 3 for very small values of D.

with the configuration where RA = $\phi/2$. On the other hand, the singularities have greater effect on the results for the extended schedule when RA = 0. This result is to be expected since ψ_1, which goes to zero with D is not interpolated with the regular schedule, but it must be used with the extended schedule thereby introducing ctn ψ_1, into the equation for σ_n.

Figure 9 shows the same data for type 5 measurements, and the same changes with r and ϕ are noted as when RA = $\phi/2$. The change in geometric configuration from RA = $\phi/2$ to RA = 0 has the same general effect on the type 5 results as on those for type 4, and for both configurations the ratios for type 5 are considerably lower than those for type 4.

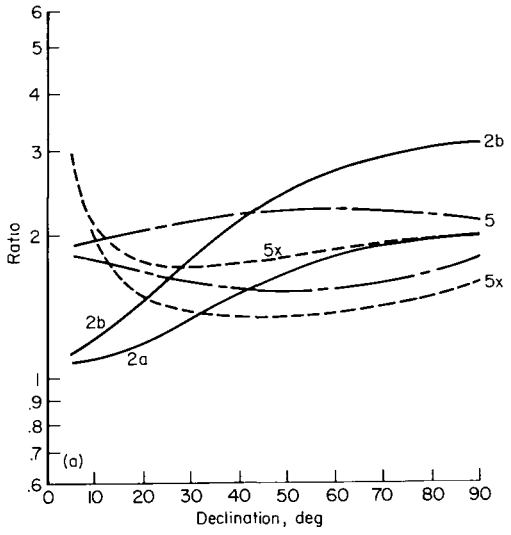

(a) $\phi = 15°$, RA = 0, r = $\sqrt{10}$

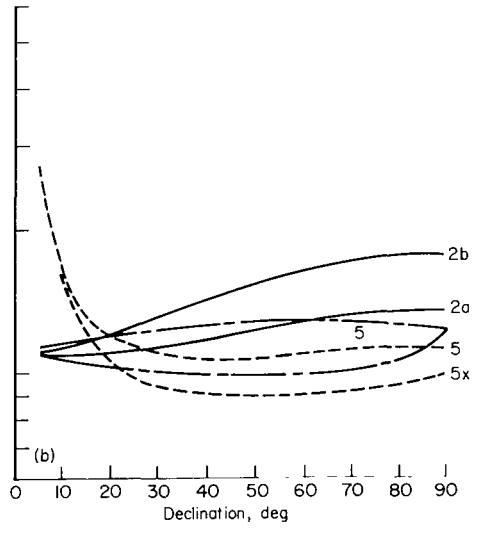

(b) $\phi = 30°$, RA = 0, r = $\sqrt{10}$

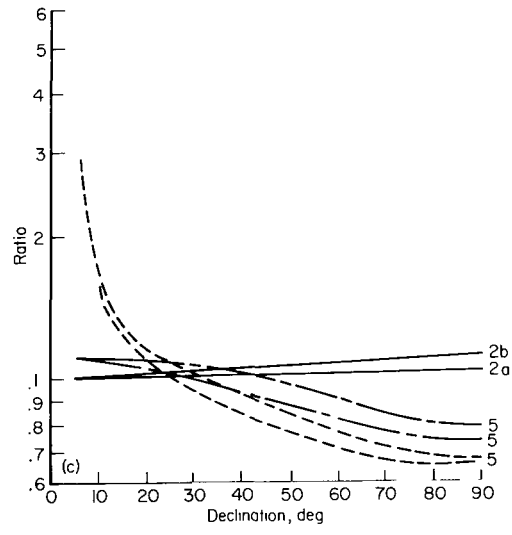

(c) $\phi = 30°$, RA = 0, r = 10

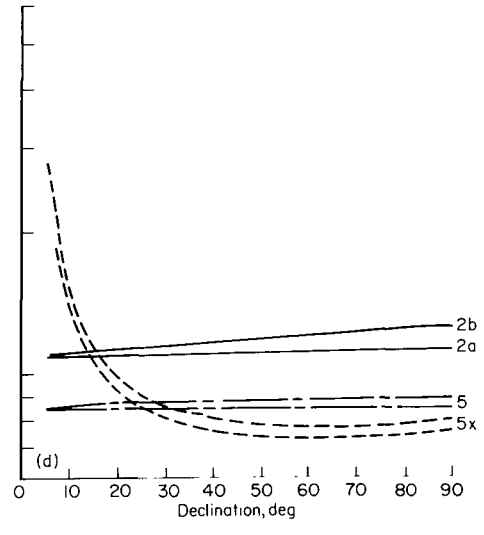

(d) $\phi = 60°$, RA = 0, r = $\sqrt{10}$

Figure 9.- Ratio of $\sqrt{\sigma_r^2 + \sigma_n^2}$ for type 2 and type 5 with RA = 0 to $\sqrt{\sigma_r^2 + \sigma_n^2}$ for type 1.

The data for the configuration (fig. 2(c)) where the projection of $\bar{r}$ onto the X-Y plane lies well outside the smaller angle between the two stars are presented in figures 10, 11, and 12. The ratios for types 2 and 3, which are shown in figure 10, are much larger than those for the other two configurations. Comparison of figures 10(a), 10(b), and 10(d) with figure 7(a), which has the same values of ϕ and r, shows that the ratios for type 2 are the same at large values of D, but the ratios in figure 7(a) are becoming relatively much smaller as D decreases. The ratios for type 3 start at larger values for D = 0 but do not increase as rapidly as those for the

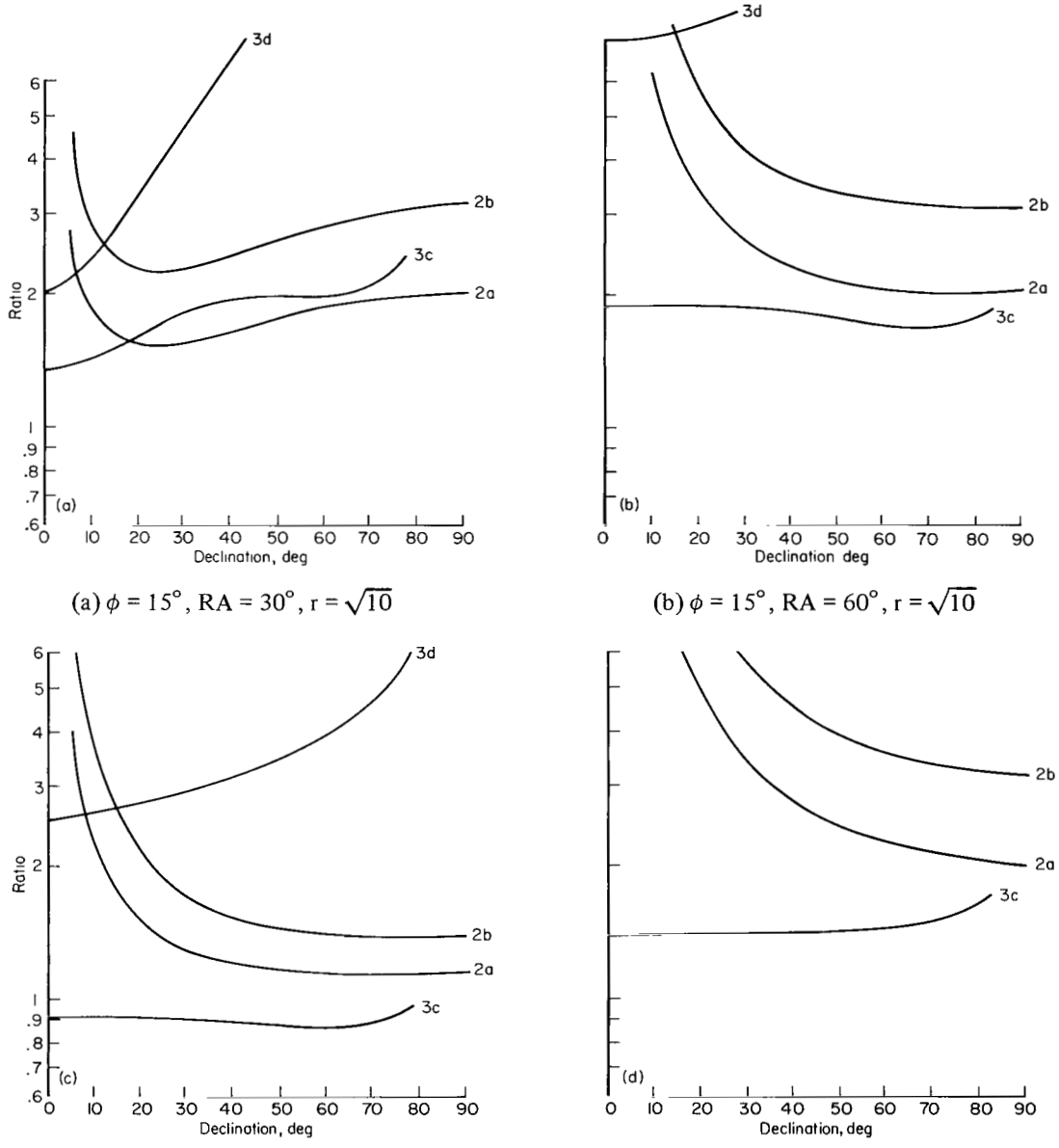

(a) $\phi = 15°$, RA = 30°, r = $\sqrt{10}$

(b) $\phi = 15°$, RA = 60°, r = $\sqrt{10}$

(c) $\phi = 15°$, RA = 60°, r = 10

(d) $\phi = 15°$, RA = 90°, r = $\sqrt{10}$

Figure 10.- Ratio of $\sqrt{\sigma_r^2 + \sigma_n^2}$ for type 2 and type 3 with RA > ϕ to $\sqrt{\sigma_r^2 + \sigma_n^2}$ for type 1.

other two configurations. Note that the ratios for types 3a and 3b are off the scale of the graphs in all cases, and in figure 12(d) the curve for type 3c has been omitted for the same reason. As with the other two configurations the ratios decrease with increasing r, but configurations of this type should be avoided for $r < 10$.

The ratios for type 4 with the third configuration are shown in figure 11, and are quite large in all cases except at very large values of D. Note that for RA = 90° (fig. 11(d)) the error for the regular schedule is independent of which limbs γ_1 and γ_2 are measured to so that only one curve is shown.

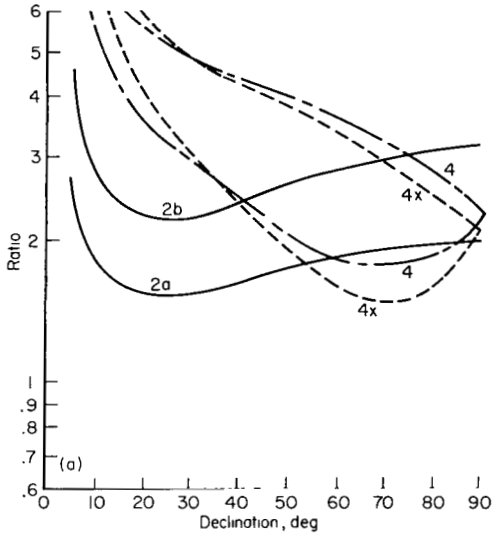

(a) $\phi = 15°$, RA = 30°, $r = \sqrt{10}$

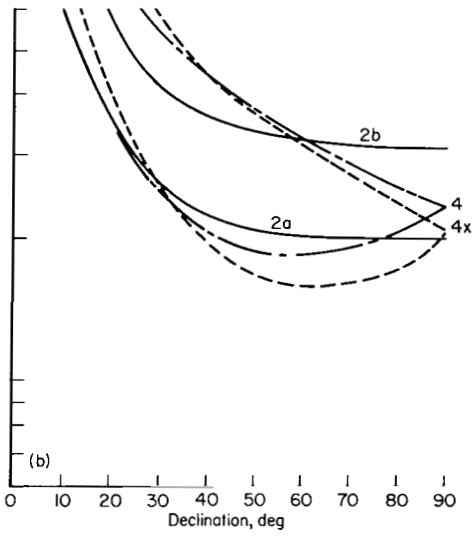

(b) $\phi = 15°$, RA = 60°, $r = \sqrt{10}$

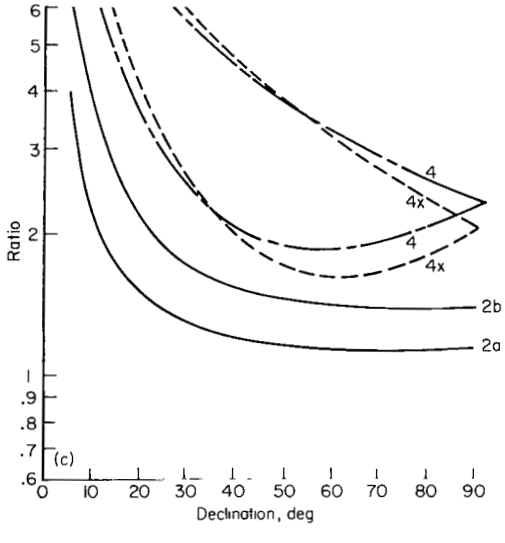

(c) $\phi = 15°$, RA = 60°, r = 10

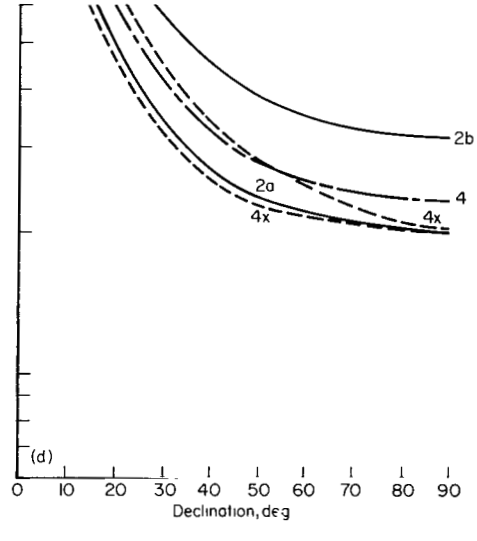

(d) $\phi = 15°$, RA = 90°, $r = \sqrt{10}$

Figure 11.- Ratio of $\sqrt{\sigma_r^2 + \sigma_n^2}$ for type 2 and type 4 with RA > ϕ to $\sqrt{\sigma_r^2 + \sigma_n^2}$ for type 1.

Figure 12 presents the same data for type 5 measurements, and, again the ratios are considerably larger than for the other two configurations. However, for $r \geqslant 10$ and $D > 25°$ the type 5 errors are comparable to those for type 1.

The preceding results show that measurements of type 2, 3, or 5 can have accuracies comparable to that of type 1, provided it is possible to choose the stars properly. Type 4 measurements appear to be decidedly inferior to the others and will not be considered further. For type 2 the stars should be chosen so that B is as near 90° as possible, while for type 5 (regular schedule) either ψ_1 or ψ_2 as well as B should be as near 90° as possible.

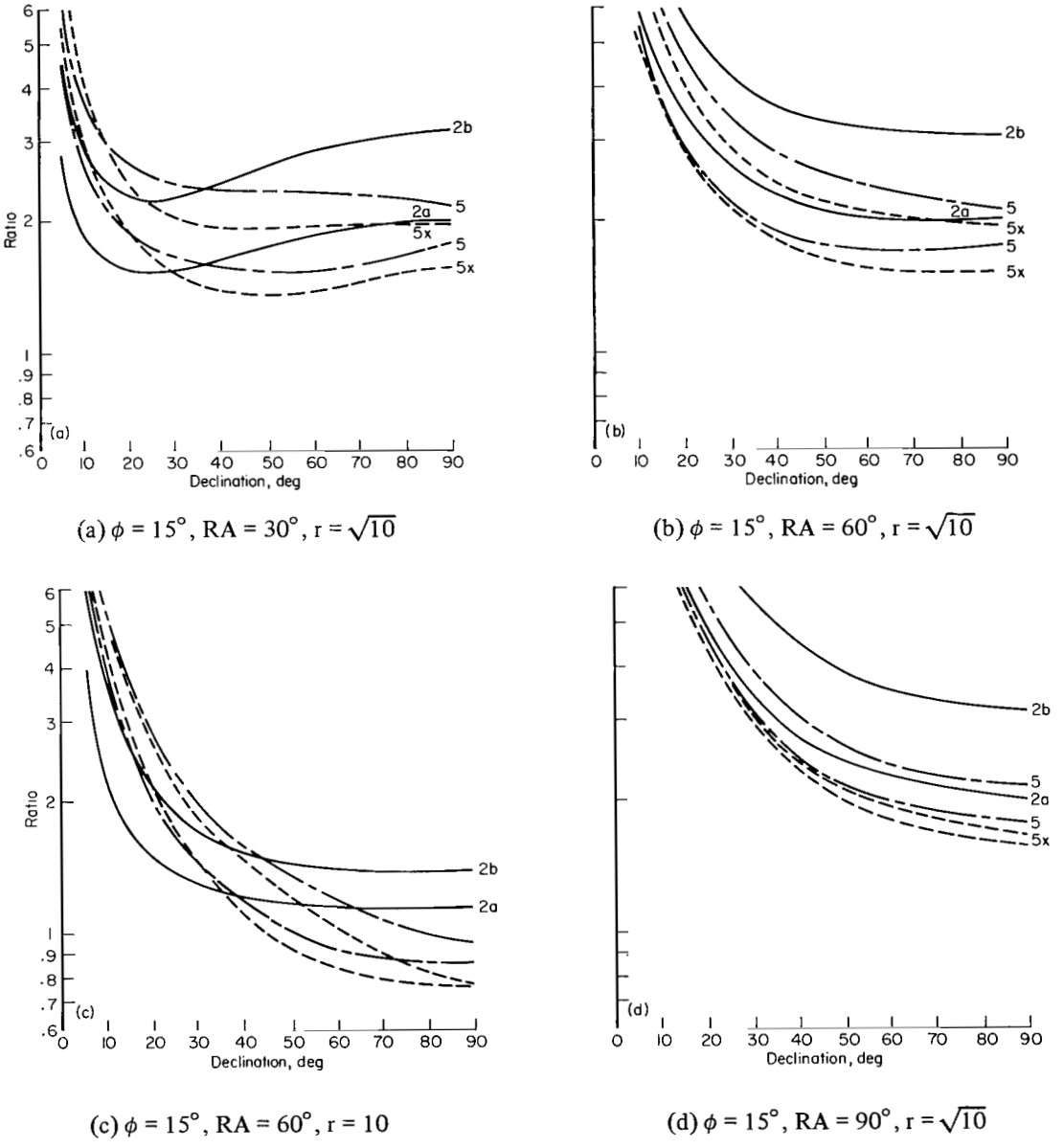

(a) $\phi = 15°$, RA = 30°, $r = \sqrt{10}$

(b) $\phi = 15°$, RA = 60°, $r = \sqrt{10}$

(c) $\phi = 15°$, RA = 60°, r = 10

(d) $\phi = 15°$, RA = 90°, $r = \sqrt{10}$

Figure 12.- Ratio of $\sqrt{\sigma_r^2 + \sigma_n^2}$ for type 2 and type 5 with $RA > \phi$ to $\sqrt{\sigma_r^2 + \sigma_n^2}$ for type 1.

These conditions are satisfied best when the projection of $\bar{r}$ onto the X-Y plane lies near one of the stars. For type 3 the best results are obtained if the two stars and the planet are nearly colinear with the projection of $\bar{r}$ onto the X-Y plane midway between the two stars. In all cases the results are poorer when the projection of r lies well outside the smaller angle between the two stars.

The practicality of making a suitable choice of stars has not been investigated in detail here, but an examination of the star chart in reference 6 indicates little difficulty if a 90° field of view is available. Reduction of the field of view to 55° makes it more difficult to locate suitable stars, and in the case of type 5 increases the minimum obtainable error since $\psi_i \leqslant \phi$.

If we assume that the proper choice of stars can be made, then the ratio of $\sqrt{\sigma_r^2 + \sigma_n^2}$ for types 2, 3, and 5 to that for type 1 can be held to less than 2. As r increases, this ratio approaches unity over an increasing range of D because the radial component becomes the dominant part of the error for all types. In view of these facts it seems reasonable to assume that the total random error for any of these observation types can be approximated by the radial error from a single subtense angle measurement. There is some improvement in the results for type 5 with the extended schedule but the change is not enough to invalidate this rough approximation.

This approximation used with equation (16) for r = 200 indicates position errors with a standard deviation of about 0.2 planet radii for each arc second standard deviation of instrument error, or, in other words, an error of 1 or 2 percent for a 10 arc sec instrument. Thus, within the present state of the art, the measurements considered in this study are useful to a maximum range of about 200 planet radii from the central body.

Bias Errors

The computation of the bias errors is complicated by the fact that different biases may either add or subtract. Therefore, the upper bound of $\sqrt{b_r^2 + b_n^2}$ was computed by assuming signs on the different biases which gave the largest total error. The instrument biases in γ, S, A, and D were assumed to have the same magnitude b, while the bias in B and that due to irradiance were assumed to be either b or 10b. It was assumed that b is equal to the standard deviation σ of the instrument errors discussed in the previous section.

The ratio of the biases for type 1 measurements to the 1σ random error for type 1 were computed and are plotted in figure 13. These ratios are nearly constant and are approximately $(1 + |b_I|/|b|)$. This approximation becomes more accurate as $|b_I|$ or r is increased.

The ratios of $\sqrt{b_r^2 + b_n^2}$ for the remaining measurement types to σ_r for type 1 were computed for the same cases as the random error and are plotted in

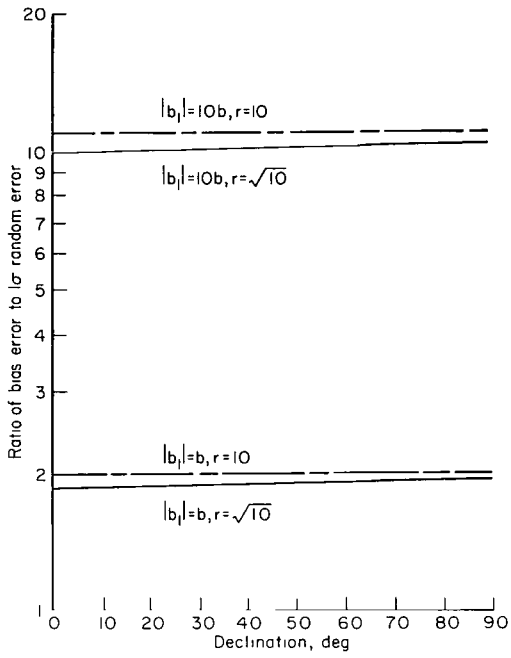

Figure 13.- Ratio of bias errors to 1σ random errors for type 1 measurements.

figures 14 through 16. Figure 3 shows that, for the values of r considered, the type 1 random error is almost entirely in the radial direction, and it is reasonable to compare these ratios directly with those in figures 4 through 12. Note that, as was pointed out earlier, the type 5 biases were computed under the assumption that the entire bias is due entirely to zero calibration error; actually the ratios for types 4 and 5 will lie somewhere between the type 2 and type 5 curves, depending on the relative magnitude of the zero calibration error. Except for one case (fig. 16(d)), the ratios for $b_I = 10b$ are about five times those for $b_I = b$ and the value of b_I is not indicated on the figures.

The ratios for the configuration with RA = $\phi/2$ (fig. 2(a)) are presented in figure 14. The curves show the same general characteristics as those for the random errors in figures 4, 5, and 6; that is, types 2 and 5 have singularities at D = 0 while type 3 has a singularity at D = 90°, and the ratios for types 3c and 3d are infinite because of the singularity when $\psi_1 = \psi_2$. Increasing r from $\sqrt{10}$ to 10 (figs. 14(b) and 14(c)) reduces the ratios for $b_I = 1$ but has little effect for $b_I = 10$. Note that the smallest value of $\sqrt{b_r^2 + b_n^2}$, type 5b with $b_I = 1$, is twice as large as σ_r for type 1, while if b_I is increased to 10 the ratio increases to 11. The biases due to zero calibration error are reduced by measuring one or both of the star-limb angles to the far limb, but the reduction is significant only at small values of D.

Figure 15 presents the corresponding data for the configuration where RA = 0 (fig. 2(b)), and, again, the curves follow the same general pattern as the corresponding ones for the random errors (figs. 7, 8, and 9). In figure 15(a) the ratio for type 2 is much larger than that for types 5c and 5d which is, in turn, much larger than the other ratios for type 5. This fact serves to show that the bias errors increase in magnitude and spread between various cases in the same manner as the random errors as a singularity is approached; in this case B becomes small with increasing D.

The configuration with the projection of $\bar{r}$ well outside the smaller angle between the two stars (fig. 2(c)) produced the ratios illustrated in

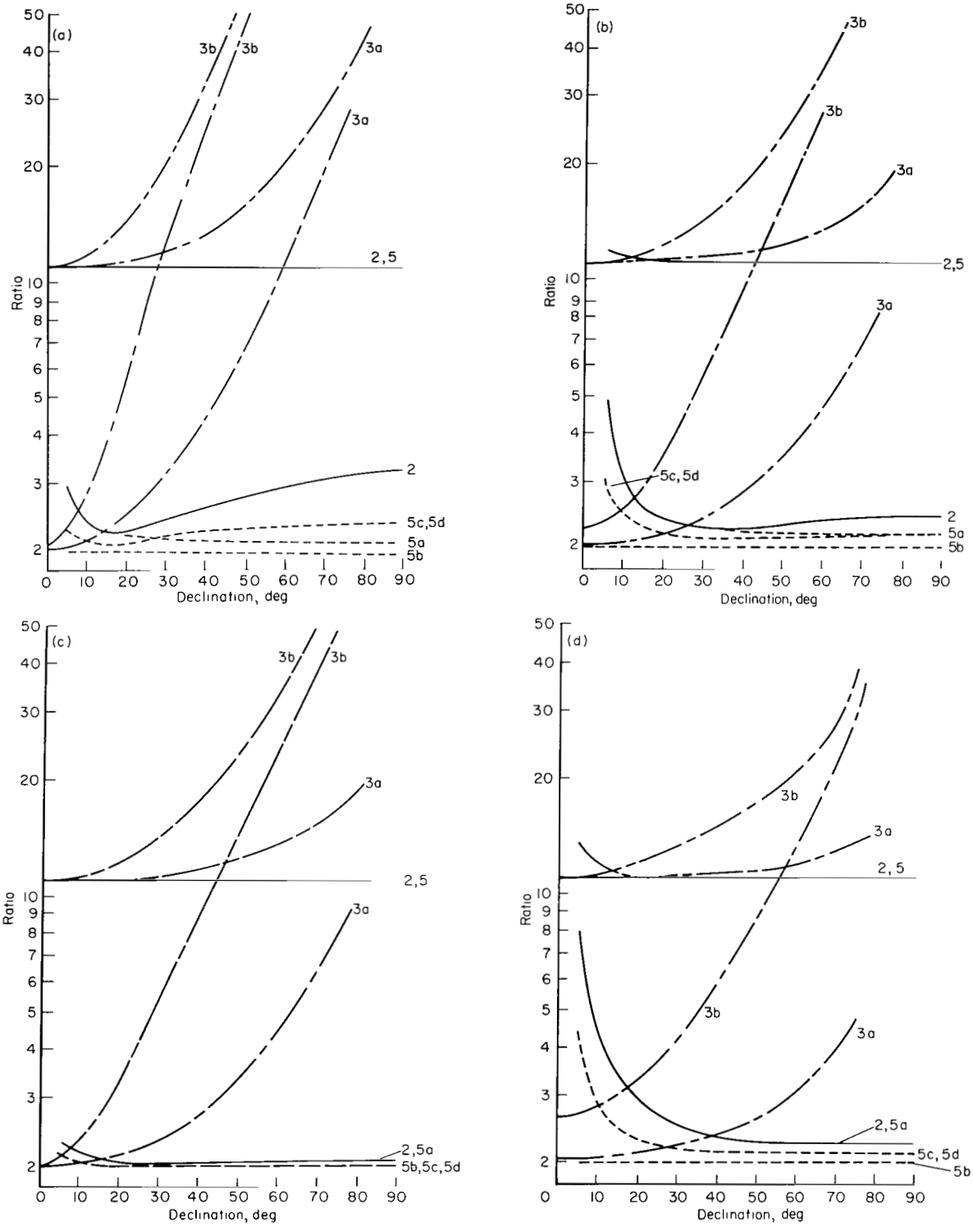

(a) $\phi = 30°$, RA = 15°, r = $\sqrt{10}$

(b) $\phi = 60°$, RA = 30°, r = $\sqrt{10}$

(c) $\phi = 60°$, RA = 30°, r = 10

(d) $\phi = 90°$, RA = 45°, r = $\sqrt{10}$

Figure 14.- Ratio of bias errors for types 2, 3, and 5 with RA $\phi/2$ to σ_r for type 1.

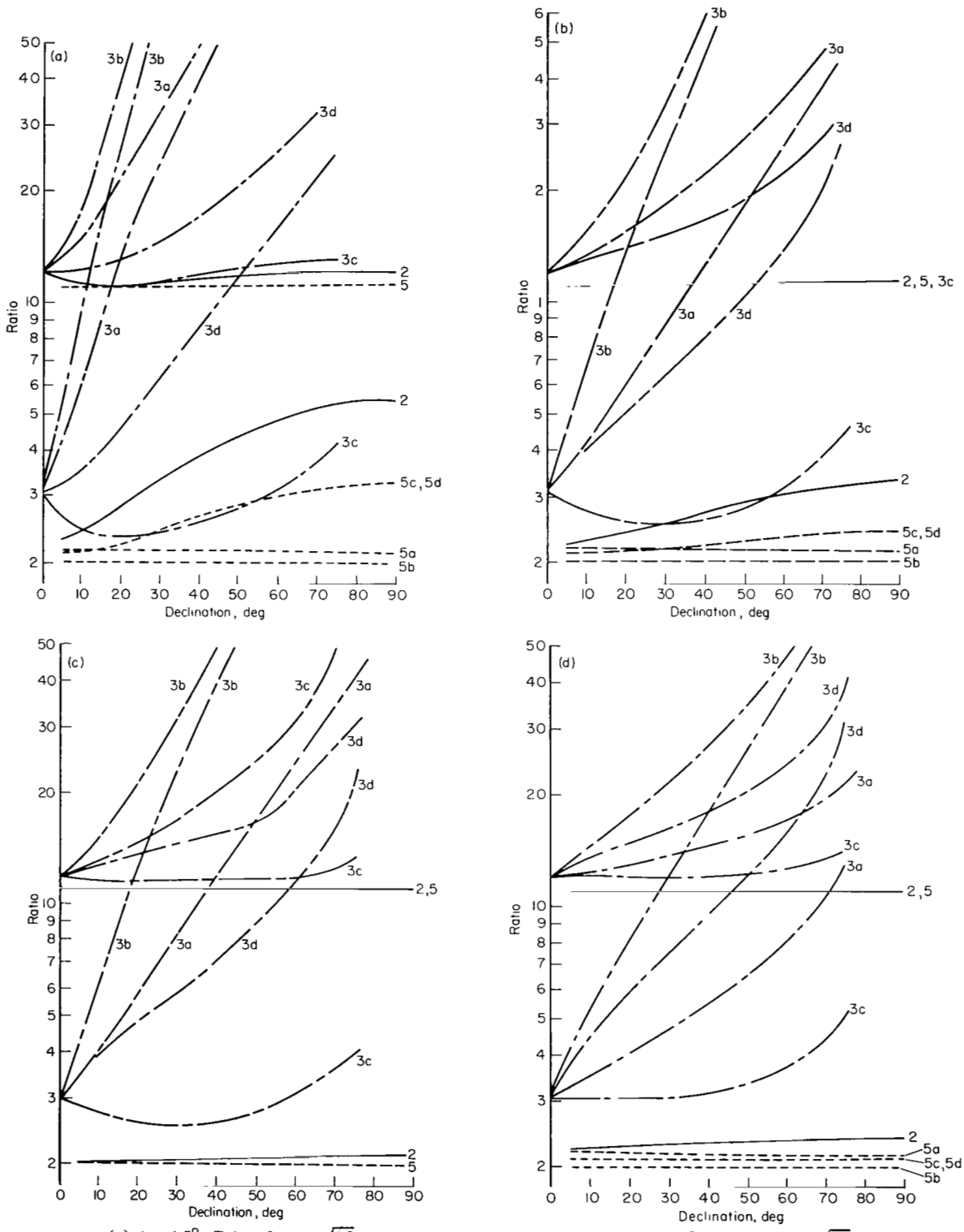

(a) $\phi = 15°$, RA = 0, r = $\sqrt{10}$

(b) $\phi = 30°$, RA = 0, r = $\sqrt{10}$

(c) $\phi = 30°$, RA = 0, r = 10

(d) $\phi = 60°$, RA = 0, r = $\sqrt{10}$

Figure 15.- Ratio of bias errors for types 2, 3, and 5 with RA = 0 to σ_r for type 1.

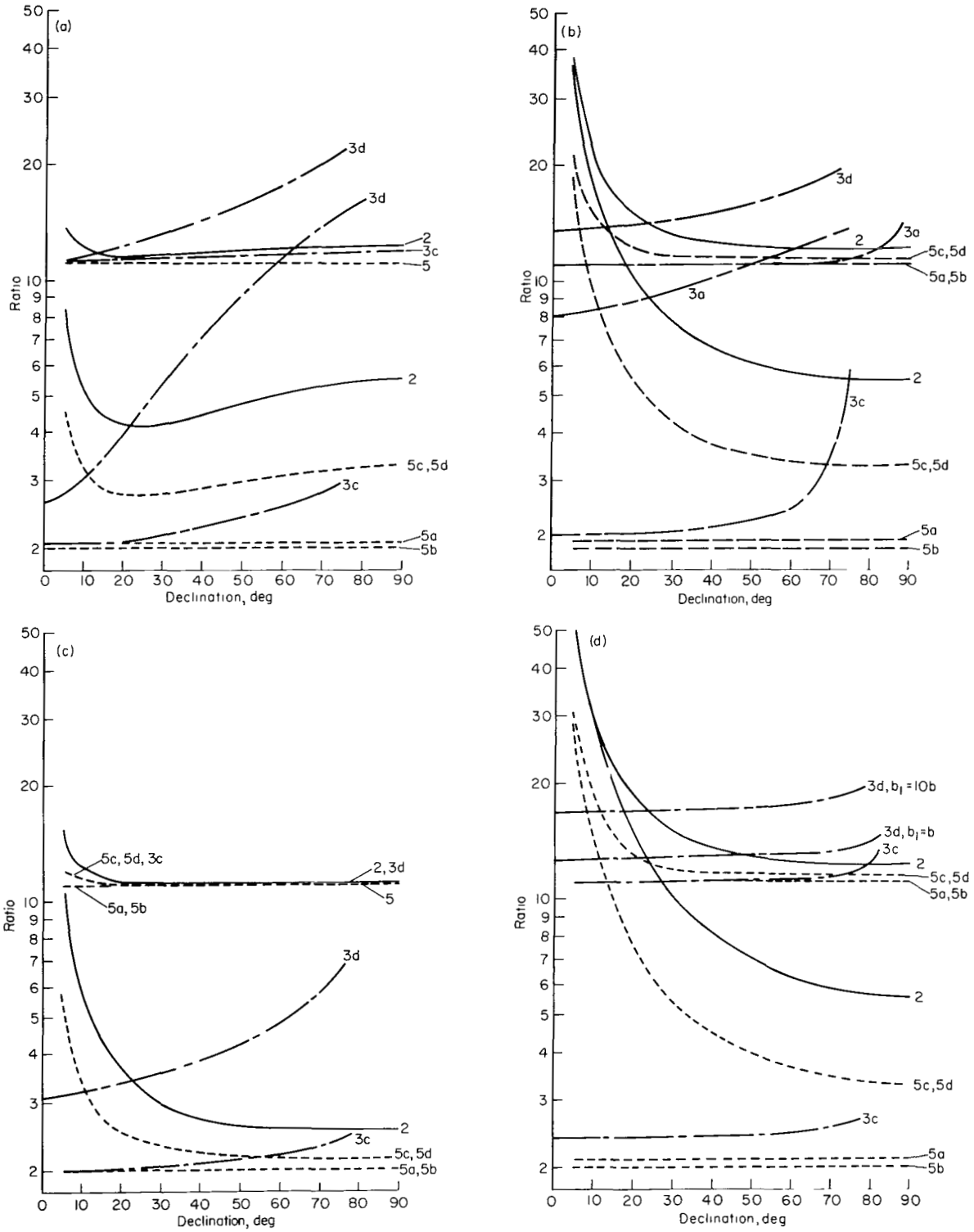

(a) $\phi = 15°$, RA = 30°, r = $\sqrt{10}$
(b) $\phi = 15°$, RA = 60°, r = $\sqrt{10}$
(c) $\phi = 15°$, RA = 60°, r = 10
(d) $\phi = 15°$, RA = 90°, r = $\sqrt{10}$

Figure 16.- Ratio of bias errors for types 2, 3, and 5 with RA = 0 to σ_r for type 1.

figure 16. As in the case of the random error (figs. 10, 11, and 12) the biases for type 2 and types 5c and 5d are much larger at lower values of D than those for $\phi = 15°$ and RA = 0 (fig. 15(a)). The other biases, types 3, 5a, and 5b, are generally a little smaller than for the other configurations.

The upper bounds on $\sqrt{b_r^2 + b_n^2}$ presented in these figures are only rough approximations and represent worst possible cases. However, they do show that in many instances a bias as large as the standard deviation of the random error can be the dominating source of position error. Even if we attribute the entire bias to zero calibration error and use type 5b measurements so that $b_n = 0$, the bias error is still about twice the random error. An increase in b_I causes a large increase in the bias error and every effort should be made to correct for irradiance bias; even a crude correction would be helpful.

As in the cases of the random errors, the bias errors for measurement types 2, 3, and 5 can be reduced to about the same value as those for type 1 by the proper choice of stars. Furthermore, the same general conclusions as to which stars should be chosen to minimize random errors also apply in the case of the bias errors.

In order to draw any further conclusions with regard to the relative importance of bias and random errors, it is necessary to make additional assumptions regarding the numerical values of the biases and standard deviations. For example, the instrument bias error from the Gemini flight described in reference 8 averages about 2.25 arc sec or about one third the average standard deviation. The irradiance error for the Moon as seen from the Earth is about five times the instrument bias error (ref. 5).

We can use these numbers with equations (15) and (16) to show that the position bias errors will be approximately twice the standard deviation of the random errors, and the total rms error is about 2.2 times the standard deviation. On the other hand, if the irradiance error could be reduced by calibration to about the same value as the instrument bias error, the total rms error would be about 1.3 times the standard deviation of the random part.

Position Errors Due to Linear Interpolation

The errors caused by the linear interpolation of r and γ are dealt with separately in this section. The derivations of the equations used and some data pertinent to neglecting higher order terms are given in appendix D.

Interpolation of r.- Appendix D gives an expression for r_{min}, the minimum value of r for which the error in the linear interpolation of r is less than $M\sigma_r$, where σ_r is evaluated for type 1 measurements. The value of

r_{min} is a function of the astrodynamic constant μ, the orbital eccentricity, e, the standard deviation of random measurement errors, σ, and Δt, which is half the time between the observations being interpolated. The computation of r_{min} requires the assignment of values to the various parameters involved. The value of μ for the Earth was used since it gives the largest value of r_{min} of any major body in the solar system (see appendix C), 10 arc sec was used for σ and values of e were used which cover the range of values likely to be encountered in manned space flight.

The data in reference 8 indicate that sextant (single angle) measurements of the same angle can be repeated on the average at intervals of about one minute. Since the alternate measurement of different angles or the simultaneous measurement of two angles will require more time, r_{min} was evaluated for Δt of 1, 2, 3, 4, and 5 minutes.

Figure 17 shows the resulting values of r_{min} for M = 0.1, plotted as a function of Δt for various values of e. It was found (eq. (D9)) that r_{min} is a function of $e\Delta t^2/M\sigma$ so that the data can be used for other values of e, M, σ, or Δt. For example, the curve shown for e = 1.0 and M = 0.1 is the same as for e = 10 and M = 1.0.

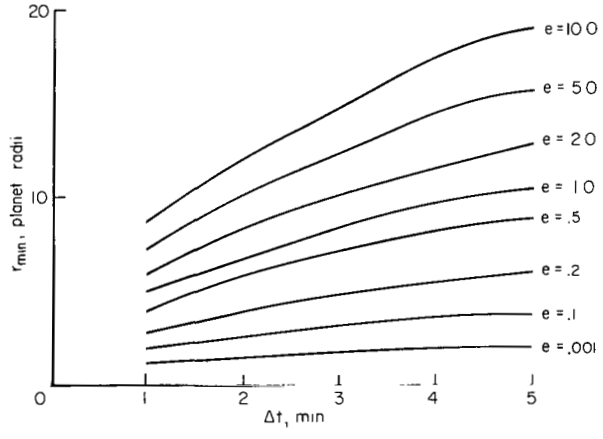

Figure 17.- Minimum radius for which linear interpolation error of radius is less than 0.1 σ_r.

If Δt is 5 minutes, M = 0.1 and e = 0.98, the equivalent of a lunar trajectory, then $r_{min} \approx 11$ Earth radii, while if Δt can be reduced to 1 minute $r_{min} \approx 5$ Earth radii. Although these are rather large distances, they are only 4.3 hours and 1.7 hours, respectively, from perigee and $r > r_{min}$ for most of the trajectory. This is also true for e = 10, in which case $r_{min} \approx 20$ Earth radii for Δt = 5 minutes and 9 Earth radii for Δt = 1 minute. These distances are about 1.7 hours and 40 minutes, respectively, from perigee. Thus, linear interpolation of r will produce negligible errors over the major portions of both lunar and interplanetary trajectories. For near-planet orbits, where $r \leqslant 4$, interpolation may be the major source of error unless e is very small. For example, if $r = \sqrt{2}$, e = 0.1 and Δt = 5 minutes, the interpolation error would exceed the measurement error by about a factor of 50. This factor decreases linearly with e and with the square of Δt, but there are many combinations of r, e, and Δt in the range considered for these parameters for which the interpolation is the dominant source of error. This fact does not necessarily preclude the use of linear interpolation for near-planet orbits, however, because the error due to measurement inaccuracy for the model assumed in the study are quite small near the planet.

Interpolation of γ- The position error due to the linear interpolation of γ is normal to the radius and contains ctn ψ_o (eq. (D31)), but since the

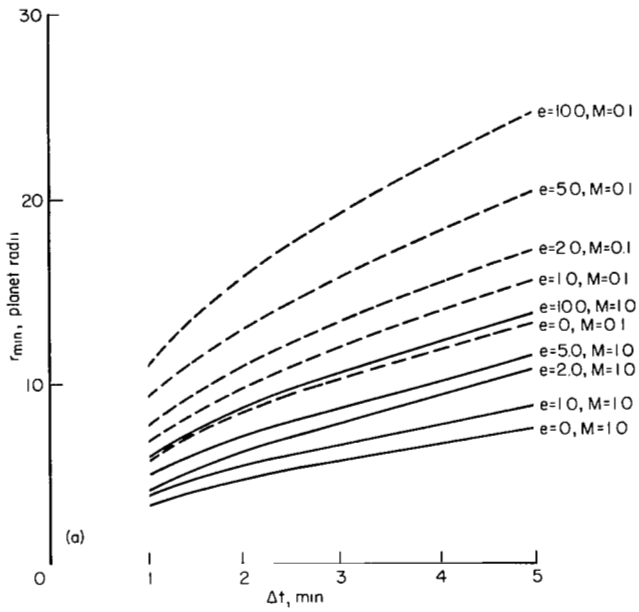

(a) sin B $\geqslant$ 0.5

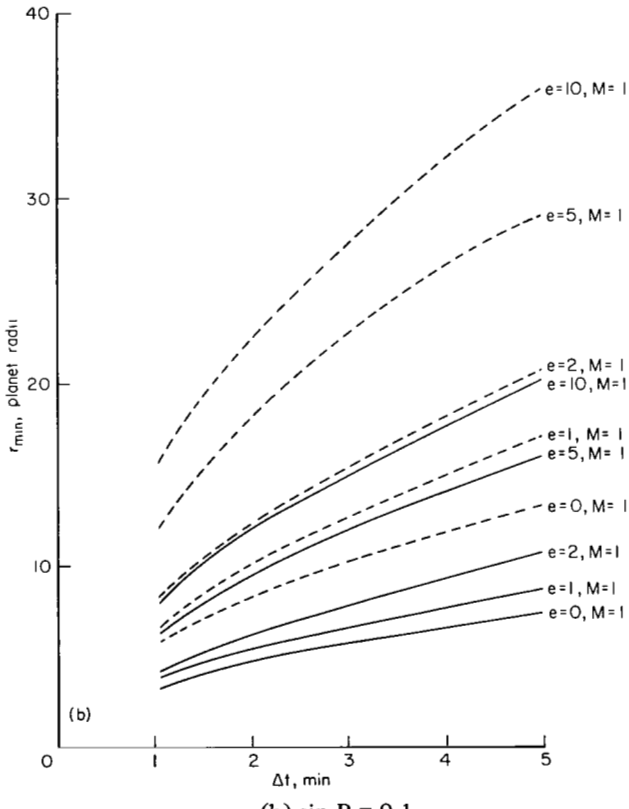

(b) sin B = 0.1

Figure 18.- Minimum radius for which error due to interpolating γ is less than $M\sqrt{\sigma_r^2 + \sigma_n^2}$.

radial portion of the measurement error is usually dominant, it should also be considered in evaluating the interpolation error. Therefore, two expressions were found (eqs. (D32) and (D34)) for which the interpolation error will not exceed $M\sqrt{\sigma_r^2 + \sigma_n^2}$; the value of $\sqrt{\sigma_r^2 + \sigma_n^2}$ for type 5 was used since it is usually smaller than that for type 4.

The value of r_{min} in this case is a function of sin B as well as e, M, σ, and Δt^2, and the last three terms occur in the expression for r_{min} in the form $\Delta t^2/M\sigma$. Thus a single curve represents a family of values of M, σ, and Δt, but e and sin B enter in a more complicated form.

The resulting values of r_{min} are plotted in figure 18 for two different values of sin B. For given values of e and μ, r_{min} is generally larger than the corresponding values in figure 17. If the data from figure 17 are used in the previous example, it is found that for the lunar trajectory, with M = 0.1, sin B $\geqslant$ 0.5 and Δt = 5 minutes, r_{min} occurs about 7.7 hours from perigee, and if Δt is reduced to 1 minute, the time is about 3 hours. For the high eccentricity (e = 10) trajectory the times are 1.8 hours and 45 minutes, respectively. For small values of sin B these times become larger, but if stars can be chosen to keep sin B large, it should be possible to use linear interpolation for γ with lunar and interplanetary trajectories. For near-planet orbits, the values of r_{min} are relatively large compared to those in figure 17, but the absolute errors due to linear interpolation at these ranges are small and may be acceptable.

Potential application- The data just presented have shown that at

sufficiently large ranges the linear-interpolation error is negligible compared to that resulting from measurement errors of 10 arc sec standard deviation. This fact implies that at such ranges it would be reasonable to use the alternate schedules for type 5, which employ only linear interpolation, as described in the section on measurement types. It was pointed out in the section on error analysis methods that the errors from the alternate schedules are about the same as those for type 2, thus comparing favorably with the regular type 5 schedule. Furthermore, some error due to linear interpolation of r is present even when Gibb's method is used for type 5. The linear-interpolation errors would, of course, become relatively more important if the instrument errors were reduced significantly or if interpolation intervals ($2\Delta t$) were larger than 10 minutes. However, these results make the alternate schedule potentially very attractive.

Velocity Errors

Once the position vectors have been obtained at two different times, the velocity is obtained by interpolation using Gibb's method. Linear interpolation could also be used to obtain velocity, but, for reasons to be discussed later, it is not considered accurate enough. The two major sources of error in velocity are the inaccuracy of the interpolation formula and random measurement errors, the measurement bias errors in velocity being zero. The standard deviation, σ_v, of the velocity error is approximately (see eq. (28)) $\sqrt{\sigma_r^2 + \sigma_n^2}/\sqrt{2}\ \Delta t$. Since this is the case, the data presented for type 1 position errors in figure 3 can be used for velocity errors by dividing the vertical scale by $\sqrt{2}\ \Delta t$. The ratios of the standard deviations of velocity errors for types 2, 3, 4, and 5 to that for type 1 are the same as the ratios for the corresponding position errors given in figures 4 through 12.

The remainder of this section is concerned with the combination of velocity errors resulting from random measurement errors and from interpolation. For this purpose a further simplification, which was pointed out in the discussion of random position errors, will be made. It will be assumed that $\sqrt{\sigma_r^2 + \sigma_n^2}$ for each position vector, can be approximated by that of the radial error arising from a single subtense angle measurement, that is, $\sigma_s r\sqrt{r^2 - 1}$.

Since the interpolation error increases with Δt while the random velocity error decreases, a value of Δt can be chosen for which the total velocity error is minimized. A rough approximation to this optimum Δt was obtained by trial and error for a few sample Earth orbits which were chosen to be circular for ease in calculating the correct $\bar{r}$ and $\bar{v}$.

Table 7 shows these approximately optimum values of Δt, along with the associated values of σ_v, σ_p, and the errors Δv in velocity and Δr in position that are due to interpolation. In the table t_2 denotes the center of the interpolation interval while the errors at t_3 apply to either end of the interval, $\Delta r(t_3)$ being omitted since it is zero. The error quantities are expressed in meters per second and kilometers. The standard deviation of

TABLE 7.- COMPARISON OF RANDOM ERRORS WITH INTERPOLATION ERRORS

r, earth radii	Δt, min	Standard deviations of random errors			Interpolation errors from Gibb's method		
		σ_V, m/s	$\sigma_p(t_2)$, km	$\sigma_p(t_3)$, km	$\Delta v(t_2)$, m/s	$\Delta r(t_2)$, km	$\Delta v(t_3)$, m/s
$\sqrt{2.0}$	1	7.3	0.31	0.44	0.2	0	1.3
$\sqrt{2.0}$	5	1.5	0.31	0.44	.4	6	25.0
$\sqrt{10}$	10	4.8	2.0	2.9	.3	1	3.2
10	50	10.3	22	31	.0	2	1.8
$\sqrt{10^3}$	500	10.3	220	310	.1	80	8.1
100	5000	10.3	2200	3100	.3	2510	14.0

instrument errors is assumed to be 10 arc sec, and the interpolation errors were calculated to an accuracy of about 0.1 m/s and 1.0 km.

The total position error (root sum square of random and interpolation errors) is smaller at the center of the interval except when $r = \sqrt{2}$ and $\Delta t = 5$, and in no case is it much greater than 1 percent of the total position vector. The total velocity error is also satisfactory both at the ends and the center of the interval, but it is much smaller at the center, indicating that interpolation to the center of the interval is preferable.

The errors in velocity which arise from the use of linear interpolation were also calculated at the center and end of the interval and found to exceed the corresponding error from Gibb's method by one or two orders of magnitude. Thus acceptable accuracy might be obtained near the center of the interval, but linear interpolation is not a generally satisfactory method for computing velocity.

At the smaller values of r the interpolation intervals ($2\Delta t$) used in table 7 would be no greater than the time required for two sets of observations; but for larger values of r the time interval becomes much greater. For example, when $r = 10$, Δt in table 7 is 50 minutes, and if Δt were reduced to 10 minutes σ_V would be about 50 m/s or about 2 percent of the total velocity. For $r = \sqrt{10^3}$ the random error for $\Delta t = 10$ minutes would exceed 0.5 km/s. The position errors at the larger ranges appear to be rather large, but the root sum square of random and interpolation errors is less than 1 percent of the total range.

Equivalent data were not obtained for orbits of higher eccentricity with the exception of one parabolic case. The interpolation errors in this case are somewhat higher than for the circular orbit, but a marked reduction in velocity errors is obtained by using large time intervals in this case also. For still higher eccentricities the orbit is essentially linear at long ranges and the velocity interpolation errors will be quite small, again indicating the desirability of large interpolation intervals.

The results just discussed indicate that all of the measurement types, except possibly type 4, can provide satisfactory preliminary trajectories, provided the time interval between the two position fixes is chosen properly. For $r > \sqrt{2}$, Δt should be 10 minutes or more and the extended schedule would be of little value. Also, the interpolation should be to a time near the center of the interval even though this choice reduced the velocity error at the expense of some increase in position error. If $r > 10$, the time interval required to reduce the random velocity error is so large that it would be best to try to reduce the position error with redundant data before attempting to determine velocity. The development of such a scheme, however, is beyond the scope of this study.

For near-planet orbits, where $r < 4$, the interpolation error from Gibb's method is not excessive if the interpolation time is near the center of the interval. Linear interpolation would be the major source of error, and this error could probably be constrained within acceptable bounds.

Near-Planet Orbits

The data presented have been restricted to $r \geqslant \sqrt{2}$ and special consideration must be given to cases with $r < \sqrt{2}$. In this case the subtense angle exceeds 90° and the planet disk fills the field of view considered in calculating data, thereby excluding all of the measurement types except type 3. While it is theoretically possible to measure angles larger than 90°, it is questionable whether it would be practical to measure subtense angles of much larger magnitude.

Since type 3 measurements do not require a view of the complete disk they can be used at small values of r, but the angle B, separating the planes defined by $\bar{r}$ and the unit vectors to the two stars, must be less than the arc of the planet's disk lying in the primary field of view. The field of view of the trisextant could probably be increased substantially from the 3° of the instrument described in reference 7, and if sufficient accuracy could be obtained, type 3 measurements would be atractive for use in near-planet orbits. These measurements in effect combine the sextant and stadimeter measurements of reference 3, and it should be possible to develop a similar manual computation method for a limited range of eccentricities. The practicality of such a system depends, of course, upon the ease and accuracy of making the measurements for $r < \sqrt{2}$.

CONCLUSIONS

An error analysis has been carried out for determining preliminary trajectories using five different types of measurements. The measurement type (type 1) consisting of simultaneous measurements of the right ascension, declination and subtense angle of the planet has been used as a standard of comparison. The following conclusions can be drawn from the results of the study:

1. If the stars used in the measurements can be chosen properly, two of the remaining methods, the photographic method (type 2) and the trisextant (type 3) need a single measurement to provide a position fix having errors within a factor of two of the standard of comparison.

2. Similar results can be obtained using a standard space sextant (type 5) to make seven angular measurements and interpolating to achieve a common epoch.

3. The measurement type (type 4) which makes simultaneous measurements of one star-limb angle and the subtense angle at three different times and interpolates is less accurate than the others and offers little advantage.

4. It is best to choose stars such that the projection of the radius vector $\bar{r}$ onto the plane of the two stars lies in or near the smaller angle between them.

5. The proper choice of stars would be enhanced by increasing the maximum measurable angle from the present 55+° to 90°.

6. For magnitudes of $\bar{r}$ greater than $\sqrt{2}$ planet radii and properly chosen stars, the random position error can be approximated roughly by the radial error from a single subtense angle measurement. The random velocity error is roughly the position error divided by half the time interval between the two position vectors used to determine the velocity.

7. Bias errors, particularly those due to irradiance, can be very important and every effort should be made to reduce the unknown biases well below the standard deviation of the random errors. For example, an instrument with a standard deviation of 10 arc sec is generally regarded as practical and it would be desirable to reduce the unknown biases to 2.5 arc sec or less.

8. For reasonably small bias errors at distances from $\sqrt{2}$ to 200 planet radii from the central body, satisfactory preliminary trajectories (position and velocity known within a few percent) can be found using any of the measurement types, provided suitable stars can be chosen.

9. For all trajectories except near-planet orbits the hand-held space sextant can provide satisfactory measurements for determining a preliminary trajectory. Furthermore, for sufficiently large radial distances from the planet, linear interpolation is sufficient for determining position, but a higher order formula such as that from Gibb's method should be used for velocity.

Ames Research Center
National Aeronautics and Space Administration
Moffett Field, Calif., 94035, July 9, 1971

APPENDIX A

EQUATIONS FOR POSITION FIX

It is pointed out in the text that some types of measurements require interpolation to refer the measured angles to a common epoch. The equations for the position fix are derived in this appendix under the assumption that the interpolation has already been carried out or, equivalently, that all of the angles used were measured simultaneously.

DETERMINATION OF RANGE

For all five types of measurements the radial distance, r, of the planet center from the spacecraft is ultimately determined from the semisubtense angle, S, as shown in sketch (d). All the equations in the report involving

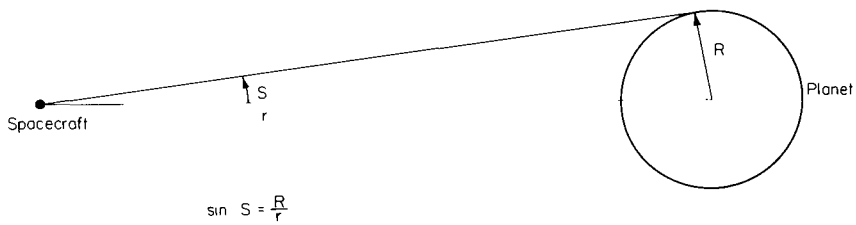

Sketch (d)

r have been normalized by defining the unit of length to be the radius of the observed planet, that is, by setting R equal to unity. Consequently,

$$r = \csc S \tag{A1}$$

COMPUTATION OF THE UNIT VECTOR $\bar{u}$

Type 1 Measurements

Type 1 measurements are direct measurements of RA, D, and S, and it is shown in the text that

$$\left.\begin{aligned} u_1 &= \cos RA \cos D \\ u_2 &= \sin RA \cos D \\ u_3 &= \sin D \end{aligned}\right\} \tag{A2}$$

Type 2, 3, 4, and 5 Measurements

These types of measurements are direct measurements of the star-limb angles γ_1 and γ_2, and, with the exception of type 3, the direct measurement of 2S. For type 3, B is measured instead of S, which must then be computed from γ_1, γ_2, and B. The details of this computation will be discussed in the next section, but for the present it will be assumed that S is known. Figure 1 is reproduced for aid in deriving the equations for the components of $\bar{u}$.

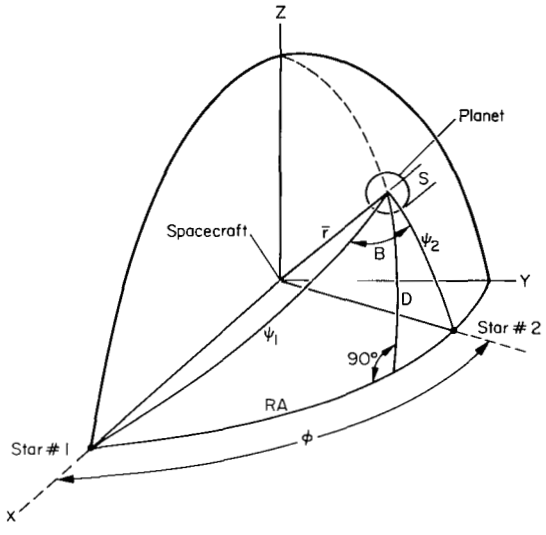

First the star-center angles ψ_1 and ψ_2 are computed using the relationship

$$\psi_i = \gamma_i + k_i S$$

where $k_i = 1$ for γ_i measured to the limb nearest the star and $k_i = -1$ for measurements to the far limb. The angle, ϕ, between the stars is taken from tabulated data, and it can be shown by spherical trigonometry that

$$\left.\begin{aligned} \cos \psi_1 &= \cos RA \cos D \\ \cos \psi_2 &= \cos(\phi - RA)\cos D \end{aligned}\right\} \qquad (A3)$$

or

$$\cos \psi_2 = \cos RA \cos D \cos \phi + \sin RA \cos D \sin \phi \qquad (A4)$$

Substitution in (A3) and (A4) for $\cos RA \cos D$ and $\sin RA \cos D$ from equations (A2) gives

$$u_1 = \cos \psi_1 \qquad (A5)$$

$$u_2 = \frac{\cos \psi_2 - \cos \psi_1 \cos \phi}{\sin \phi} \qquad (A6)$$

Since $\bar{u}$ is a unit vector

$$u_3 = \pm \sqrt{1 - u_1^2 - u_2^2} \qquad (A7)$$

Combining equations (A5), (A6), and (A7) into a single vector equation gives

$$\bar{u} = \begin{bmatrix} \cos \psi_1 \\ \dfrac{\cos \psi_2 - \cos \psi_1 \cos \phi}{\sin \phi} \\ \pm \sqrt{1 - u_1^2 - u_2^2} \end{bmatrix} \tag{A8}$$

Special Computation for Type 3

In the case of type 3 measurements, γ_1, γ_2, and B are measured simultaneously, and S must be calculated. The law of cosines for spherical triangles gives

$$\cos \phi = \cos \psi_1 \cos \psi_2 + \sin \psi_1 \sin \psi_2 \cos B \tag{A9}$$

or

$$\cos \phi = \cos(\gamma_1 + k_1 S)\cos(\gamma_2 + k_2 S) + \sin(\gamma_1 + k_1 S)\sin(\gamma_2 + k_2 S)\cos B$$

It can be shown that since $k_i = \pm 1$

$$\cos(\gamma_i + k_i S) = \cos(k_i \gamma_i + S)$$

$$\sin(\gamma_i + k_i S) = k_i \sin(k_i \gamma_i + S)$$

so that

$$\cos \phi = \cos(k_1 \gamma_1 + S)\cos(k_2 \gamma_2 + S) + k_1 k_2 \sin(k_1 \gamma_1 + S)\sin(k_2 \gamma_2 + S)\cos B \tag{A10}$$

Expanding the trigonometric functions of sums of angles in equation (A10) with the appropriate formulas gives

$$\begin{aligned} \cos \phi = {} & (\cos k_1 \gamma_1 \cos k_2 \gamma_2 + k_1 k_2 \sin k_1 \gamma_1 \sin k_2 \gamma_2 \cos B)\cos^2 S \\ & - (\sin k_1 \gamma_1 \cos k_2 \gamma_2 + \cos k_1 \gamma_1 \sin k_2 \gamma_2)(1 - k_1 k_2 \cos B)\sin S \cos S \\ & + (\sin k_1 \gamma_1 \sin k_2 \gamma_2 + k_1 k_2 \cos k_1 \gamma_1 \cos k_2 \gamma_2 \cos B)\sin^2 S \end{aligned} \tag{A11}$$

We note that

$$\left.\begin{aligned} \cos^2 S &= \frac{1 + \cos 2S}{2} \\ \sin^2 S &= \frac{1 - \cos 2S}{2} \\ \sin S \cos S &= \frac{\sin 2S}{2} \end{aligned}\right\} \tag{A12}$$

so that

$$\begin{aligned} 2 \cos \phi = {} & \cos(k_1\gamma_1 - k_2\gamma_2)(1 + k_1k_2 \cos B) \\ & + \cos(k_1\gamma_1 + k_2\gamma_2 + 2S)(1 - k_1k_2 \cos B) \end{aligned}$$

$$\cos(k_1\gamma_1 + k_2\gamma_2 + 2S) = \frac{2 \cos \phi - \cos(k_1\gamma_1 - k_2\gamma_2)(1 + k_1k_2 \cos B)}{1 - k_1k_2 \cos B} \tag{A13}$$

Once equation (A13) has been solved for S we can compute ψ_1 and ψ_2 and use equations (A5) and (A6) for u_1 and u_2. Equation (A8) can be used for u_3 or the law of sines for spherical triangles can be used to show that

$$\sin D = \frac{\sin \psi_1 \sin \psi_2 \sin \phi}{\sin B}$$

so that

$$u_3 = \pm \frac{\sin \psi_1 \sin \psi_2 \sin \phi}{\sin B} \tag{A14}$$

Equations (A5), (A6), and (A14) can be combined to give

$$\bar{u} = \begin{bmatrix} \cos \psi_1 \\ \dfrac{\cos \psi_2 - \cos \psi_1 \cos \phi}{\sin \phi} \\ \dfrac{\pm \sin \psi_2 \sin \psi_1 \sin B}{\sin \phi} \end{bmatrix} \tag{A15}$$

Equations (A8) and (A15) are equivalent and the one to be used for type 3 measurements could be chosen for ease in computation.

APPENDIX B

INTERPOLATION FORMULAS FOR POSITION AND VELOCITY FROM GIBB'S METHOD

Following the approach given in reference 9 (p. 147), we expand the position vector, $\bar{r}$, in a series in time as follows:

$$\bar{r}(t) = \bar{a} + \bar{b}t + \bar{c}t^2 + \bar{d}t^3 + \ldots \tag{B1}$$

We assume that $\bar{r}(t_1)$ and $\bar{r}(t_3)$ have been calculated from measurements and wish to determine $\bar{r}(t_2)$ by means of interpolation. For convenience assume that $t_2 = 0$ and write

$$\left.\begin{aligned} \bar{r}(t_1) &= \bar{a} + \bar{b}t_1 + \bar{c}t_1^2 + \bar{d}t_1^3 \\ \bar{r}(t_2) &= \bar{a} \\ \bar{r}(t_3) &= \bar{a} + \bar{b}t_3 + \bar{c}t_3^2 + \bar{d}t_3^3 \end{aligned}\right\} \tag{B2}$$

Differentiation of equation (B1) twice and evaluation at t_1, t_2, t_3 gives

$$\left.\begin{aligned} \ddot{\bar{r}}(t_1) &= \bar{A}(t_1) = 2\bar{c} + 6\bar{d}t_1 \\ \ddot{\bar{r}}(t_2) &= \bar{A}(t_2) = 2\bar{c} \\ \ddot{\bar{r}}(t_3) &= \bar{A}(t_3) = 2\bar{c} + 6\bar{d}t_3 \end{aligned}\right\} \tag{B3}$$

where $\bar{A}$ is the vector of gravitational force acting on the spacecraft, which can be calculated if the corresponding $\bar{r}$ (plus necessary ephemeris information in n-body cases) is known. Therefore $\bar{A}(t_2)$ is unknown, but the first and third of equations (B3) can be solved for $\bar{c}$ and $\bar{d}$ in terms of known quantities to give

$$\left.\begin{aligned} \bar{c} &= \frac{1}{2}\left[\frac{t_3\bar{A}(t_1) - t_1\bar{A}(t_3)}{t_3 - t_1}\right] \\ \bar{d} &= \frac{1}{6}\left[\frac{\bar{A}(t_3) - \bar{A}(t_1)}{t_3 - t_1}\right] \end{aligned}\right\} \tag{B4}$$

and from equations (B2)

$$[\bar{r}(t_3) - \bar{r}(t_1)](t_3 - t_1) = \bar{b}(t_3 - t_1) + \bar{c}(t_3^2 - t_1^2) + \bar{d}(t_3^3 - t_1^3) \tag{B5}$$

Equations (B4) and (B5) can be solved for $\bar{b}$, which is equal to the velocity at t_2, giving

$$\bar{b} = \bar{v}(t_2) = \frac{1}{t_3 - t_1}\left[\bar{r}(t_3) - \bar{r}(t_1) - \frac{\bar{A}(t_1)}{6}(2t_3^2 + 2t_1t_3 - t_1^2) - \frac{\bar{A}(t_3)}{6}(t_3^2 - 2t_1t_3 - 2t_1^2)\right] \tag{B6}$$

We can solve for $\bar{a}$ by substituting for $\bar{b}$, $\bar{c}$, and $\bar{d}$ in the equation for either $\bar{r}(t_1)$ or $\bar{r}(t_3)$ giving

$$\bar{a} = \bar{r}(t_2) = \frac{1}{t_3 - t_1}\left[t_3\bar{r}(t_1) - t_1\bar{r}(t_3) - \frac{\bar{A}(t_1)}{6}t_1t_3(t_1 - 2t_3) - \frac{\bar{A}(t_3)}{6}t_1t_3(2t_1 - t_3)\right] \tag{B7}$$

Note that equation (B6) can be solved with either t_1 or t_3 set equal to t_2, which has been taken to be zero; that is, given $\bar{r}(t_1)$ and $\bar{r}(t_3)$ Gibb's method can be used to find the velocity at either end of the interval. In this case interpolation of $\bar{r}$ is unnecessary, and the solution of equation (B7) is trivial.

APPENDIX C

FORMULAS FOR EVALUATING MEASUREMENT ERRORS

This appendix is divided into four sections. The first section shows that the acceleration terms resulting from Gibb's interpolation method can be neglected in computing the errors in position and velocity. The next section gives derivations of the formulas used for evaluating position errors resulting from measurement errors when only enough data are obtained for a single position fix. The third section presents derivations of equivalent formulas for the extended schedules. Finally equations are developed for evaluating the errors in determining velocity.

SIMPLIFICATION OF ERROR FORMULAS FOR GIBB'S METHOD

The purpose of this section is to show that the acceleration terms from Gibb's method can be neglected for the purposes of computing errors resulting from instrument inaccuracies. We differentiate equations (7) and (10) to get

$$d\bar{r}(t_2) = \frac{1}{t_3-t_1}\left[t_3 d\bar{r}(t_1) - t_1 d\bar{r}(t_3) - \frac{d\bar{A}(t_1)}{6} t_1 t_3 (t_1-2t_3) - \frac{d\bar{A}(t_3)}{6} t_1 t_3 (2t_1-t_3)\right] \tag{C1}$$

and

$$d\bar{v}(t_2) = \frac{1}{t_3-t_1}\left[d\bar{r}(t_3) - d\bar{r}(t_1) - \frac{d\bar{A}(t_1)}{6}(2t_3^2 + 2t_1t_3 - t_1^2) - \frac{d\bar{A}(t_3)}{6}(t_3^2 - 2t_1t_3 - 2t_1^2)\right] \tag{C2}$$

If conic orbits are assumed and

$$\bar{r} = r\bar{u}$$

then

$$\bar{A} = -\frac{\mu\bar{u}}{r^2}$$

and

$$d\bar{A}(t_i) = -\mu\left[\frac{d\bar{u}(t_i)}{r^2(t_i)} - \frac{2\bar{u}(t_i)dr(t_i)}{r^3(t_i)}\right]$$

Substitution for $d\bar{A}(t_i)$ and $d\bar{r}(t_i)$ in (C1) and (C2) gives

$$d\bar{r}(t_2) = \frac{1}{t_3 - t_1}\left[t_3 r(t_1) d\bar{u}(t_1)\left(1 + \frac{P_1}{2}\right) + t_3 \bar{u}(t_1) dr(t_1)(1 - P_1)\right.$$
$$\left. -t_1 r(t_3) d\bar{u}(t_3)\left(1 + \frac{P_2}{2}\right) - t_1 \bar{u}(t_3) dr(t_3)(1 - P_2)\right]$$

$$d\bar{v}(t_2) = \frac{1}{t_3 - t_1}\left[r(t_3) d\bar{u}(t_3)\left(1 + \frac{P_3}{2}\right) + dr(t_3)\bar{u}(t_3)(1 - P_3)\right.$$
$$\left. -r(t_1) d\bar{u}(t_1)\left(1 + \frac{P_4}{2}\right) - dr(t_1)\bar{u}(t_1)(1 - P_4)\right]$$

where

$$P_1 = \frac{\mu}{3r^3(t_1)}(t_1^2 - 2t_1 t_3)$$

$$P_2 = \frac{\mu}{3r^3(t_3)}(t_3^2 - 2t_1 t_3)$$

$$P_3 = \frac{\mu}{3r^3(t_3)}(t_3^2 - 2t_1 t_3 - 2t_1^2)$$

$$P_4 = \frac{\mu}{3r^3(t_1)}(t_1^2 - 2t_1 t_3 - 2t_3^2)$$

We wish to know when the P_i are negligible with respect to unity. If we let $t_1 = t_3 - 2\Delta t$, thereby defining $2\Delta t$ as the interval between t_1 and t_3, then $0 \leqslant t_3 \leqslant 2\Delta t$ and

$$|t_1^2 - 2t_1 t_3| = |4\Delta t^2 - t_3^2| \leqslant 4\Delta t^2$$
$$|t_3^2 - 2t_1 t_3| = |4t_3\Delta t - t_3^2| \leqslant 4\Delta t^2$$
$$|t_3^2 - 2t_1 t_3 - 2t_1^2| = |-8\Delta t^2 + 12t_3\Delta t - 3t_3^2| \leqslant 8\Delta t^2$$
$$|t_1^2 - 2t_1 t_3 - 2t_3^2| = |4\Delta t^2 - 3t_3^2| \leqslant 8\Delta t^2$$

Therefore we wish to know when $8\mu\Delta t^2/3r^3$ is negligible compared to unity.

The values of μ for the major bodies in the solar system, in units of (planet radii)^3/sec^2, are tabulated below in order of decreasing size.

Body	μ (planet radii)^3/sec^2
Earth	1.54×10^{-6}
Mercury	1.49×10^{-6}
Venus	1.37×10^{-6}
Mars	1.18×10^{-6}
Moon	0.993×10^{-6}
Neptune	0.403×10^{-6}
Sun	0.394×10^{-6}
Jupiter	0.349×10^{-6}
Uranus	0.280×10^{-6}
Saturn	0.112×10^{-6}

This table shows that the maximum value of μ is that of the Earth so that

$$\frac{8\mu\Delta t^2}{3r^3} \leqslant 4.11\times10^{-6}\ \frac{\Delta t^2}{r^3}$$

If the acceleration term is to be less than 0.1, then, in seconds,

$$\Delta t \leqslant 156\ r^{3/2}$$

and for $r = \sqrt{2}$ the interval $(2\Delta t)$ between t_1 and t_3 is about 8.4 minutes. This would require two type 3 measurements no more than 8.4 minutes apart while two independent sets of type 5 measurements would require the individual measurements to be about 1 minute apart. For $r = 2$, Δt is increased to 7 minutes, requiring type 5 measurements at 2 minute intervals. If interpolation is carried out to the center of the interval, the maximum acceleration term is reduced to $\mu\Delta t^2/r^3$ and Δt is increased by 60 percent. Therefore, even for near planet orbits, it is reasonable to neglect the acceleration terms in most cases. Equations (C1) and (C2) may be written

$$d\bar{r}(t_2) = \frac{t_3 d\bar{r}(t_1) - t_1 d\bar{r}(t_3)}{t_3 - t_1} \tag{C3}$$

$$d\bar{v}(t_2) = \frac{d\bar{r}(t_3) - d\bar{r}(t_1)}{t_3 - t_1} \tag{C4}$$

POSITION ERRORS FOR REGULAR SCHEDULES

In the text the radial and normal components of the position error due to measurement bias are defined as b_r and b_n, respectively. To compute b_r and b_n set the random measurement errors equal to zero in which case

$$\left.\begin{aligned} b_r &= dr \\ b_n &= r\sqrt{du_1^2 + du_2^2 + du_3^2} \end{aligned}\right\} \quad \text{(C5)}$$

and (see eq. (13))

Since the random measurement errors produce no mean position errors, the standard deviations of the components of position error are given by

$$\left.\begin{aligned} \sigma_r &= \sqrt{E(dr^2) - b_r^2} \\ \sigma_n &= \sqrt{r^2 E(du_1^2 + du_2^2 + du_3^2) - b_n^2} \end{aligned}\right\} \quad \text{(C6)}$$

the equations for b_r, b_n, σ_r and σ_n are derived by substituting the measurement biases and random errors into the appropriate differentials as shown in the following paragraphs.

Type 1 Measurements

For this type of measurement

$$r = \csc S \quad \text{(C7)}$$

and differentiation gives

$$dr = \operatorname{ctn} S \csc S \, dS = -r\sqrt{r^2 - 1} \, dS \quad \text{(C8)}$$

From equations (14) in the text

$$ds = \delta_s + b_I + b_s$$

Therefore,

$$E(dr^2) = [\sigma_s^2 + (b_I + b_s)^2]r^2(r^2 - 1)$$

and

$$b_r = -(b_I + b_s)r\sqrt{r^2 - 1} \quad \text{(C9)}$$

so that

$$\sigma_r = \sigma_s r\sqrt{r^2 - 1} \quad \text{(C10)}$$

From equations (2) in the text

$$u_1 = \cos RA \cos D$$

$$u_2 = \sin RA \sin D$$

$$u_3 = \sin D$$

Differentiating and substituting for dRA and dD gives

$$du_1 = -(\delta_{RA} + b_{RA})\sin RA \cos D + (\delta_D + b_D)\cos RA \sin D$$

$$du_2 = (\delta_{RA} + b_{RA})\cos RA \cos D - (\delta_D + b_D)\sin RA \sin D$$

$$du_3 = (\delta_D + b_D)\cos D$$

so that

$$du_1^2 + du_2^2 + du_3^2 = (\delta_D + b_D)^2 + (\delta_{RA} + b_{RA})^2 \cos^2 D$$

therefore

$$b_n = r\sqrt{b_D^2 + b_{RA}^2 \cos^2 D} \tag{C11}$$

and

$$\sigma_n = r\sqrt{\sigma_D^2 + \sigma_{RA}^2 \cos^2 D} \tag{C12}$$

Basic Equations for Types 2, 3, 4, and 5

All the types of measurements except type 1 use the same basic position fix equations, namely (C7) and

$$u_1 = \cos \psi_1 \tag{C13}$$

$$u_2 = \frac{\cos \psi_2 - \cos \psi_1 \cos \phi}{\cos \phi} \tag{C14}$$

$$u_3 = \pm \sqrt{1 - u_1^2 - u_2^2} \tag{C15}$$

It is shown in appendix A that for type 3 we can also write

$$u_3 = \pm \frac{\sin \psi_1 \sin \psi_2 \sin B}{\sin \phi}$$

but the derivative of this expression and that of (C15) are identical so only (C15) will be considered.

The expression for dr is given in equation (C8) and differentiating equations (C13), (C14), and (C15) gives

$$du_1 = -\sin \psi_1 \, d\psi_1 \tag{C16}$$

$$du_2 = -\frac{\sin \psi_2 \, d\psi_2}{\sin \phi} - du_1 \operatorname{ctn} \phi \tag{C17}$$

$$du_3 = -\frac{(u_1 du_1 + u_2 du_2)}{u_3} \tag{C18}$$

From equations (C15) and (C18)

$$du_1^2 + du_2^2 + du_3^2 = \frac{1}{u_3^2}\left[(1 - u_2^2)du_1^2 + (1 - u_1^2)du_2^2 + 2u_1u_2 \, du_1 \, du_2\right]$$

Substituting for du_1 and du_2 from (C16) and (C17) gives

$$\begin{aligned} du_1^2 + du_2^2 + du_3^2 = \frac{1}{u_3^2}\Big\{ & d^2\psi_1 \sin^2 \psi_1 [(1 - u_2^2) + (1 - u_1^2)\operatorname{ctn}^2 \phi \\ & -2u_1u_2 \operatorname{ctn} \phi] + d\psi_2^2 \frac{\sin^2 \psi_2}{\sin^2 \phi}(1 - u_1^2) \\ & - \frac{2d\psi_1 \, d\psi_2 \sin \psi_1 \sin \psi_2}{\sin \phi}[(1 - u_1^2)\operatorname{ctn} \phi - u_1u_2]\Big\} \end{aligned} \tag{C19}$$

If substitutions are made for u_1 from (C13), u_2 from (C14), u_3 from (A14) and $\cos \phi$ from (A9), equation (C19) is reduced to

$$r^2(du_1^2 + du_2^2 + du_3^2) = \frac{r^2}{\sin^2 B}(d\psi_1^2 + d\psi_2^2 - 2d\psi_1 \, d\psi_2 \cos B) \tag{C20}$$

The appropriate expressions for $d\psi_1$, $d\psi_2$, and ds can be substituted into equations (C8) and (C20) in order to find b_r, b_n, σ_r and σ_n for the different measurement types.

Type 2 Measurements

In this case measure γ_1, γ_2, and S simultaneously. The equation for dr is the same as for type 1 so that (C9) and (C10) are used for b_r and σ_r.

From the definition of the star-center angles

$$\left.\begin{aligned}\psi_1 &= \gamma_1 + k_1 S \\ \psi_2 &= \gamma_2 + k_2 S\end{aligned}\right\} \tag{C21}$$

Differentiating and substituting the differentials from equations (12) gives

$$\left.\begin{aligned}d\psi_1 &= (\delta_1 + b_1) + k_1(\delta_s + b_s) \\ d\psi_2 &= (\delta_2 + b_2) + k_2(\delta_s + b_s)\end{aligned}\right\} \tag{C22}$$

Substitution of $d\psi_1$ and $d\psi_2$ into (C20) gives

$$b_n = \frac{r}{\sin B}\left[(b_1 + k_1 b_s)^2 + (b_2 + k_2 b_s)^2 - 2(b_1 + k_1 b_s)(b_2 + k_2 b_s)\cos B\right]^{1/2} \tag{C23}$$

and

$$\sigma_n = \frac{r}{\sin B}\left[2\sigma_\gamma{}^2 + 2\sigma_s{}^2(1 - k_1 k_2 \cos B)\right]^{1/2} \tag{C24}$$

Type 3 Measurements

With this type of measurement γ_1, γ_2, and B are measured and S must be calculated from equation (6) which is

$$\cos(k_1\gamma_1 + k_2\gamma_2 + 2S) = \frac{2\cos\phi - \cos(k_1\gamma_1 - k_2\gamma_2)(1 + k_1 k_2 \cos B)}{(1 - k_1 k_2 \cos B)}$$

If this expression is differentiated, it is found that

$$ds = -\frac{1}{2}\left\{(k_1 d\gamma_1 + k_2 d\gamma_2) + (k_1 d\gamma_1 - k_2 d\gamma_2)\left[\frac{\sin(k_1\gamma_1 - k_2\gamma_2)(1 + k_1 k_2 \cos B)}{\sin(k_1\gamma_1 + k_2\gamma_2 + 2S)(1 - k_1 k_2 \cos B)}\right]\right.$$

$$\left. + \frac{dB k_1 k_2 \sin B[2\cos(k_1\gamma_1 - k_2\gamma_2) - 2\cos\phi]}{\sin(k_1\gamma_1 + k_2\gamma_2 + 2S)(1 - k_1 k_2 \cos B)^2}\right\} \tag{C25}$$

It can be shown from equations (C21) that

$$\left.\begin{aligned}k_1\gamma_1 &= k_1\psi_1 - S \\ k_2\gamma_2 &= k_2\psi_2 - S\end{aligned}\right\} \tag{C26}$$

Substitution of equations (C26) into (A10) gives

$$\cos\phi = \cos k_1\psi_1 \cos k_2\psi_2 + k_1 k_2 \sin k_1\psi_1 \sin k_2\psi_2 \cos B \tag{C27}$$

Equations (C26) and (C27) can be used to reduce (C25) to

$$ds = -\frac{1}{2}\left\{(k_1\, d\gamma_1 + k_2\, d\gamma_2) + (k_1\, d\gamma_1 - k_2\, d\gamma_2)\left[\frac{\sin(k_1\psi_1 - k_2\psi_2)(1 + k_1k_2\cos B)}{\sin(k_1\psi_1 + k_2\psi_2)(1 - k_1k_2\cos B)}\right] + \frac{2\sin\psi_1\sin\psi_2\sin B\, dB}{\sin(k_1\psi_1 + k_2\psi_2)(1 - k_1k_2\cos B)}\right\}$$

If we define

$$\rho_1 = \frac{\sin(k_1\psi_1 - k_2\psi_2)(1 + k_1k_2\cos B)}{\sin(k_1\psi_1 + k_2\psi_2)(1 - k_1k_2\cos B)}$$

and

$$\rho_2 = \frac{\sin\psi_1\sin\psi_2\sin B}{\sin(k_1\psi_1 + k_2\psi_2)(1 - k_1k_2\cos B)}$$

then

$$ds = -\frac{1}{2}\left[k_1\, d\gamma_1(1 + \rho_1) + k_2\, d\gamma_2(1 - \rho_1) + 2\, dB\rho_2\right] \tag{C28}$$

and

$$d\psi_1 = d\gamma_1 + k_1\, ds = \left(\frac{d\gamma_1 - k_1k_2\, d\gamma_2}{2}\right)(1 - \rho_1) - k_1\rho_2\, dB$$

$$d\psi_2 = d\gamma_2 + k_2\, ds = \left(\frac{d\gamma_2 - k_1k_2\, d\gamma_1}{2}\right)(1 + \rho_1) - k_2\rho_2\, dB$$

Substituting for $d\gamma_1$, $d\gamma_2$, and dB from equations (12) gives

$$ds = -\frac{1}{2}\left[k_1(\delta_1 + b_1)(1 + \rho_1) + k_2(\delta_2 + b_2)(1 - \rho_1) - 2b_I + 2(\delta_B + b_B)\rho_2\right]$$

$$\left.\begin{aligned} d\psi_1 &= \left[\frac{(\delta_1 - k_1k_2\delta_2) + (b_1 - k_1k_2b_2)}{2}\right](1 - \rho_1) - (\delta_B + b_B)k_1\rho_2 \\ d\psi_2 &= \left[\frac{(\delta_2 - k_1k_2\delta_1) + (b_2 - k_1k_2b_1)}{2}\right](1 + \rho_1) - (\delta_B + b_B)k_2\rho_2 \end{aligned}\right\} \tag{C29}$$

When equations (C29) are used with (C8) and (C20), it is found that

$$b_r = -r\sqrt{r^2 - 1}\;\frac{1}{2}\left[k_1b_1(1 + \rho_1) + k_2b_2(1 - \rho_1) + 2b_B\rho_2 - 2b_I\right] \tag{C30}$$

$$\sigma_r = r\sqrt{r^2 - 1}\left[\frac{\sigma_\gamma^2}{2}(1 + \rho_1^2) + \sigma_B^2\rho_2^2\right]^{1/2} \tag{C31}$$

$$b_n = \frac{r}{\sin B}\left\{\frac{(k_1b_1 - k_2b_2)^2}{2}[(1 + \rho_1^2) + k_1k_2(1 - \rho_1^2)\cos B]\right.$$

$$+ 2b_B(k_1b_1 - k_2b_2)\rho_1\rho_2(1 - k_1k_2\cos B)$$

$$\left. + 2b_B^2\rho_2^2(1 - k_1k_2\cos B)\right\}^{1/2} \tag{C32}$$

$$\sigma_n = \frac{r}{\sin B}\left\{\sigma_\gamma^2[(1 + \rho_1^2) + k_1k_2(1 - \rho_1^2)\cos B]\right.$$

$$\left. + 2\sigma_B^2\rho_2^2(1 - k_1k_2\cos B)\right\}^{1/2} \tag{C33}$$

Type 4 Measurements

This method consists in measuring S and γ_1 at times t_1 and t_3 and interpolating to find $\cos\psi_1$ at t_2 while we measure S and γ_2 at t_2. Therefore $d\psi_2$ and ds are the same as for type 2 and b_r and σ_r are given by equations (C9) and (C10).

$\cos\psi_1(t_2)$ is given by equation (9) as

$$\cos\psi_1(t_2) = \frac{1}{r(t_3 - t_1)}\left\{r_1\left[t_3 - \frac{\mu t_1t_3}{6r^3}(t_1 - 2t_3)\right]\cos\psi_1(t_1)\right.$$

$$\left. - r_3\left[t_1 - \frac{\mu t_1t_3}{6r_3^3}(t_3 - 2t_1)\right]\cos\psi_1(t_3)\right\}$$

It was shown earlier in this appendix that the term involving μ/r^3 can be neglected in computing the errors. Thus, replacing r by $1/\sin S$

$$\cos\psi_1(t_2) = \frac{\sin S(t_2)}{t_3 - t_1}\left[\frac{t_3\cos\psi_1(t_1)}{\sin S(t_1)} - t_1\frac{\cos\psi_1(t_3)}{\sin S(t_3)}\right] \tag{C34}$$

Differentiate (C34) and then, since relatively small time intervals are considered, it can be assumed that $\psi_1(t_1) = \psi_1(t_3) = \psi_1$ and $S(t_1) = S(t_3) = S$. This gives

$$d\psi_1(t_2) = -dS(t_2)\text{ctn }\psi_1\text{ ctn S} + \left[\frac{t_3\, dS(t_1) - t_1\, dS(t_3)}{t_3 - t_1}\right]\text{ctn }\psi_1\text{ ctn S}$$

$$+ \frac{t_3\, d\psi_1(t_1) - t_1\, d\psi_1(t_3)}{t_3 - t_1} \qquad \text{(C35)}$$

Since the biases are constants, equation (C20) can be used to write $d\psi_1(t_i) = [\delta_1(t_i) + b_1] + k_1[\delta_S(t_i) + b_S]$ and from equation (12)

$$dS(t_i) = \delta_S(t_i) + b_S + b_I$$

Substitution of these expressions into equation (C35) gives

$$d\psi_1(t_2) = \left[\frac{t_3\delta_S(t_1) - t_1\delta_S(t_3)}{t_3 - t_1}\right](k_1 + \text{ctn }\psi_1\text{ ctn S})$$

$$-\delta_S(t_2)\text{ctn }\psi_1\text{ ctn S} + \left[\frac{t_3\delta_1(t_1) - t_1\delta_1(t_3)}{t_3 - t_1}\right] + b_1 + k_1 b_S \qquad \text{(C36)}$$

From equation (C22)

$$d\psi_2(t_2) = [\delta_2(t_2) + k_2\delta_S(t_2)] + (b_2 + k_2 b_S) \qquad \text{(C37)}$$

It can be seen that the bias terms in equation (C36) are the same as those for $d\psi_1$ in equations (C22) so that b_n is given by (C23). Substituting equations (C36) and (C37) into (C20) gives

$$\sigma_n = \frac{r}{\sin B}\left\{\sigma_\gamma^2\left[1 + \frac{t_3^2 + t_1^2}{(t_3 - t_1)^2}\right] + \sigma_s^2\left[\text{ctn}^2\,\psi_1\,\text{ctn}^2\,S + 1\right.\right.$$

$$\left.\left. + \frac{t_3^2 + t_1^2}{(t_3 - t_1)^2}(k_1 + \text{ctn }\psi_1\text{ ctn S})^2 + 2k_2\,\text{ctn }\psi_1\,\text{ctn S cos B}\right]\right\}^{1/2} \qquad \text{(C38)}$$

The quantity $(t_3^2 + t_1^2/(t_3 - t_1)^2)$ varies from a maximum of unity for t_1 or t_3 equal to zero to a minimum of 0.5 for $-t_1 = t_3 = \Delta t$. Since the latter would be more nearly true in practice, the results will not be greatly degraded by making this approximation, in which case

$$\sigma_n = \frac{r}{\sin B}\left\{\frac{3}{2}\sigma_\gamma^2 + \frac{\sigma_S^2}{2}\left[3(r^2 - 1)\operatorname{ctn}^2 \psi_1 + 3 + 2\sqrt{r^2 - 1}\ \operatorname{ctn} \psi_1 (2k_2 \cos B + k_1)\right]\right\}^{1/2} \tag{C39}$$

If ψ_2 is interpolated instead of ψ_1, it replaces ψ_1 in equation (C39).

Type 5 Measurements

The schedule for this method is as follows:

Time	t_1	t_2	t_3	$t_4=0$	t_5	t_6	t_7
Angle measured	S	γ_1	S	γ_2	S	γ_1	S

If the intervals between the t_i are assumed equal, then from linear interpolation

$$\left.\begin{aligned} dS(t_2) &= \frac{dS(t_1) + dS(t_3)}{2} \\ dS(t_4) &= \frac{dS(t_3) + dS(t_5)}{2} \\ dS(t_6) &= \frac{dS(t_5) + dS(t_7)}{2} \end{aligned}\right\} \tag{C40}$$

Since $r = \csc S(t_4)$, equations (12) and (C40) give

$$dr = -r\sqrt{r^2 - 1}\left[\frac{\delta_S(t_3) + \delta_S(t_5)}{2} + b_I + b_S\right]$$

from which

$$b_r = -(b_I + b_S) r \sqrt{r^2 - 1} \tag{C41}$$

and

$$\sigma_r = \sigma_S r \sqrt{\frac{r^2 - 1}{2}} \tag{C42}$$

Equation (C20) can be used for this type of measurement if t_1, t_2, and t_3 are replaced with t_2, t_4, and t_6, respectively, Then using equations (C40) for the appropriate $dS(t_i)$ gives the equation

$$d\psi_1(t_4) = \frac{\text{ctn } \psi_1 \text{ ctn } S}{4} [dS(t_1) - dS(t_3) - dS(t_5) + dS(t_7)]$$

$$+ \frac{k_1}{4} [dS(t_1) + dS(t_3) + dS(t_5) + dS(t_7)]$$

$$+ \left[\frac{d\gamma_1(t_2) + d\gamma_1(t_6)}{2}\right]$$

Substitution for the differentials from equations (12) gives

$$d\psi_1(t_4) = \frac{\text{ctn } \psi_1 \text{ ctn } S}{4} [\delta_s(t_1) - \delta_s(t_3) - \delta_s(t_5) + \delta_s(t_7)] + \frac{k_1}{4} [\delta_s(t_1) + \delta_s(t_3)$$

$$+ \delta_s(t_5) + \delta_s(t_7)] + \left[\frac{\delta_1(t_2) + \delta_1(t_6)}{2}\right] + b_1 + k_1 b_s$$

Similarly, it can be shown that

$$d\psi_2(t_4) = \delta_2(t_4) + k_2\left[\frac{\delta_s(t_3) + \delta_s(t_5)}{2}\right] + b_2 + k_2 b_s$$

The bias terms in these equations are the same as for types 2 and 4 so that b_n is given by equation (C23). Using $d\psi_1(t_4)$ and $d\psi_2(t_4)$ in equation (C20) gives

$$\sigma_n = \frac{r}{\sin B}\left\{\frac{3\sigma_\gamma^2}{2} + \frac{\sigma_s^2}{4}\left[(r^2 - 1)\text{ctn}^2 \psi_1 + 2k_2(\sqrt{r^2 - 1}\ \text{ctn } \psi_1 - k_1)\cos B + 3\right]\right\}^{1/2} \tag{C43}$$

Position Errors for Extended Schedules

It was pointed out earlier in the computation of instrument errors that the acceleration terms from Gibb's method may be neglected to give a formula of the form

$$d\bar{r}(t_2) = \frac{t_3\, d\bar{r}(t_1) - t_1\, d\bar{r}(t_3)}{t_3 - t_1} \tag{C44}$$

from which

$$|d\bar{r}(t_2)|^2 = \frac{t_3^2|d\bar{r}(t_1)^2 - 2t_1t_3[d\bar{r}(t_1) \cdot d\bar{r}(t_3)] + t_1^2|d\bar{r}(t_3)|^2}{(t_3 - t_1)^2}$$

If we assume that $t_3 = -t_1 = \Delta t$ then

$$|d\bar{r}(t_2)|^2 = \frac{|d\bar{r}(t_1)|^2 + 2[d\bar{r}(t_1) \cdot d\bar{r}(t_3)] + |d\bar{r}(t_3)|^2}{4} \tag{C45}$$

By definition

$$\bar{r} = r\bar{u}$$

$$d\bar{r} = dr\ \bar{u} + r\ d\bar{u}$$

and $\bar{u}$ and $d\bar{u}$ are orthogonal. Therefore we can write

$$|d\bar{r}(t_i)|^2 = dr^2(t_i) + r^2(t_i)|d\bar{u}(t_i)|^2 \tag{C46}$$

and

$$d\bar{r}(t_1) \cdot d\bar{r}(t_3) = dr(t_1)dr(t_3)[\bar{u}(t_1) \cdot \bar{u}(t_3)] + r(t_3)dr(t_1)[\bar{u}(t_1) \cdot d\bar{u}(t_3)]$$

$$+ r(t_1)dr(t_3)[\bar{u}(t_3) \cdot d\bar{u}(t_1)] + r(t_1)r(t_3)[d\bar{u}(t_1) \cdot d\bar{u}(t_3)] \tag{C47}$$

If the change in true anomaly between t_1 and t_3 is small, then the approximations may be made that

$$\bar{u}(t_1) \cdot \bar{u}(t_3) = 1$$

$$\bar{u}(t_1) \cdot d\bar{u}(t_3) = \bar{u}(t_3) \cdot d\bar{u}(t_1) = 0$$

$$r(t_1) = r(t_2) = r(t_3) = r$$

Then equation (C47) reduces to

$$d\bar{r}(t_1) \cdot d\bar{r}(t_3) = dr(t_1)dr(t_3) + r^2\ d\bar{u}(t_1) \cdot d\bar{u}(t_3) \tag{C48}$$

where the first term on the right-hand side comes from the radial components and the second from the normal components.

Equations (C46) and (C48) can be used to separate equation (C45) into its radial and normal components to give

$$dr^2(t_2) = \left[\frac{dr(t_1) + dr(t_3)}{2}\right]^2 = r^2(r^2 - 1)\left[\frac{dS(t_1) + dS(t_3)}{2}\right]^2 \tag{C49}$$

and

$$r^2|d\bar{u}(t_2)|^2 = \frac{r^2[|d\bar{u}(t_1)|^2 + 2d\bar{u}(t_1) \cdot d\bar{u}(t_3) + |d\bar{u}(t_3)|^2]}{4} \tag{C50}$$

The terms $r^2|d\bar{u}(t_1)|^2$ and $r^2|d\bar{u}(t_3)|^2$ can be found by substituting the proper time arguments into equation (C20), and if equations (C16), (C17), and (C18) are used with the proper time arguments,

$$[d\bar{u}(t_1) \cdot d\bar{u}(t_3)] = \frac{1}{\sin^2 B}\{d\psi_1(t_1)d\psi_1(t_3) + d\psi_2(t_1)d\psi_2(t_3)$$

$$-[d\psi_1(t_1)d\psi_2(t_3) + d\psi_1(t_3)d\psi_2(t_1)]\cos B\}$$

Making these substitutions into (C50) results in

$$r^2|d\bar{u}(t_2)|^2 = \frac{r^2}{4\sin^2 B}\{[d\psi_1(t_1) + d\psi_1(t_3)]^2 + [d\psi_2(t_1) + d\psi_2(t_3)]^2$$

$$-2[d\psi_1(t_1)d\psi_2(t_1) + d\psi_1(t_3)d\psi_2(t_3) + d\psi_1(t_1)d\psi_2(t_3)$$

$$+ d\psi_1(t_3)d\psi_2(t_1)]\cos B\} \qquad \text{(C51)}$$

Since biases are constants, it can be seen from equation (C49) that b_r is the same as for a single measurement of S and, hence, is given by (C9). Likewise, examination of equation (C36) shows that the biases in $d\psi_i$ are not affected by interpolation so that b_n is given by (C23). We can evaluate σ_r and σ_n for types 4 and 5 with the extended schedule by setting the measurement biases to zero and taking expected values in equations (C49) and (C51).

Type 4 Measurements

The extended schedule for this type of measurement is

Time	t_1	t_2	t_3	t_4	t_5
Angles measured	γ_1,S	γ_2,S		γ_1,S	γ_2,S
Angle computed	ψ_1	ψ_2		ψ_1	ψ_2

In this case interpolate to get $\psi_1(t_2)$, and use it with $\psi_1(t_2)$ and $S(t_2)$ to compute $\bar{r}(t_2)$. Then interpolate to get $\psi_2(t_4)$ for use in computing $\bar{r}(t_4)$. The assumptions made in deriving equations (C49) and (C51) require that $t_4 = -t_2 = \Delta t/2$ and $t_5 = t_1 = 3\Delta t/2$.

Substituting the appropriate time arguments into equation (C49) gives

$$dr^2(t_3) = r^2(r^2 - 1)\left[\frac{dS(t_2) + dS(t_4)}{2}\right]^2$$

and since $S(t_2)$ and $S(t_4)$ are measured directly the random components are independent and

$$\sigma_r = \sigma_s r \sqrt{\frac{r^2 - 1}{2}} \tag{C52}$$

If we omit the biases and assume the values of t_i given above, then

$$d\psi_1(t_2) = \left[\frac{\delta_s(t_1) + \delta_s(t_4)}{2}\right](k_1 + \text{ctn } \psi_1 \text{ ctn } S)$$

$$-\delta_s(t_2)\text{ctn } \psi_1 \text{ ctn } S + \left[\frac{\delta_1(t_1) + \delta_1(t_4)}{2}\right]$$

$$d\psi_2(t_2) = \delta_2(t_2) + k_2\delta_s(t_2)$$

$$d\psi_1(t_4) = \delta_1(t_4) + k_1\delta_s(t_4)$$

$$d\psi_2(t_4) = \left[\frac{\delta_s(t_2) + \delta_s(t_5)}{2}\right](k_2 + \text{ctn } \psi_2 \text{ ctn } S)$$

$$-\delta_s(t_4)\text{ctn } \psi_2 \text{ ctn } S + \left[\frac{\delta_1(t_2) + \delta_1(t_5)}{2}\right]$$

When these differentials are substituted into (C51) we can show that

$$\sigma_n = \frac{r}{2 \sin B}\left\{5\sigma_\gamma^2 + \frac{\sigma_s^2}{2}\left[(r^2 - 1)(3 \text{ ctn}^2 \psi_1 + 3 \text{ ctn}^2 \psi_2\right.\right.$$

$$+ 4 \text{ ctn } \psi_1 \text{ ctn } \psi_2 \cos B) + \sqrt{r^2 - 1}\,(4k_1 + 6k_2 \cos B)\text{ctn } \psi_1$$

$$\left.\left. + \sqrt{r^2 - 1}\,(4k_2 + 6k_2 \cos B)\text{ctn } \psi_2 + 10\right]\right\}^{1/2} \tag{C53}$$

Type 5 Measurements

The extended schedule for this type of measurement is:

Time	t_1	t_2	t_3	t_4	t_5	t_6	t_7	t_8	t_9
Angle measured	S	γ_1	S	γ_2	S	γ_1	S	γ_2	S

This schedule is the same as for type 4 except that in order to compute ψ_i associated with each measured γ_i we must interpolate S using the measured values at adjacent times. Then following the procedure used for type four we compute $\bar{r}(t_4)$ and $\bar{r}(t_6)$ and then interpolate to get $\bar{r}(t_5)$.

Substituting the appropriate time arguments into (C49) gives

$$dr^2(t_5) = r^2(r^2 - 1)\left[\frac{dS(t_4) + dS(t_6)}{2}\right]^2$$

and taking account of linear interpolation

$$dr^2(t_5) = \frac{r^2(r^2 - 1)}{4}\left[\frac{dS(t_3) + dS(t_5)}{2} + \frac{dS(t_5) + dS(t_7)}{2}\right]^2$$

Assuming the biases to be zero and taking the expected value gives

$$\sigma_r = \sigma_s r\sqrt{\frac{3(r^2 - 1)}{8}} \tag{C54}$$

Similarly, by making the proper substitutions into equation (C51) we can show that

$$\sigma_n = \frac{r}{2 \sin B}\left\{5\sigma_\gamma^2 + \frac{\sigma_s^2}{8}\left[(r^2 - 1)(2 \operatorname{ctn}^2 \psi_1 + 2 \operatorname{ctn}^2 \psi_2 + \operatorname{ctn} \psi_1 \operatorname{ctn} \psi_2 \cos B\right] + 5\sqrt{r^2 - 1}\,(k_1 \operatorname{ctn} \psi_2 + k_2 \operatorname{ctn} \psi_1)\cos B - 15k_1k_2 \cos B + 20\right\}^{1/2} \tag{C55}$$

VELOCITY ERRORS

The errors in velocity are determined by differentiating equation (10). It was shown earlier in this appendix that, for the purpose of computing the position and velocity errors due to measurement errors, the acceleration terms in equation (10) may be omitted. The resulting equation is of the form

$$d\bar{v}_2 = \frac{d\bar{r}(t_3) - d\bar{r}(t_1)}{t_3 - t_1} \tag{C56}$$

Since the bias errors are constants, it can be seen from (C56) that there are no errors in velocity due to measurement biases. Therefore we will compute the random errors in velocity under the assumption that the biases are zero. Hence,

$$E[|d\bar{v}(t_2)|^2] = E\left\{\frac{|d\bar{r}(t_3)|^2 - 2[d\bar{r}(t_1) \cdot d\bar{r}(t_3)] + |d\bar{r}(t_1)|^2}{(t_3 - t_1)^2}\right\} \tag{C57}$$

If $\bar{r}(t_1)$ and $\bar{r}(t_3)$ are determined from two independent sets of measurements, which is the case except when the extended schedules are used, the random components of $d\bar{r}(t_1)$ and $d\bar{r}(t_3)$ are independent, and the expected value of the dot product is zero.

From equation (13)

$$|d\bar{r}(t_i)|^2 = dr^2(t_i) + r^2(t_i)[du_1^2(t_i) + du_2^2(t_i) + du_3^2(t_i)]$$

so that substitution from (14), assuming $b_r = b_n = 0$ into (C57) gives

$$E[|d\bar{v}(t_2)|] = \frac{1}{t_3 - t_1}\sqrt{2(\sigma_r^2 + \sigma_n^2)}$$

If Δt is defined by

$$t_3 - t_1 = 2\Delta t$$

then

$$E[|d\bar{v}(t_2)|] = \frac{1}{\Delta t}\sqrt{\frac{\sigma_r^2 + \sigma_n^2}{2}} \tag{C58}$$

Similarly, if the acceleration terms are neglected,

$$d\bar{r}(t_2) = \frac{t_3 d\bar{r}(t_1) - t_1 d\bar{r}(t_3)}{\Delta t}$$

and

$$|d\bar{r}(t_2)|^2 = \frac{t_3^2|d\bar{r}(t_1)|^2 - 2t_1t_3[d\bar{r}(t_1) \cdot d\bar{r}(t_3)] + t_1^2|d\bar{r}(t_3)|^2}{4\Delta t^2} \tag{C59}$$

Therefore, for two independent sets of measurements and assuming $b_r = b_n = 0$

$$E[|d\bar{r}(t_2)|] = \sqrt{\frac{t_1^2 + t_3^2}{\Delta t}}\sqrt{\frac{\sigma_r^2 + \sigma_n^2}{4}} \tag{C60}$$

From equations (C58) and (C60)

$$E[|d\bar{v}(t_2)|] = \frac{E[|d\bar{r}(t_2)|]}{\sqrt{t_1^2 + t_3^2}} \tag{C61}$$

The quantity $(t_1^2 + t_3^2)$ varies from a maximum of $4\Delta t^2$ for interpolation to one of the ends of the interval, where $t_1 = t_2 = 0$ or $t_3 = t_2 = 0$, to a

minimum of $2\Delta t^2$ if $t_3 = -t_1 = \Delta t$. Therefore, for interpolation to the center of the interval

$$\frac{E[|d\bar{v}(t_2)|]}{E[|d\bar{r}(t_2)|]} = \frac{1}{\Delta t} \tag{C62}$$

While for interpolation to the ends of the interval the ratio is reduced by $\sqrt{2}$. Note that this change is caused by an increase in the standard deviation of the position error while that of the velocity remains the same.

For the extended schedules assume that $t_3 = -t_1 = \Delta t$ so that equation (C59) reduces to (C45), while (C57) is the same except that the sign of the dot product is reversed. Making this sign change in the derivations for the standard deviations of the position error gives for type 4 measurements

$$\sigma_r' = \frac{\sigma_s r}{\Delta t}\sqrt{\frac{r^2 - 1}{2}}$$

$$\sigma_n' = \frac{r}{2\Delta t \sin B}\left\{5\sigma_\gamma^2 + \frac{\sigma_s^2}{2}[(r^2 - 1)(3\ \mathrm{ctn}^2\ \psi_1 + 3\ \mathrm{ctn}^2\ \psi_2 - 4\ \mathrm{ctn}\ \psi_1\ \mathrm{ctn}\ \psi_2 \cos B) + \sqrt{r^2 - 1}\,(4k_1 - 6k_2 \cos B)\mathrm{ctn}\ \psi_1 + \sqrt{r^2 - 1}\,(4k_2 - 6k_1 \cos B)\mathrm{ctn}\ \psi_2 + 10]\right\}^{1/2}$$

For type 5 measurements

$$\sigma_r' = \frac{\sigma_s r}{\Delta t}\sqrt{\frac{(r^2 - 1)}{8}}$$

$$\sigma_n' = \frac{r}{2\Delta t \sin B}\left\{5\sigma_\gamma^2 + \frac{\sigma_s^2}{8}[(r^2 - 1)(2\ \mathrm{ctn}^2\ \psi_1 + 2\ \mathrm{ctn}^2\ \psi_2 - \mathrm{ctn}\ \psi_1\ \mathrm{ctn}\ \psi_2 \cos B) - 5\sqrt{r^2 - 1}\,(k_1\ \mathrm{ctn}\ \psi_2 + k_2\ \mathrm{ctn}\ \psi_1)\cos B + 15k_1k_2 \cos B + 20]\right\}^{1/2}$$

where σ_r' and σ_n' are the standard deviations of radial and normal errors in velocity. Numerical evaluation over the range of measured angles considered indicates that if $t_3 = -t_1 = \Delta t$ then equation (C62) holds for the extended schedule within a factor of 2.

APPENDIX D

EQUATIONS FOR ANALYSIS OF ERRORS DUE TO LINEAR INTERPOLATION

The purpose of this appendix is to compare the magnitude of position errors arising from the linear interpolation of the range r or a star-limb angle γ with the errors due to measurement inaccuracy. Since the interpolation errors are a function of the spacecraft trajectory, the state of the vehicle must be accounted for. This has been done by finding the minimum value of r for which the maximum interpolation errors are less than some fraction, M, of those due to measurement inaccuracy. An expression for the error was found in terms of the gravitational constant μ, the true anomaly θ, the orbital eccentricity e, the range r, and Δt which is half the interpolation interval. The largest value of μ, in (planet radii)^3/sec^2, of the major bodies in the solar system was used, and θ was chosen to maximize the error. This choice of θ was made in order to simplify the calculations. The minimum value of r was then found for various values of eccentricity and Δt.

The errors in range, which can be evaluated directly from a Taylor series expansion of r, are considered in the first section. Errors due to linear interpolation of γ are dealt with in the second section by an indirect method because the Taylor series expansion of γ contains a singularity.

Interpolation of Range

If $r(t)$ is known at times t_1 and t_3, an appropriate value, $\hat{r}(t_2)$, can be obtained for $r(t_2)$ under the assumption that r is a linear function of time. Then

$$\hat{r}(t_2) = \frac{(t_3 - t_2)r(t_1) + (t_2 - t_1)r(t_3)}{t_3 - t_1}$$

and if $t_2 = 0$

$$\hat{r}(t_2) = \frac{t_3 r(t_1) - t_1 r(t_3)}{t_3 - t_1} \tag{D1}$$

Since r is not a linear function of time, we can estimate the error in $\hat{r}(t_2)$ by expanding r in a Taylor series about t_2. This gives

$$\left.\begin{aligned} r(t_1) &= r(t_2) + t_1\dot{r}(t_2) + \frac{t_1^2}{2!}\ddot{r}(t_2) + \frac{t_1^3}{3!}\dddot{r}(t_2) + \ldots \\ r(t_3) &= r(t_2) + t_3\dot{r}(t_2) + \frac{t_3^2}{2!}\ddot{r}(t_2) + \frac{t_3^3}{3!}\dddot{r}(t_2) + \ldots \end{aligned}\right\} \tag{D2}$$

Substituting (D2) into (D1) gives

$$\hat{r}(t_2) - r(t_2) = \ddot{r}(t_2) \frac{t_1 t_3}{2!} - \dddot{r}(t_2) \frac{t_1 t_3 (t_1 + t_3)}{3!} \ldots$$

or, dropping the time argument,

$$\Delta r \approx -\ddot{r} \frac{t_1 t_3}{2} - \dddot{r} \frac{t_1 t_3}{6} (t_1 + t_3) \tag{D3}$$

This is the error in interpolating with a first-order formula as compared with a third-order formula such as those derived by Gibb's method. It should give a good indication of the total error when $(t_3 - t_1)$ is small. Note that if t_2 lies at t_1 or t_3 or half way between t_1 and t_3 $(-t_1 = t_3 = \Delta t)$, the third-order term disappears. Define Δr_2 and Δr_3 as the maximum values of the second- and third-order terms, respectively, in equation (D3) and determine the minimum value of r for which $|\Delta r_2| \leqslant M\sigma_r$. In this case σ_r is the standard deviation of position error due to a single subtense angle measurement of 10 arc seconds standard deviation. Next find the minimum value of r for which $|\Delta r_3|_{max}$ is negligible compared to $|\Delta r_2|_{max}$ and hence compared to the measurement error. If this latter condition is true, then the second-order term is a valid representation of the total interpolation error. If the trajectory is assumed conic

$$r = \frac{h^2}{\mu(1 + e \cos \theta)} \tag{D4}$$

$$\dot{r} = \frac{\mu e \sin \theta}{h} \tag{D5}$$

$$\ddot{r} = \frac{\mu e \cos \theta}{r^2} \tag{D6}$$

$$\dddot{r} = - \frac{2\mu^2 e^2 \sin \theta \cos \theta}{hr^3} - \frac{\mu e h \sin \theta}{r^4}$$

or substituting for r in the second term from (D4)

$$\dddot{r} = - \frac{\mu^2 e \sin \theta}{hr^3} (3e \cos \theta + 1) \tag{D7}$$

where e is the orbital eccentricity, θ is the true anomaly and h is the angular momentum.

From equations (D3) and (D6) the second-order error is

$$\Delta r_2 = - \frac{t_1 t_3}{2} \frac{\mu e \cos \theta}{r^2}$$

and $t_1 t_3$ is maximum for $t_1 = t_3 = \Delta t$ so that

$$|\Delta r_2| \leqslant \frac{\Delta t^2 \mu e}{2r^2} \tag{D8}$$

The standard deviation of the random error in determining range from a single subtense angle measurement is $\sigma r\sqrt{r^2 - 1}$ where σ is the standard deviation of the instrument error. For the ratio of the maximum of $|\Delta r_2|$ to this quantity to be less than or equal to some number, M requires

$$r^3\sqrt{r^2 - 1} \geqslant \frac{\mu e \Delta t^2}{2\sigma M} \tag{D9}$$

The minimum values of r from equation (D9) are plotted in figure 17 for M = 0.1 and 10 arc seconds, and are discussed in the section on results in the text.

From equations (D3) and (D7)

$$\Delta r_3 = -\frac{t_1 t_3 (t_1 + t_3)}{6} \frac{\mu^2 e \sin\theta}{hr^3} (3e \cos\theta + 1) \tag{D10}$$

Since $h = \sqrt{\mu r_p (1 + e)}$ and planet radii are the units of length

$$h \geqslant \sqrt{\mu (1 + e)} \tag{D11}$$

and since

$$\left.\begin{aligned} \sin\theta(3e \cos\theta + 1) &= \frac{3}{2} e \sin 2\theta + \sin\theta \\ \sin\theta(3e \cos\theta + 1) &< \frac{3e + 2}{2} \end{aligned}\right\} \tag{D12}$$

Therefore substituting from equations (D11) and (D12) into (D10) gives

$$|\Delta r_3| \leqslant \left|\frac{t_1 t_3 (t_1 + t_3)}{6}\right| \frac{\mu^{3/2}}{r^3} \frac{e(3e + 2)}{2\sqrt{1 + e}} \tag{D13}$$

If the interval between t_1 and t_3 is $2\Delta t$ then $|t_1 t_3 (t_1 + t_3)|$ is maximum if $t_1 = -\Delta t(1 \pm 1/\sqrt{3})$ so that

$$\left|\frac{t_1 t_3 (t_1 + t_3)}{6}\right| \leqslant \frac{2\Delta t^3}{9\sqrt{3}}$$

then

$$|\Delta r_3| \leqslant \frac{\Delta t^3}{9\sqrt{3}} \frac{\mu^{3/2}}{r^3} \frac{e(3e + 2)}{2\sqrt{1 + e}} \tag{D14}$$

Dividing equation (D14) by (D8) gives the ratio of the maximum value of $|\Delta r_3|$ to the maximum value of $|\Delta r_2|$ as

$$\frac{|\Delta r_3|_{max}}{|\Delta r_2|_{max}} = \frac{2\sqrt{\mu}}{9\sqrt{3}} \frac{3e + 2}{\sqrt{1 + e}} \frac{\Delta t}{r}$$

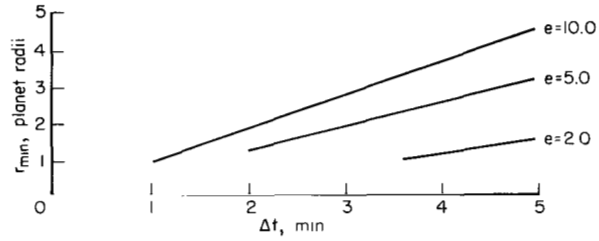

Figure 19.- Minimum radius for neglecting third-order term in analyzing error due to linear interpolation of radius.

The third-order term can be considered negligible if this ratio does not exceed 0.1, which requires

$$r \geqslant \frac{20\sqrt{\mu}}{9\sqrt{3}} \left(\frac{3e + 2}{\sqrt{1 + e}} \right) \tag{D15}$$

The minimum values of r for various values of e and Δt, using μ for the Earth, are plotted in figure 19. All these values are considerably smaller than the corresponding ones for $|\Delta r_2| \leqslant M\sigma_r$, thus indicating that the second-order error term is a valid approximation for the total interpolation error.

Linear Interpolation of Star-Limb Angles

In this section of the appendix sets of equations similar to (D14) and (D15) are derived for the case where linear interpolation is used with a star-limb angle instead of r. For this purpose it is convenient to deal with the star-center angle ψ at first. The error in position due to errors in ψ_1 and ψ_2 is normal to the radius vector and can be shown from equation (C20) to be

$$r\sqrt{du_1^2 + du_2^2 + du_3^2} = \frac{r}{\sin B} \sqrt{d\psi_1^2 + d\psi_2^2 - 2d\psi_1\, d\psi_2 \cos B}$$

For simplicity interpolation will be assumed for only one angle (ψ_1 or ψ_2) at a time and $\Delta\psi$ will be the interpolation error. Then

$$r\sqrt{du_1^2 + du_2^2 + du_3^2} = \frac{r\,\Delta\psi}{\sin B} \tag{D16}$$

Since actually γ instead of ψ is interpolated, the "interpolated" value $\hat{\psi}$ of $\psi(t_2)$ can be written

$$\hat{\psi} = \frac{t_3\gamma(t_1) - t_1\gamma(t_3)}{t_3 - t_1} + kS(t_2) \tag{D17}$$

Equation (D17) can be written

$$\hat{\psi} = \tilde{\psi} - k\tilde{S} + kS(t_2)$$

where

$$\tilde{\psi} = \frac{t_3\psi(t_1) - t_1\psi(t_3)}{t_3 - t_1}$$

and

$$\tilde{S} = \frac{t_3S(t_1) - t_1S(t_3)}{t_3 - t_1}$$

It can be seen that $\tilde{\psi}$ and $\tilde{S}$ are the values of $\psi(t_2)$ and $S(t_2)$ obtained by linear interpolation and

$$\Delta\psi = \hat{\psi} - \psi(t_2) = [\tilde{\psi} - \psi(t_2)] - k[\tilde{S} - S(t_2)]$$

is the difference of the errors in interpolating ψ and S. Furthermore,

$$|\Delta\psi| \leqslant |\tilde{\psi} - \psi(t_2)| + |\tilde{S} - S(t_2)| \tag{D18}$$

The second term can be evaluated directly by means of a Taylor series expansion, but the first term requires an indirect approach. For this purpose, define ψ with different geometric equations from those used in the text as illustrated by sketch (e). The X-Y plane is the orbital plane of the

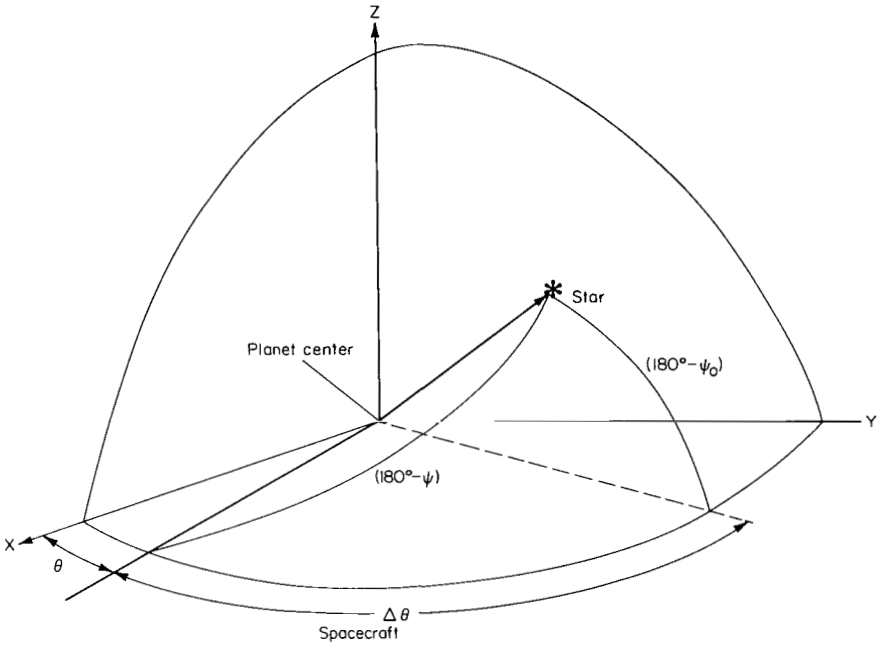

Sketch (e)

spacecraft with the origin at the center of the planet and X axis at periapsis. The star-spacecraft angle is the compliment of the star-center angle, ψ, defined in the text, and the elevation angle of the star above the orbital plane is defined as $(180^\circ - \psi_o)$. Note that ψ_o is the minimum value attained by ψ during a complete orbit. The angle θ is the true anomaly of the spacecraft, while $\Delta\theta$ is the change in true anomaly from the spacecraft's position to the projection of the star on the orbital plane.

For spherical trigonometry

$$\cos(180^\circ - \psi) = \cos(180^\circ - \psi_o)\cos \Delta\theta$$

which can be reduced to

$$\cos \psi = \cos \psi_o \cos \Delta\theta \qquad \text{(D19)}$$

we can write

$$\dot{\psi} = \dot{\theta} \frac{d\psi}{d\Delta\theta}$$

so that if the time interval is small enough for $\dot{\theta}$ to be assumed constant, then $\Delta\theta$ can be used as the independent variable instead of time. The minimum value of r for which this approximation is valid is found by expanding $\Delta\theta$ in a Taylor series to give

$$\Delta\theta = \Delta\theta_o + \Delta t\dot{\theta}_o + \frac{\Delta t^2\ddot{\theta}_o}{2:} + \cdots$$

and requiring that the second-order term be less than 10 percent of the first order.

If the trajectory is assumed conic

$$\dot{\theta} = \frac{h}{r^2} = \frac{\sqrt{\mu r_p(1 + e)}}{r^2} \tag{D20}$$

$$\ddot{\theta} = -\frac{2\mu e \sin\theta}{r^3} \tag{D21}$$

then setting r_p equal to one planet radius and $|\sin\theta|$ to unity gives

$$\frac{|\Delta t^2(\ddot{\theta}/2)|}{|\Delta t\dot{\theta}|} \leqslant \frac{\sqrt{\mu}\ e}{r\sqrt{1 + e}}$$

The minimum value of r for this ratio to be less than one tenth is given by

$$r \geqslant \frac{10\sqrt{\mu}\ e\Delta t}{\sqrt{1 + e}}$$

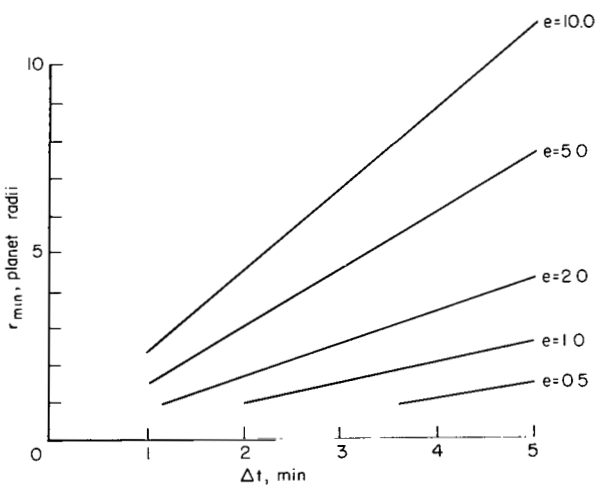

Figure 20.- Minimum radius for assuming $\dot{\theta}$ constant.

the resulting value of r_{min} is plotted in figure 20 for various values of r and e using a geocentric orbit.

If r is assumed to be greater than the minimum values in figure 20, then $\Delta\theta$ can be used as the independent variable for interpolating ψ. Since $d\psi/d\Delta\theta$ is singular for $\psi = 0$, it is impractical to use a Taylor series, and we make further simplifications by considering the plot (obtained from eq. (D19)) of ψ as a

function of $\Delta\theta$, shown in figure 21. It can be seen from the two examples of linear interpolation in this figure that the maximum interpolation error occurs when the epoch t_2 is at the center of the time interval and $\Delta\theta(t_2) = 0$. Under these conditions $\psi(t_2) = \psi_o$, $-\Delta\theta(t_1) = \Delta\theta(t_3) = \Delta\theta$,

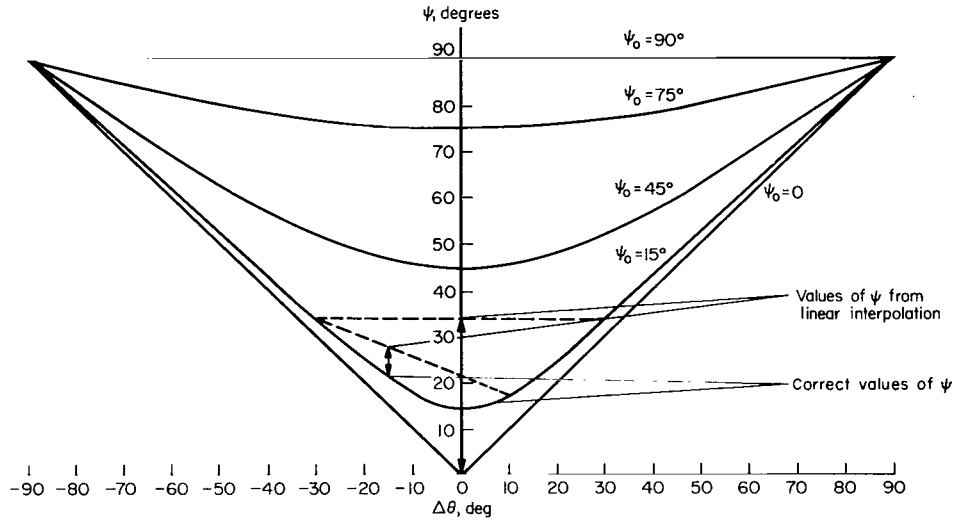

Figure 21.- Variation of ψ with $\Delta\theta$ and ψ_o, with two examples of linear interpolation.

$\tilde{\psi} = \psi(t_1) = \psi(t_3)$ and $t_3 = -t_1 = \Delta t$. Therefore from equation (D19)

$$\cos \tilde{\psi} = \cos \psi_o \cos \Delta\theta$$

and since

$$\cos \psi(t_2) = \cos \psi_o$$

then

$$\cos \tilde{\psi} - \cos \psi(t_2) = -\cos \psi_o(1 - \cos \Delta\theta) \tag{D22}$$

and from trigonometry

$$\cos \tilde{\psi} - \cos \psi_o = -2 \sin \left(\frac{\tilde{\psi} + \psi_o}{2} \right) \sin \left(\frac{\tilde{\psi} - \psi_o}{2} \right) \tag{D23}$$

From equation (D19) $\tilde{\psi} \geqslant \psi_o$ for $\Delta\theta \leqslant 90°$ so that

$$\sin \left(\frac{\tilde{\psi} + \psi_o}{2} \right) \geqslant \sin \psi_o$$

Therefore, combining equations (D22) and (D23) gives

$$2 \sin\left(\frac{\tilde{\psi} - \psi_o}{2}\right) \leqslant \text{ctn } \psi_o(1 - \cos \Delta\theta)$$

or

$$\sin\left(\frac{\tilde{\psi} - \psi_o}{2}\right) \leqslant \text{ctn } \psi_o \sin^2 \frac{\Delta\theta}{2} \tag{D24}$$

For the fastest orbit considered ($u = 1.54\times10^{-6}$, $r_p = 1$ and $e = 10$) it can be shown that the change in true anomaly from perigee in 5 minutes is about 0.89 radian. Since $\Delta\theta/2 \leqslant 0.445$ radian, it is reasonable to make the approximation that

$$\sin \frac{\Delta\theta}{2} \approx \frac{\Delta\theta}{2}$$

and from figure 21

$$\left(\frac{\psi - \psi_o}{2}\right) \leqslant \frac{\Delta\theta}{2}$$

then

$$\sin\left(\frac{\tilde{\psi} - \psi_o}{2}\right) \approx \frac{\tilde{\psi} - \psi_o}{2}$$

these approximations reduce equation (D24) to

$$|\tilde{\psi} - \psi_o| = |\tilde{\psi} - \psi(t_2)| \leqslant \frac{\Delta\theta^2}{2} \text{ctn } \psi_o$$

and if r is less than the appropriate minimum value from figure 19

$$|\tilde{\psi} - \psi(t_2)| \leqslant \frac{\dot{\theta}^2 \Delta t^2}{2} \text{ctn } \psi_o$$

We can replace $\dot{\theta}^2$ with h^2/r^4 and eliminate h by using equation (D4) to get

$$\dot{\theta}^2 = \frac{\mu(1 + e \cos \theta)}{r^3}$$

so that

$$|\tilde{\psi} - \psi(t_2)| \leqslant \frac{\mu(1 + e)\Delta t^2 \text{ ctn } \psi_o}{r^3} \tag{D25}$$

Now consider the second term in equation (D18), $|\tilde{S} - S(t_2)|$. By definition

$$\tilde{S} = \frac{t_3 S(t_1) - t_1 S(t_3)}{t_3 - t_1}$$

and we can expand $S(t_1)$ and $S(t_3)$ in a Taylor series about t_2 to give

$$\tilde{S} - S(t_2) = \frac{t_1 t_3}{2} \ddot{S}(t_2) + \frac{t_1 t_3 (t_1 + t_3)}{6} \dddot{S}(t_2) + \ldots$$

It was shown in the section on the linear interpolation of r that

$$\frac{t_1 t_3 (t_1 + t_3)}{6} \leqslant \frac{2\Delta t^3}{9\sqrt{3}}$$

and

$$\frac{t_1 t_3}{2} \leqslant \frac{\Delta t^2}{2}$$

so that

$$|\tilde{S} - S(t_2)| \leqslant \frac{\Delta t^2}{2} |\ddot{S}(t_2)| + \frac{2\Delta t^3}{9\sqrt{3}} |\dddot{S}(t_2)| + \ldots \tag{D26}$$

We wish to be able to approximate $|\tilde{S} - S(t_2)|$ by the second-order term and therefore find the minimum value of r for which the maximum magnitude of the third-order term does not exceed 10 percent of the second-order one. By definition

$$\sin S = 1/r$$

where the equation has been normalized by using planet radii as units of length. Differentiation gives

$$\dot{S} = -\dot{r} \sin S \tan S$$

$$\ddot{S} = -\ddot{r} \sin S \tan S - \dot{S}\dot{r} \sin S(1 + \sec^2 S)$$

or, substituting for $\dot{S}$

$$\ddot{S} = -\ddot{r} \sin S \tan S + \dot{r}^2 \sin^2 S \tan S(1 + \sec^2 S)$$

Differentiating and substituting for $\dot{S}$ gives

$$\dddot{S} = -\sin S \tan S[\dddot{r} - 3\dot{r}\ddot{r} \sin S(1 + \sec^2 S)$$

$$+\dot{r}^3 \sin^2 S(2 + \sec^2 S + 3 \sec^4 S)]$$

Substitution of the derivatives of r from equations (D5), (D6), and (D7) gives

$$\dddot{S} = \sin S \tan S \left[\frac{\mu^2 e \sin \theta}{hr^3} (3e \cos \theta + 1)\right.$$

$$+ \frac{3\mu^2 e^2 \sin \theta \cos \theta}{hr^2} \sin S(1 + \sec^2 S)$$

$$\left. - \frac{2\mu^3 e^3 \sin^3 \theta}{h^3} \sin^2 S(2 + \sec^2 S + 3 \sec^4 S)\right]$$

and substitution for $\sin B$ and $\tan S$ using the definition of $\sin S$ gives

$$\dddot{S} = \frac{\mu^2 e \sin \theta}{hr^3\sqrt{r^2 - 1}} \left[\frac{3e \cos \theta + 1}{r} + \frac{3e \cos \theta}{r} (1 + \sec^2 S)\right.$$

$$\left. - \frac{\mu e^2 \sin^2 \theta}{h^2} (2 + \sec^2 S + 4 \sec^4 S)\right]$$

Substituting from (D4) for r inside the bracket and from (D12) for h gives

$$|\dddot{S}| \leq \frac{\mu^{3/2} e}{(1 + e)^{3/2}} r^3\sqrt{r^2 - 1} \left|\sin \theta[1 + e \cos \theta(7 + 3 \sec^2 S]\right|$$

$$+e^2 \cos^2 \theta(6 + 3 \sec^2 S) - e^2 \sin^2 \theta(2 + \sec^2 S + 3 \sec^4 S)| \quad \text{(D27)}$$

Substitution for r, $\sin S$, $\tan S$, and h in the expression for $\ddot{S}$ gives

$$|\ddot{S}| \leq \frac{\mu e}{(1 + e)r^2\sqrt{r^2 - 1}} \left|e \sin^2 \theta(1 + \sec^2 S) - e \cos^2 \theta - \cos \theta\right|$$

or

$$|\ddot{S}| \leq \frac{\mu e}{(1 + e)r^2\sqrt{r^2 - 1}} \left|e(1 + \sec^2 S) - e(2 + \sec^2 S)\cos^2 \theta - \cos \theta\right| \tag{D28}$$

We can rewrite (D27) and (D28) as

$$|\dddot{S}| \leq \frac{\mu^{3/2} eF}{(1 + e)^{3/2}} r^3\sqrt{r^2 - 1} \tag{D29}$$

and

$$|\dddot{S}| \leq \frac{\mu eG}{1 + e} r^2\sqrt{r^2 - 1} \tag{D30}$$

where F and G are defined as the maximum magnitudes of the terms in the absolute value signs. In order for the maximum magnitude of the third-order term in equation (D26) to be less than 10 percent of that of the second-order term

$$r \geq \frac{40}{9\sqrt{3}} \frac{\mu^{1/2}}{\sqrt{1 + e}} \frac{F}{G} \Delta t \tag{D31}$$

The values of F and G depend on θ and $\sec^2 S$ as well as e, and successive approximations were used to find their values for various values of e and Δt. The resulting values of r_{min} are plotted in figure 22 for geocentric orbits as functions of Δt for various values of e. If r is larger than these values and those in figure 20, equations (D25), (D26), and (D30) combine to give

$$|\Delta\psi| \leq \frac{\Delta t^2}{2}\left[\frac{\mu(1 + e)}{r^3} \operatorname{ctn} \psi_o + \frac{\mu eG}{(1 + e)r^2\sqrt{r^2 - 1}}\right]$$

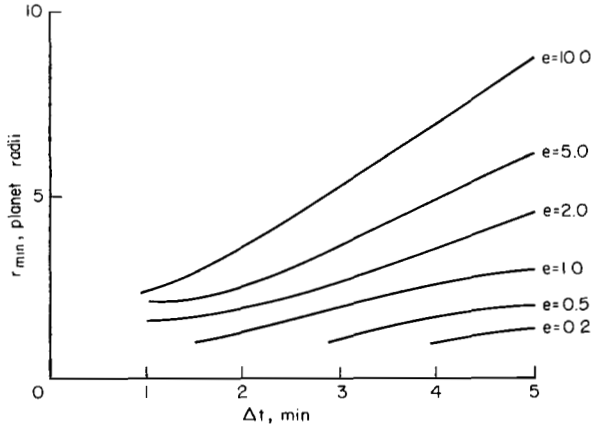

Figure 22.- Minimum radius for neglecting third-order term in analyzing error due to linear interpolation of subtense angle.

This expression can be used with (D16) to show that the upper bound on the position error $\tilde{r}$ due to the interpolation of γ is given by

$$|\tilde{r}| \leq \frac{r}{\sin B}\left[\frac{\mu\Delta t^2(1+e)}{2r^3}\operatorname{ctn}\psi_o + \frac{\mu\Delta t^2 eG}{2(1+e)r^2\sqrt{r^2-1}}\right] \tag{D32}$$

This error is compared with $\sqrt{\sigma_r^2 + \sigma_n^2}$ for type 5 since it has been found (see the section on results in the text) that this quantity is usually smaller for type 5 than for type 4. From equations (C42) and (C43)

$$(\sigma_r^2 + \sigma_n^2) = r^2\sigma^2\left\{\left(\frac{r^2-1}{2}\right) + \frac{3}{2} + \frac{1}{\sin^2 B}\left[\left(\frac{r^2-1}{4}\right)\operatorname{ctn}^2\psi_1 + \frac{k_2\sqrt{r^2-1}\operatorname{ctn}\psi_1 + k_1k_2}{2}\cos B + \frac{3}{4}\right]\right\}$$

Note that it has been assumed that $\sigma_\gamma = \sigma_s = \sigma$ and that if ψ_2 is interpolated instead of ψ_1, it would replace ψ_1 in the equation and k_1 and k_2 would be interchanged. From this equation it is seen that dropping the subscript on ψ, that

$$\sigma_r^2 + \sigma_n^2 \geq r^2\sigma^2\left[\left(\frac{r^2+2}{2} + \frac{3}{4\sin^2 B}\right) + \frac{\sqrt{r^2-1}\operatorname{ctn}\psi}{2\sin^2 B} + \frac{(r^2-1)\operatorname{ctn}^2\psi_1}{4\sin^2 B}\right]$$

This expression is of the form

$$(\sigma_r^2 + \sigma_n^2) \geq r^2\sigma^2(C_1^2\operatorname{ctn}^2\psi + 2C_2\operatorname{ctn}\psi + C_3^2)$$

and from equation (D32)

$$|\tilde{r}|^2 \geq r^2(D_1^2\operatorname{ctn}^2\psi + 2D_1D_3\operatorname{ctn}\psi + D_3^2)$$

Therefore if the maximum magnitude of interpolation error is to be less than M times the maximum of $\sqrt{\sigma_r^2 + \sigma_n^2}$

$$D_1 \leq M\sigma C_1$$

$$D_1D_3 \leq M^2\sigma^2C^2$$

$$D_3 \leq M\sigma C_3$$

Substituting for the D_i and C_i gives

$$\frac{\mu \Delta t^2 (1 + e)}{r^3} \leqslant M\sigma\sqrt{r^2 - 1} \tag{D33}$$

$$\frac{\mu^2 \Delta t^4 eG}{r^5\sqrt{r^2 - 1}} < M^2\sigma^2\sqrt{r^2 - 1} \tag{D34}$$

$$\frac{\mu \Delta t^2 eG}{2(1 + e)r^2\sqrt{r^2 - 1}} \sin B \leqslant M\sigma\sqrt{\frac{r^2 + 2}{2} + \frac{3}{4 \sin^2 B}} \tag{D35}$$

It can be shown that if the first condition is satisfied, the second will also be, and only the first and last conditions will be considered.

The minimum values of r, using μ for the Earth and 10 arc seconds for σ, for the two conditions were computed for each case and the largest taken as r_{min}. These values of r_{min} are plotted in figure 18 for two different values of sin B. The value of r_{min} from equation (D35) goes to zero with e so that for the smaller values of e the value of r_{min} from (D33) is the larger and the curves do not change with sin B. For the larger values of e the errors increase rapidly as sin B decreases, and for very small values of sin B the interpolation error would become very large compared to the measurement error. However, the measurement error is also large in this region and such measurements would be avoided.

Note that the values of r_{min} in figure 18 are always greater than the corresponding values in figures 20 and 22, so that the second-order terms used in obtaining the curves of figure 18 are valid measures of the error. The curves in figure 18 are discussed further in the text.

REFERENCES

1. Nordtvedt, Kenneth, Jr.: A Theory of Manual Space Navigation. NASA CR-841, 1967.

2. Havill, C. Dewey: An Emergency Midcourse Navigation Procedure for a Space Vehicle Returning From the Moon. NASA TN D-1765, 1963.

3. Silva, Robert M.; and Mills, Jon Gary: Analytic Development of Optimum Astronaut Procedures for Use of the Air Force Space Navigation System in the Manual Mode. Final Report Air Force Avionics Laboratory Technical Report AFAL-TR-69-14, 22 May 1967 - Dec. 1968.

4. Hamer, Harold A.; and Mayo, Alton P.: Error Analysis of Several Methods of Determining Vehicle Position in Earth-Moon Space From Simultaneous Onboard Optical Measurements. NASA TN D-1805, 1963.

5. Lampkin, Bedford A.; and Smith, Donald W.: A Hand-Held Sextant Qualified for Space Flight. NASA TN D-4585, 1968.

6. Walsh, Thomas M.: Factors Affecting the Design and Use of a Photographic Sextant for Space Navigation. NASA TN D-4285, 1967.

7. Novak, Donald H.: Trisextant - A Space Navigation Instrument. AIAA Paper 63-191, 1963.

8. Smith, Donald W.; and Lampkin, Bedford A.: Sextant Sighting Measurements From On Board the Gemini XII Spacecraft. NASA TN D-4952, 1968.

9. Danby, J. M. A.: Fundamentals of Celestial Mechanics. The Macmillan Company, N. Y., 1962.

10. Gadeberg, Burnett L.; and White, Kenneth C.: Theory of the Correction of Celestial Observations Made for Space Navigation or Training. NASA TN D-5239, 1970.

NASA-Langley, 1971 —— 21 A-3522

"The aeronautical and space activities of the United States shall be conducted so as to contribute . . . to the expansion of human knowledge of phenomena in the atmosphere and space. The Administration shall provide for the widest practicable and appropriate dissemination of information concerning its activities and the results thereof."

—NATIONAL AERONAUTICS AND SPACE ACT OF 1958

NASA SCIENTIFIC AND TECHNICAL PUBLICATIONS

TECHNICAL REPORTS: Scientific and technical information considered important, complete, and a lasting contribution to existing knowledge.

TECHNICAL NOTES: Information less broad in scope but nevertheless of importance as a contribution to existing knowledge.

TECHNICAL MEMORANDUMS: Information receiving limited distribution because of preliminary data, security classification, or other reasons.

CONTRACTOR REPORTS: Scientific and technical information generated under a NASA contract or grant and considered an important contribution to existing knowledge.

TECHNICAL TRANSLATIONS: Information published in a foreign language considered to merit NASA distribution in English.

SPECIAL PUBLICATIONS: Information derived from or of value to NASA activities. Publications include conference proceedings, monographs, data compilations, handbooks, sourcebooks, and special bibliographies.

TECHNOLOGY UTILIZATION PUBLICATIONS: Information on technology used by NASA that may be of particular interest in commercial and other non-aerospace applications. Publications include Tech Briefs, Technology Utilization Reports and Technology Surveys.

Details on the availability of these publications may be obtained from:

SCIENTIFIC AND TECHNICAL INFORMATION OFFICE

NATIONAL AERONAUTICS AND SPACE ADMINISTRATION

Washington, D.C. 20546